Technical University of Denmark

DTU

Modeling and Control of Electrodynamic Tethers - an Energy and Topology Approach

Larsen, Martin Birkelund; Blanke, Mogens

Publication date:
2010

Document Version
Publisher's PDF, also known as Version of record

Link back to DTU Orbit

DTU Library
Technical Information Center of Denmark

Technical University of Denmark

DTU

Martin Birkelund Larsen

Modeling and control of Electrodynamic Tethers – an Energy and Topology Approach

PhD thesis, May, 2010

DTU Electrical Engineering
Department of Electrical Engineering

Modeling and Control of Electrodynamic Tethers
– an Energy and Topology Approach

Martin Birkelund Larsen

Summary

A space tether is a cable used to connect spacecrafts in an orbiting structure. If an electrical current is lead through the tether, it can be utilized to provide propulsion for the spacecraft. In this case the cable is referred to as an electrodynamic tether. The system utilizes the magnetic field of the Earth for creating a Lorentz force along the tether which occur when a current carrying wire operates in a magnetic field. The use of electrodynamic tethers are interesting since they operate solely on electrical energy, which can be provided by solar panels of the spacecrafts. In this way the amount of propellant a spacecraft need to bring from Earth can be reduced.

In this thesis the modeling and control of electrodynamic tethers are investigated, both when a single tether is used to connect two spacecrafts, and when the tethers are used i more general formations of spacecrafts. One of the main challenges when using electrodynamic tethers is that the force created along the tether is based on an external uncontrollable condition, namely the magnetic field. Even whit a known model of the magnetic field, limitations to the creation of the Lorentz force still exists, since the force can only be generated perpendicular to the instantaneous magnetic field. Furthermore, the control problem is complicated by the time variations in the magnetic field. This thesis solves these problems by utilizing an energy-based system description and a passivity-based control design. An advantage of the energy-based approach is that the stability of the system can easily be investigated, based on the energy flow in the system.

Systems of several spacecrafts connected by tethers has many applications, for example in connection with space telescopes and space stations. Tethered formations are advantageous, compared to formations of free-flying spacecrafts, since a predetermined geometry of spacecrafts is easily maintained. This thesis investigates the use of electrodynamic tethers for such tethered satellite forma-

tions with focus on the modeling and control aspects. One can think of many different structures for solving tasks in space, and separate derivations of the dynamical equations can be cumbersome. It can therefore be advantageous to be able to model a formation independent of its topology, i.e. the way tethers and satellites are interconnected. The thesis treats a class of formations in a generic framework, using graph theory to describe the topology of the formations. The framework can be used both to deduce the equations of motion for the attitude motion of the formation and for control design regarding the same motion.

The main part of the thesis consists of five scientific papers which have been submitted for international journals and conferences during the PhD project.

Resumé

Et rumkabel (*space tether*) er et kabel, der forbinder rumfartøjer i en formation. Ledes en elektrisk strøm gennem dette kabel, kan det anvendes til at påvirke fremdriften af rumfartøjet. I dette tilfælde benævnes kablet elektrodynamisk (*electrodynamic tether*). Systemet udnytter jordens magnetfelt til at danne en Lorentzkraft distribueret langs kablet. Denne kraft opstår ved en vekselvirkning mellem det strømførende kabel og magnetfeltet. Brugen af elektrodynamiske kabler er interessant, da de kan fungere alene ved tilførslen af elektrisk energi, som kan leveres af solpaneler på rumfartøjerne i formationen. På denne måde kan mængden af brændstof, der skal medbringes fra jorden, reduceres.

I denne afhandling er modelleringen og styringen af elektrodynamiske kabler undersøgt, både i forbindelse med et enkelt kabel der forbinder to rumfartøjer og i forbindelse med formationer af flere rumfartøjer. Et af hovedproblemerne ved brugen af elektrodynamiske kabler er, at kraften der dannes langs kablet, er afhængig af en ekstern størrelse, nemlig jordens magnetfelt. Selv med en kendt model af jordens magnetfelt, er dannelsen af Lorentzkraften underlagt restriktioner, da den kun kan dannes ortogonalt på den aktuelle feltvektor. Reguleringsproblemet bliver ydermere vanskeliggjort af tidsvariationerne i jordens magnetfelt. I denne afhandling er disse problemer løst ved anvendelsen af en energibaseret systembeskrivelse samt en passivitetsbaseret reguleringsmetode. Metoden har blandt andet den fordel at stabiliteten af systemet let kan undersøges gennem energistrømmen i systemet.

Flere rumfartøjer forbundne med kabler har flere anvendelsesområder, blandt andet i forbindelse med rumteleskoper og rumstationer. Forbundne formationer har den fordel, frem for formationer af frie rumfartøjer, at en fast struktur let kan opretholdes. Denne afhandling undersøger brugen af elektrodynamiske kabler i sådanne forbundne formationer, med fokus på modellering og styring. Man kan forstille sig mange forskellige formationer til løsning af opgaver i rummet, og det

kan være tidskrævende at finde de dynamiske ligninger for alle formationerne separat. Det er derfor fordelagtigt at kunne modellere formationerne uafhængigt af deres topologi dvs. hvordan kabler og rumfartøjer er forbundne. Afhandlingen undersøger en gruppe formationer med en fælles beskrivelse, hvor formationernes topologi er udtrykt ved hjælp af grafteori. Beskrivelsen kan bruges både til at finde bevægelsesligningerne for formationen, samt til at designe regulatorer.

Hoveddelen af nærværende afhandling består af fem artikler indsendt til internationale tidsskrifter og konferencer i løber af ph.d. projektet.

Preface

This thesis is written based on the research conducted during my PhD project at the Technical University of Denmark, Department of Electrical Engineering. The project was carried out from May 2007 to May 2010 founded by a DTU scholarship. The supervisor of the project was Professor Mogens Blanke.

The thesis constitutes a collection of articles which have been submitted for conferences and journals during the project. Since the articles represent work carried out over a three year period, a consistent nomenclature have not been possible.

This thesis treats the use of electrodynamic tethers in connection with single tether systems and tethered satellite formations. For clarity the thesis is divided according to these research areas. This division can, in some contexts, appear enforced due to the gradual transition between the areas. The main focus of the thesis is on the modeling and control aspects of such tethered satellite systems.

<div align="right">

Martin Birkelund Larsen
Copenhagen, May 2010

</div>

Papers included in the thesis

[A] Larsen, M. B., Blanke M. Control by damping injection of electrodynamic tether system in an inclined orbit. *In proceedings of American Control Conference ACC'09*, 2009, 4824-4829, St. Louis, USA. Published

[B] Larsen, M. B., Blanke M. Stabilization of periodic solutions in a tethered satellite system by damping injection. *In proceedings of European Control Conference ECC'09*, 2009, 2169-2174, Budapest, Hungary. Published

[C] Larsen, M. B., Blanke M. Passivity-based control of a rigid electrodynamic tether. *Journal of Guidance, Control, and Dynamics*, 2010. Submitted

[D] Larsen, M. B., Smith, R. S., Blanke M. Modeling of tethered satellite formations using graph theory. *Acta Astronautica*, 2010. Submitted

[E] Larsen, M. B., Smith, R. S., Blanke M. Decentralized control of tethered satellite formations using electrodynamic tethers. *Journal of Guidance, Control, and Dynamics*, 2010. Submitted

The following paper was published during the PhD project, but not included in this thesis. The paper was based on my MSc project and related to the work in this thesis.

- Larsen, M. B., Blanke M. Nonlinear control of electrodynamic tether in equatorial or somewhat inclined orbits. *In proceedings of Mediterranean Conference on Control & Automation MED '07*, 2007, 1-6, Athens, Greece. Published

Acknowledgements

Contents

CHAPTER 1

Introduction

This thesis treats some of the modeling and control aspects of space tether technology. The basic idea of the technology is quite simple, nevertheless its potential is huge and the use of space tethers have been proposed in connection with a large number of missions. The technology has been studied since the middle of the 1960's, and several missions have been flown to prove and investigate the concepts, especially during the 1990's. The proposed concepts aim to solve a variety of different tasks in space and covers numerous configurations. Only a couple of the concepts will be highlighted here, but comprehensive descriptions of many others are collected in [10].

A tethered satellite system (TSS) has been proposed in connection with the creation of artificial gravity on spacecrafts. When two tethered satellites are orbiting the Earth aligned with the local vertical axis, the center of mass (CM) of the system will be placed somewhere along the tether. Each satellite will experience a force directed away from the CM, due to the mismatch between the gravitational and the centrifugal force. This force can constitute an artificial gravity force. The force is, however, quite small, about one percent of the gravity on Earth [31]. The magnitude of the artificial gravity can be increased by spinning the system around its CM, and thereby create an additional centrifugal force. Tethers could also be useful in connection with momentum exchange between satellites. The idea is to use a TSS capable of capturing satellites in low Earth orbits. The TSS will then, by inducing a librational or rotational motion, be able to transfer the satellites to orbits of higher orbital energy, at the cost of orbital energy of the TSS itself. Satellites in a tethered formation have

also been proposed in connection with space interferometers, for example the Submillimeter Probe of the Evolution of Cosmic Structure (SPECS) proposed by NASA [30]. The relative distances between the satellites are crucial in this context and a TSS can reduce the use of propellant in connection with formation control compared to a formation of free-flying satellites. The use of tethers are also proposed in connection with re-entering the atmosphere of space capsules, the so-called tethered spacemail concept. The idea is to deploy a capsule in a tether from the main spacecraft, transport it to a lower orbit, and induce pendulum like oscillation in the system. By cutting the tether at the right position the capsule will lose orbital energy and move to a lower orbit from where it will be reenter the atmosphere.

The concept of electrodynamic tethers (EDT's) is one of the most innovative proposal regarding TSS's. The basic idea is to use the tether as a conducting wire, along which a voltage is induced when the system is orbiting the Earth through the magnetic field. The part of the atmosphere called the ionosphere is ionized and contains free electrons. By collecting these electrons at one end of the tether and emitting them at the other end, a current will flow through the tether. The electrical circuit can be seen as being closed through a phantom loop in the ionosphere. Since the electrons are moving in a magnetic field, the current will furthermore give rise to an electrodynamic force (the Lorentz force) acting along the tether. The collection of electrons can be done either by use of a spherical collector or by a partly uninsulated tether called a bare tether. The bare tether has the advantage that higher currents through the tether can be obtained. Two properties of the concept can be utilized by space missions: the generated electrical energy and the force acting on the tether. The electrical energy can be used to power spacecrafts. The electrical energy is converted from the orbital energy of the TSS, which as a consequence will be transferred to a lower orbit. In case the TSS is intended to stay in orbit, another force should be used to counteract the drag from the EDT. Utilizing the electrodynamic force acting along the tether, an electrodynamic tether can be used to perform orbit maneuvers. The system can either by used in generator mode, which will decrease the orbital energy of the system or in thruster or motor mode, which will increase the energy. For this reason the system is also referred to as a plasma motor generator (PMG) system. When used in thruster mode additional electrical energy must be supplied for example from solar panels. Hence, in thruster mode electrical energy is converted to orbital energy, while it is the other way around when using the system in generator mode. In generator mode, the system has mainly been proposed in connection with deorbiting [20, 21, 24, 43] of obsolete satellites, which is an important task in order to mitigate the increasing amount of space debris. In thruster mode, the system has been proposed to cancel out air-drag on the International Space Station (ISS), a proposal that potentially can save one billion dollars over ten years in connection with transportation of propellant to the ISS [22]. The

concepts can also be used on a momentum exchange system in order to regain the orbital energy lost by the exchange [57].

When connecting several satellites in a tethered satellite formation, a basic concern is to ensure that the tethers are kept in tension. This can be achieved using the gravity gradient or a drag force, in which case the formation is characterized as a static formation. Alternatively, it can be done by spinning the formation and thereby creating a centrifugal force, in which case the formation is dynamic. A single tether system is considered as a static formation in most investigations. In case the tethers are kept in tension, the modeling can be simplified by substituting the flexible tethers with rigid rods.

A single tether system consists of a main satellite connected to a sub-satellite or an endmass by a tether. The typical mission of a TSS is divided into three phases: First, a deployment phase, where the tether is deployed from the main satellite. Then an operational phase where the system performs a task. Last, a retrieval phase where the system is put back in the initial configuration. Each phase requires a control scheme, and these are typically treated separately due to different dynamic properties of each phase.

The main problem when using TSS's is the safety risk connected with the length of the tether. Depending on the purpose of the tether and the masses of the satellites involved, a tether can range from less than hundred meter to close to fifty kilometers. When planing a mission with such a widespread structure, the potential collision risk with other spacecrafts must be considered very carefully. As an example of this, it can be mentioned that the configuration of the ProSEDS mission was changed due to a collisions risk with the International Space Station (ISS). The changes included a shortening of the tether and was introduced due to a change in the launch of the mission [15].

1.1 Tethered satellite systems in orbit

Several missions have been flown using space tether technology. Table 1.1 presents an overview of some of these. The purpose of the missions have in general been to investigate the fundamental dynamics and, in case of an electrodynamic tether, the electrodynamic properties of the TSS.

In 1992 and 1996 the missions TSS-1 and TSS-1R were flown as experiments on the space shuttle missions STS-46 and STS-75, respectively. The experiments investigated a 20 km long electrodynamic tether equipped with a spherical electron collector. During TSS-1 about 260 m of tether was deployed before the

Name	Year	Tether	Main investigation
TSS-1[1]	1992	~ 260 m	Electrodynamic tether
SEDS-1	1993	20 km	Deployment (open-loop)
PMG[1]	1993	500 m	Electrodynamic tether
SEDS-2	1994	20 km	Deployment (closed-loop)
TSS-1R[1]	1992	~ 20 km	Electrodynamic tether
TiPS	1996	4 km	Long-time dynamics
ProSEDS[1]	(2003)[2]	15 km	Bare electrodynamic tether
YES2	2007	~ 31 km	Spacemail concept

[1] Using electrodynamic tether.
[2] Cancelled.

Table 1.1: Data of space missions involving tethers [10, 26, 31].

experiment was interrupted by a malfunction in the deployment mechanism. TSS-1R repeated the experiment, and got about 19.5 km tether deployed, before the tether was broken. In spite of less successful course of events, the experiment proved the concept of electrodynamic tethers and was able to create the first experimental data for the current-voltage characteristics of the system [39]. The concept of electrodynamic tethers was also investigated during the PMG mission. The mission was able to reverse the current along the tether using an additional voltage source and thereby using the system in thruster mode [23]. In connection with electrodynamic tethers the proposed mission ProSEDS [1] should also be mentioned even though it was canceled. The mission was supposed to test the concept of bare electrodynamic tethers, using a 15 km long tether of which 5 km was uninsulated and conducting to increase its capability of collecting electrons. The remaining 10 km was non-conductive and used to increase the gravity gradient affecting the system. In connection with the ProSEDS mission the overview in Figure 1.1 was made of past and future missions. Non of the future proposals have, however, been realized yet.

As regards electrodynamic tether systems that have been implemented, the Termination Tether[TM] and nanoTerminator[TM] should be mentioned. These are commercial products designed for deorbiting of satellites by the company Tethers Unlimited, Inc[1]. The Termination Tether[TM] [13] is designed for satellites with a mass of less than 500 kg, while nanoTerminator[TM] is intended for nano-satellites like a CubeSat.

Beside the missions investigating the concept of electrodynamic tethers, a series of missions have investigated the dynamics of non-conduction tethers. The missions SEDS-1 and SEDS-2 have investigated the deployment dynamics of a TSS. The missions accomplished the deployment, controlling the tension along

---

[1] http://www.tethers.com
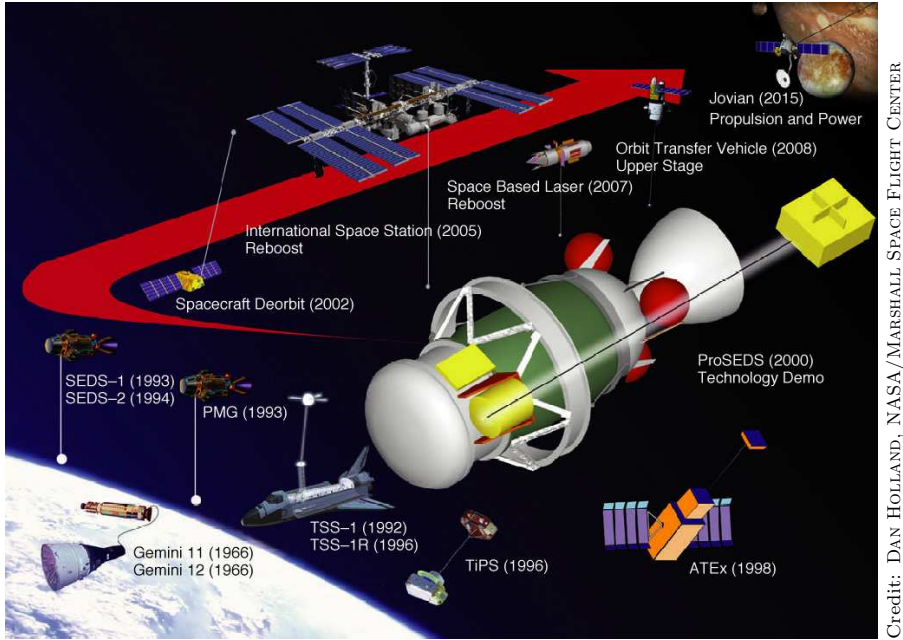
Figure 1.1: Space tether mission overview.

the tether using an open-loop and a closed-loop strategy, respectively. The missions were successful in the way that the observed pendulum oscillations were smaller than excepted [10]. The TiPS mission also investigated the dynamics of the TSS, but at a longer time scale. The mission showed how tether oscillation will be damped over time and the tether robustness against space debris was established [49]. Recently, the YES2 mission tested the concept of spacemail, using an over 30 km long tether. Even though the tether was deployed further than planed, the capsule was released for reentering the atmosphere. The capsule itself was never found due to lack of a beacon signal [26].

1.2   Literature survey

The survey, presented in this section, is divided according to the two main research areas of this thesis: Single tether systems and tethered satellite formations. The survey will mainly focus on the fundamental results regarding the modeling and control of the TSS and on the research regarding electrodynamic tethers. More detailed reviews can be found in [27] and [4].

1.2.1 Single tether systems

Modeling. One of the most comprehensive treatments of the modeling regarding space tethers was given in the book by Beletsky and Levin [2]. The book deduced the equations of motion using a Newtonian approach for both massless and massive tethers. This division made it possible to separate the attitude and the flexible motions of the system, and the corresponding equations of motion were given as ordinary and partial differential equations, respectively. A comprehensive list of the forces affecting the tether, and estimations of their magnitude were given. The various oscillations of an massive tether were also treated, together with ways to damp these. The basic properties of an electrodynamic tether were also studied and the effect of the Lorentz force was investigated in a simplified approached.

The modeling of a flexible tether was also treated in [58], which covered the computational aspects of solving the equations of motion. The equations of motion were deduced taking gravity and air drag into account and the resulting partial differential equations were discretized using a Gelerkin modal approach and a finite elements approach, respectively. The oscillations of a flexible electrodynamic tether were investigated in [50] using modal analysis. Periodic solutions induced by the magnetic field were found, and numerical simulations showed them to be unstable. The electrodynamic tether was also investigated in [56] for an inextensible tether. An linear stability analysis of the lateral oscillation, concluded that the source of the instability were resonance between the forcing term and the out-of-plane dynamics.

The dynamic model of a single tether system, where the satellites are modeled as point masses and the tether as a rigid rod, was the subject of much research. The unforced system was identical to a dumbbell satellite and its basic dynamics was treated in [5, 38, 42]. When used in a electrodynamic setup with a constant tether current, the Lorentz force will act as a periodic forcing term of the dynamics and periodic solutions are induced. These periodic solutions were approximated and investigated by Peláez et al. [47]. The solutions were approximated for small tether currents using power series found by a perturbation method. Furthermore, the solutions were found to be unstable using Floquet theory. This conclusion was also reached by simulations of the energy flow in the system. The periodic solutions were further investigated in [45] and numerical approximations of the solutions were found for larger values of the tether current than the power series allowed. The paper also investigated the periodic solution of the unforced system using a Poincaré section in state space. The main attitude control problem, when using electrodynamic tethers, occur due to the torque originating from the Lorentz force used to actuate the orbit motion. In the concept of self balanced electrodynamic tethers this problem

was solved by canceling the total Lorentz torque [44]. The simple idea behind the concept was to cancel out the torques acting on the upper and lower parts of the tether, relative to the CM. This requires that the electric current profile along the tether can be controlled or that the masses of the satellites and the tether can be chosen to fulfill a balancing condition.

A fundamental treatment of the electrodynamic parts of an EDT system is given in [20]. An equivalent electrical circuit was given for an uncontrolled single tether, and the components of the circuit were treated based on the data from the TSS-1R mission. The main challenge when using electrodynamic tethers is to maximize the current flowing in the tether. To do this the concept of bare tethers was introduced in [51]. The main idea behind the concept is to leave a part of the tether uninsulated to increase the area for collecting electrons. This will, however, lead to a variable current profile along the tether.

Control. The control of oscillations along an electrodynamic tether was investigated in [19]. This work included two control algorithms that used the current through the tether as input. The first algorithm used motion feedback from several point along the tether while the second only used feedback from the sub-satellite. Simulations showed that the controllers could reduce the unstable behavior of the tether oscillations. In [12] the vibrations along a nonconducting tether were damped by an active control law. The system was actuated by controlling the tether tension at the attachment with the main satellite. A control law for damping the longitudinal oscillations was used and the control gains were found to optimize an energy based performance index.

The attitude control, or libration control, has been often treated for rigid EDT systems. One simple approach was presented in [9] in connection with deorbiting. The system was controlled by switching the current through the tether on and off, based on the energy in the tether motion. The simplicity of this approach prevented an asymptotically stable motion, but simulation showed that the magnitude of the libration motion was limited. A controller for the libration motion in the orbit plane was treated in [34]. The tether current was controlled by means of a variable resistor in series with the tether and feedback linearization was applied for the system. Stabilization of an equilibrium point for both the in-plane and the out-of-plane motion is not possible, when only the current through the tether is controlled. Therefore, a common control strategy is to stabilize periodic solutions, e.g. the solutions induced by the magnetic field when a constant current is applied to the tether. In [46] two controllers using this strategy were investigated. The first approach used a feedback signal of the difference between the states and a periodic solution, while the second used the difference between the states and a delayed version of the states. The control

laws were applied by means of additional actuators for in-plane and out-of-plane motions. In [63] the periodic solutions were stabilized, using synchronization of the libration energy with a known reference signal. This control law was applied varying only the current through the tether. Lately, a predictive control law has been investigated in [65] varying the tether current. The control law was based on a delayed feedback signal and included both the libration motion and the orbit motion. Using a discrete version of the dynamics, the control signal was found by minimizing the difference between the present and the delayed libration motion.

The use of an electrodynamic tether will change the orbit of the TSS, hence orbit control is an important control task in this connection. The orbital changes induced by a tether were investigated in [28]. The work included the attitude dynamics of a rigid tether, a high fidelity model of the magnetic field, and a detailed model of the electrodynamics. The changes in the orbit were modeled using the equinoctial elements, to avoid the singularities for small orbit eccentricities and orbit inclinations when using the classical orbital parameters. In [59] a guidance scheme for an orbit maneuver was considered. The scheme was based on a simple model ignoring the attitude dynamics and used the tether current to actuate the orbital motion. The approach was expanded in [62] by taking attitude dynamics into account. Ref. [64] used a similar approach, but assumed that the tether was spinning with constant velocity in the orbit plane and that no out-of-plane motion was excited.

1.2.2   Tethered satellite formations

Modeling.   A variety of different types of tethered satellite formations have been investigated in the literature. Figure 1.2 provides an overview of some of the different configurations. The chain structure (see Figure 1.2a) is probably the most investigated type of formation. The study of chain structures can both be motivated by multi-tether formations or by discretized versions of single tether systems. A chain structure containing three satellites connected by rigid rods was investigated in [37]. The equations of motion were found for both fixed-length and variable-length tethers, and the stationary configurations of the system were treated. A general chain structure with N satellites was investigated by Misra and Modi [36]. The equations of motion were found for the combined in-plane and out-of-plane motion, using variable-length tethers modeled as massless rigid rods. It was shown that the in-plane natural frequencies $\omega_{\theta j}$ and the out-of-plane frequencies $\omega_{\varphi j}$ fulfill the relation $(\omega_{\varphi j}/\Omega)^2 = (\omega_{\theta j}/\Omega)^2 + 1$, for $j = 1, \ldots, N-1$, assuming a system in a circular orbit with orbit rate Ω. This work was expanded to take flexible tethers into account in [25]. The stationary configurations of a chain containing three satellites were investigated in

(a) Chain

(b) Triangle

(c) Hub-and-Spoke   **(d)** Closed-Hub-and-Spoke   **(e)** Double pyramid
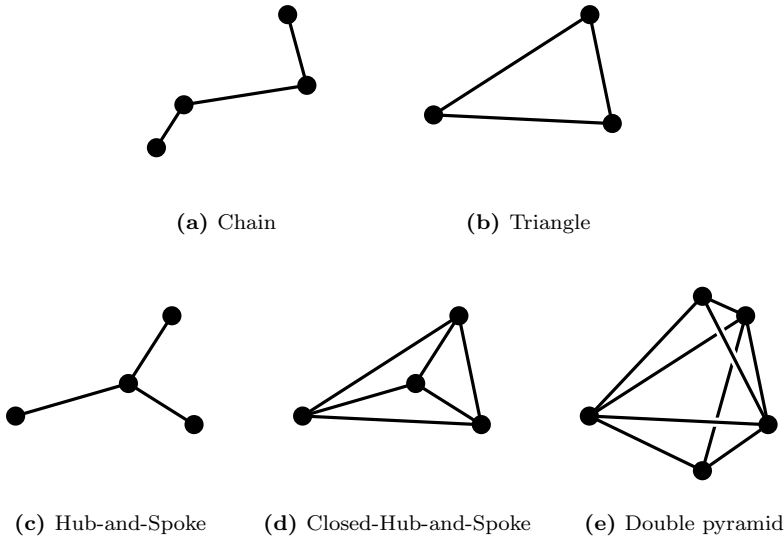
Figure 1.2: Examples of different kinds of tethered satellite formations. The figures are only examples of the structures.

[35]. The configurations were divided into collinear and triangular configurations. All triangular configurations were shown to be unstable, while one of the collinear ones was stable. Guerman [18] investigated the stationary configuration situated in the orbit plane of an N-body chain connected by rigid rods. It was shown that the stationary configurations were a combination of groups of either vertical or horizontal rods, connected by no more than one rod. An upper limit of configurations was stated as $2^{2(N-1)}$. This work was expanded to include general stationary configurations in three dimensions in [17]. When taking both the in-plane and the out-of-plane dimensions into account the stationary configurations follow much more complicated structures.

More complicated tethered formations have also been investigated. In [11] a planar triangle formation (see Figure 1.2b) was investigated in connection with interferometry. The formation was assumed to be spinning around an axis perpendicular to the plane of the satellite and the dynamics was deduced assuming rigid tethers. The validity of this assumption was investigated by considering the forces along the tethers. A hub-and-spoke formation (see Figure 1.2c) consists of a main satellite, to which a number of sub-satellites are tethered. In case the sub-satellites are tethered to each other as well, the formation is called closed-hub-and-spoke (see Figure 1.2d). A double pyramid formation consist of a planar formation, tethered to an anchor satellite at each side (see Figure

1.2e). The formation is spinning around an axis perpendicular to the formation plane, through the two anchor satellites. The hub-and-spoke and the closed-hub-and-spoke formations were investigated in [48] assuming the parent body followed a circular orbit. The formations were investigated with an initial spin around the axis perpendicular to the orbit plane and around the position vector of the system relative to the Earth. The hub-and-spoke formation was, in general, unstable when rotating in the orbit plane, while the closed-hub-and-spoke was stable. When spinning around the radial vector the closed-hop-and-spoke formation was found to exhibit an unstable behavior. The formation could, however, be stabilized by two additional anchor satellites, turning the formation into a double pyramid. A double pyramid formation spinning around the axis through the anchors was also treated in [60]. The rotational axes leading to a stationary configuration were stated as a function of the size of the formation and the spinning rate, and their stability properties were investigated through simulations. Furthermore, a relation, between the system parameters guaranteeing positive tension along the tethers, was given.

Control. The main task of the motion control in connection with tethered satellite formations is to maintain a desired formation structure, i.e. to control the relative positions of the satellites in a formation. When using rigid approximations of the tethers, the investigation of the control strategy can include an analysis of the tension along the tether to be sure that the rigid approximation is valid. In the case that a spinning formation is considered it can also be an objective to control the rate of spinning along with the plane of rotation.

In [36] a control law was considered for a three satellite chain structure, where the length of both tethers was assumed to vary exponentially. The rate of change in the length of the tethers is controlled by a velocity feedback, and the energy flow of the system was considered to obtain stability. A chain structure were also considered in [32], where one satellite constituted an elevator which could move along the tether. The movement of this elevator was controlled by an open-loop strategy and induced oscillations in the system were investigated through simulations. An open-loop retargeting strategy for an interferometer was developed in [3], considering a formation consisting of three satellites in a spinning chain formation. The strategy applied electrical thrusters on two of the satellites, to actuate the system. The retargeting maneuver, i.e. changing the plane of rotation, was investigated using a perturbation method, and the equations of motion were solved analytically in this way. In [7, 8] a decentralized control strategy was applied to a chain structure of two and three satellites. The strategy considered a planar motion of a spinning satellite formation. The control law considered the attitude of each satellite and the spin rate of the formation, and was decentralized in the sense that the torque applied at each

satellite was based only on the attitude of the same satellite. Control of a triangle and a hub-and-spoke formation was investigated in [53] for a planar motion. The formation was controlled, using reaction wheels at each satellite. The work also investigated the alternative of using an electromagnetic formation flight (EMFF), instead of a tethered one. In an EMFF the formation structure is maintained through interconnection of controllable electromagnetic fields generated at each satellite.

1.3   Outline

The outline of the remaining parts of this thesis is as follows. The next two chapters contain a review of the research conducted in the two main areas of this thesis: Single tether systems are considered in Chapter 2, and tethered satellite formations are treated in Chapter 3. The reviews are intended to give an overview of the work done in the areas. Each chapter is concluded with a summery of the papers included in this thesis, where the main ideas and contributions will be highlighted. Chapter 4 contains reflections and conclusions of the work. Afterwards follows the five papers included in the thesis in chronological order. The papers are included as independent chapters with separate bibliographies to reflect the way the papers was published.

Single Tether Systems

The research in the area of single tether systems has focus on the attitude motion of the TSS. The attitude motion is important for two main reasons: First, to be able to perform an orbit maneuver using an EDT, the thrust generated by the Lorentz force must be properly directed in order to obtain the desired orbit correction. This direction is determined by the orientation of the system. Second, to minimize the potential safety risk the TSS constitutes. With a tether close to 50 km in length the risk of collision with other spacecrafts must be considered very carefully, and control of the tether motion is crucial to be able to estimate this risk.

2.1 Modeling

The model of the attitude dynamics includes two degrees of freedom (DOF), the in-plane motion and the out-of-plane motion. The model is nonlinear, underactuated, and time-periodic, and is deduced in a dimensionless formulation. The electrodynamic tether will be considered as the only actuator of the system, and the current through the tether is, therefore, the sole input of the model. The model is the basis for the work in [A,B,C]. The derivation of the model is treated in further detail in Paper C.

2.1.1   Equations of motion

The equations of motion are deduced in a Hamiltonian framework, for an assumed constant-length tether. This framework is mainly chosen, since it is based on an energy function which can be utilized during the control design. The motion is described in the orbit frame, with origin at the center of mass (CM) of the TSS. To capture the attitude motion of the system, the frame follows the orbit motion. The x-axis of the frame is placed along the position vector from the Earth to the CM, and the z-axis is perpendicular to the orbit plane. The y-axis completes the right-handed coordinate system. Figure 2.1 illustrate the
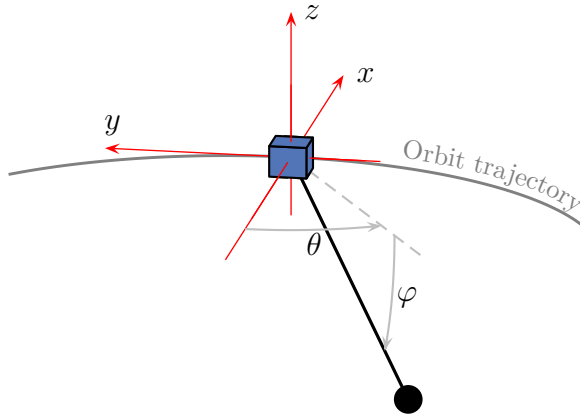
Figure 2.1: Description of a TSS in the orbit frame.

single tether system described in the orbit frame. The CM coincides with the main satellite, since this satellite is assumed the main contributor of the total mass. The orbit is assumed circular, hence the orbit velocity is aligned with the y-axis. Tether positions situated along the x-axis are denoted vertical, while tethers placed along the y-axis are horizontal. The Hamiltonian is given as,

$$H = \frac{1}{2}\left(p_\varphi^2 + \frac{(p_\theta + 1)^2}{\cos^2\varphi} - 2p_\theta - 3\cos^2\theta\cos^2\varphi\right) + 1. \tag{2.1}$$

where θ and φ are the in-plane and the out-of-plane angles, respectively, shown in Figure 2.1. The generalized momenta associated with θ and φ are denoted p_θ and p_φ. The Hamiltonian includes the kinetic energy and the gravitational potential. Furthermore, the centrifugal and the Coriolis potentials are included, since the motion is described in a rotation frame. The Hamiltonian is positive definite around the origin. The function is a dimensionless quantity, and all parameters for the formulations are collected as a gain of the input. The equations of motion

are given by Hamilton's equation,

$$\dot{\boldsymbol{q}} = \frac{\partial H}{\partial \boldsymbol{p}}, \tag{2.2a}$$

$$\dot{\boldsymbol{p}} = -\frac{\partial H}{\partial \boldsymbol{q}} + \boldsymbol{Q}, \tag{2.2b}$$

where $\boldsymbol{Q}$ is a dimensionless version of the generalized force originating from the Lorentz force. The generalized coordinates are collected in $\boldsymbol{q} = [\theta \; \varphi]^T$ and the momenta in $\boldsymbol{p} = [p_\theta \; p_\varphi]^T$, while the partial derivatives of H are defined as column vectors. The time-derivatives are taken with respect to the true anomaly ν that describes the position in the orbit. The orbit velocity is constant along the orbit, due to the circular orbit assumption, and ν is linearly increasing with time. The true anomaly is therefore easily adopted as the time-variable of the system description, and is sometimes referred to as the non-dimensional time. The use of ν as time-variable induces that the periodic variations originating from the orbit motion have a fundamental period of 2π. The level curves of the Hamiltonian are shown in Figure 2.2a in the configuration space for zero momenta. It is seen that there exist a potential well around the origin. To escape this well a dimensionless energy of $H = 1.5$ must be obtained. As seen from (2.2) the equilibria of the unforced system are placed at the stationary points of the Hamiltonian. There exist four equilibria on the sphere defined by $\boldsymbol{q}$, three of which are shown in Figure 2.2a. All four equilibria are situated in

(a) Contour plot of Hamiltonian   **(b)** Equilibria
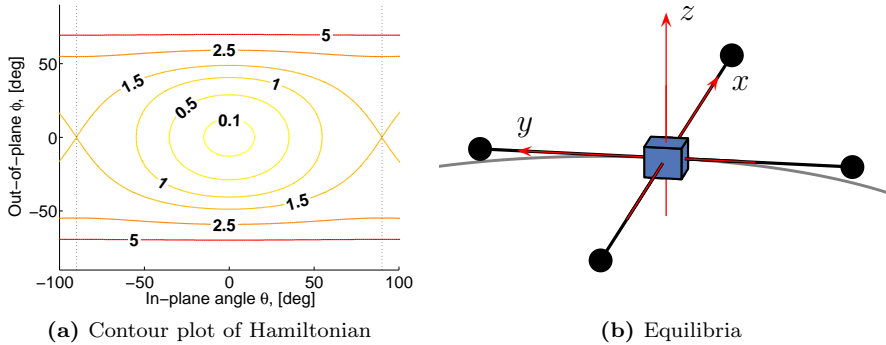
Figure 2.2: Illustrations of the open-loop equilibria.

the orbit plane, in vertical and horizontal positions as shown in Figure 2.2b. The horizontal equilibria are stable and the vertical are unstable, which is also clear from the level curves of H. The orbit frame is introduced such that the equilibrium pointing towards the Earth coincides with the origin. The choice to describe the motion around the lower instead of the upper horizontal equilibrium has only minor effect due to the symmetry of the Hamiltonian.

The main simplification of the formulation is to model the tether as a rigid rod. This assumption has the obvious advantage that flexible modes along the tether are ignored, and the attitude motion is thereby isolated. The assumption can be justified when working around a vertical equilibrium, where the gravity gradient will ensure tension along the tether. Another assumption is that the TSS follows a circular orbit. This assumption is mainly introduced to avoid the periodic disturbance originating from an elliptic orbit. The introduction of a slightly elliptic orbit would introduce a periodic motion around the equilibrium of the circular case. These periodic trajectories can be found using a perturbation method, similar to the one that will be used later to determine the periodic solution originating from the Lorentz force. The in-plane component of this motion was investigated in [67] and was found to be stable for eccentricities up to about $e = 0.3$.

2.1.2   Actuator modeling

The attitude motion is actuated by the torque originating from the Lorentz force, which can be written as,

$$\boldsymbol{F} = I\boldsymbol{r} \times \boldsymbol{B}, \tag{2.3}$$

where I is the tether current, $\boldsymbol{r}$ is a unit vector along the tether, and $\boldsymbol{B}$ the magnetic field. The cross product in (2.3) introduces some limitations in the actuation of the system. The cross product vanishes when the tether orientation is perpendicular to the magnetic field, in which case the system in unactuated. This orientation will, however, change with the orbit position, and thereby be time-varying. This phenomenon is well known when using B-dot control for the attitude motion of satellites [66], where torques around the magnetic field vector is not possible. The control problem of the electrodynamic tether becomes even more complicated, since it is underactuated when the current I constitute the only control input. The underactuated nature can be seen from the cross product in (2.3) where the magnitude of the Lorentz force can be controlled, while the direction is determined by the time-varying magnetic field and the attitude of the system.

A model of the magnetic field of the Earth is essential to the modeling of the actuator and can be done with almost arbitrary precision. The International Geomagnetic Reference Field provides a high fidelity model, based on a spherical harmonic expansion [33]. It is, however, common to simplify the modeling using a dipole model, especially when used in an analytical context. The dipole approximation can either be done as a so-called aligned dipole or tilted dipole as shown in Figure 2.3. The aligned, or non-tilted, dipole has its dipole moment along the rotational axis of the Earth, while the dipole moment of the tilted

(a) Aligned dipole   **(b)** Tilted dipole
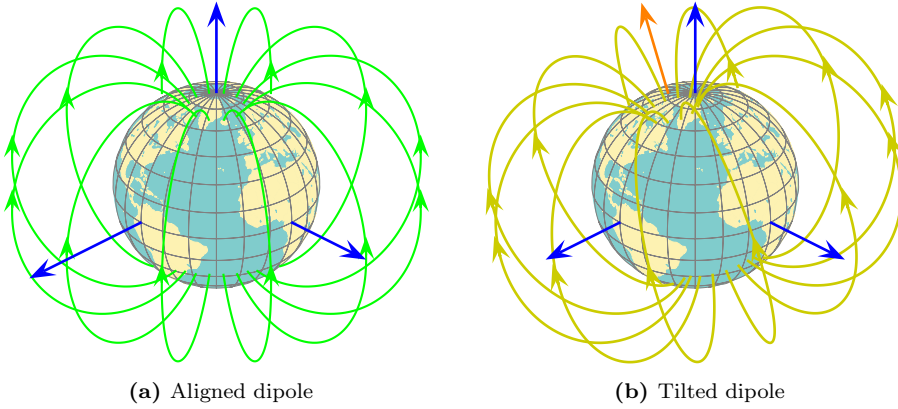
Figure 2.3: Dipole approximation of the magnetic field of the Earth.

dipole is inclined to reflect the fact that the magnetic and geographic north pole do not coincide. From a modeling point of view the advantage of the aligned dipole is that the magnetic field is symmetric around the rotational axis of the Earth, and thereby independent of the rotation of the Earth. In this work the aligned dipole model has been used to model the magnetic field. In [C] the tilted dipole have been utilized to model perturbations in the magnetic field, with the advantage that limits on these perturbations can be determined. The field from an aligned dipole model can be expressed in the orbit frame as,

$$\boldsymbol{B} = \frac{\mu_m}{R^3} \begin{bmatrix} -2\sin\nu\sin i \\ \cos\nu\sin i \\ \cos i \end{bmatrix}, \tag{2.4}$$

where i is the orbit inclination, ν the true anomaly expressing the orbit position, and R the orbit radius. The strength of the magnetic field is determined by $\mu_m \approx 7.79 \times 10^{15}$ Tm^3. As seen from (2.4) the magnetic field will be constant and perpendicular to the orbit plane in case of circular-equatorial orbit. In this case, only the in-plane motion is affected by the Lorentz force, and it is therefore a common assumption when investigating the in-plane motion separately. The periodic variation in the magnetic field, for an inclined orbit, is induced by the periodic orbit motion through the magnetic field. In case a more precise, but still static, model of the magnetic field is used, the periodic changes would be induced by the orbit motion and the rotation of the Earth, in combination. This combination will change the period of the variation, or lead to quasi periodic changes.

2.1.3   Total system description

Combining all parts of the modeling the equations of motion (2.2) can be written in the compact Hamiltonian form,

$$\dot{\boldsymbol{x}} = \boldsymbol{J}\,\frac{\partial H}{\partial \boldsymbol{x}} + \boldsymbol{g}\left(\nu, \theta, \varphi, i\right) u, \tag{2.5}$$

where u is a dimensionless input proportional to the tether current and $\boldsymbol{x} = [\theta\ \varphi\ p_\theta\ p_\varphi]^T$ is the state vector. The matrix $\boldsymbol{J}$ is given as,

$$\boldsymbol{J} = \begin{bmatrix} \boldsymbol{0} & \boldsymbol{I}_{2\times 2} \\ -\boldsymbol{I}_{2\times 2} & \boldsymbol{0} \end{bmatrix} \tag{2.6}$$

with $\boldsymbol{I}_{2\times 2}$ being a 2×2 identity matrix. The system is actuated through the input function $\boldsymbol{g}$, which is 2π periodic in time ν. The function also depends on the generalized coordinates and the orbit inclination i.

2.1.4   Open-loop periodic solutions

When using a constant tether current $u \neq 0$ the input function acts as a time-periodic forcing term, which will give rise to families of periodic solutions. This constant input term can be seen as a bias term for the system. Such a family was investigated by Peláez et al. [47]. The solutions were approximated by power series for small inputs, using a perturbation method treated in the next section. A stability analysis showed that the solutions were unstable, although the instability evolved quite slowly. The solutions were characterized as weakly unstable up to a certain limit u^*, since the larges characteristic multiplier was placed on the unit circle for $u < u^*$, when analysing a linear approximation of the dynamics. An eight order series approximation of the periodic solutions are shown in Figure 2.4 for some constant values of u. The series is only valid for small u, and the deviation from the real solutions increase with u due to the finite number of terms. The real solutions are, however, hard to simulate due to their unstable nature.

2.1.5   Perturbation theory

The input current affecting the system can be seen as a small quantity perturbing the system behavior. For this reason perturbation theory is a useful tool when analyzing the EDT system. The purpose of perturbation theory is to approximate a solution of a perturbed equation, based on a know solution
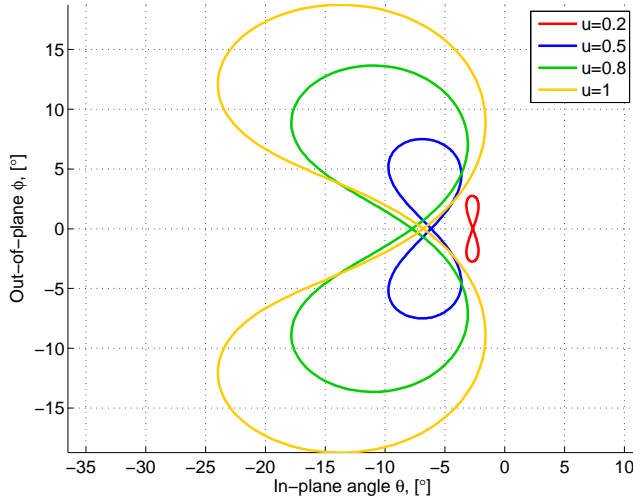
Figure 2.4: Periodic open-loop solutions for different bias values.

of the unperturbed equation. The theory can be applied both to algebraic and differential equations. The main idea is to expand the quantities of the equation in power series in the small perturbation quantity ε. Inserting these series, the equation can be divided into an equation for each power of ε. In case of a linear system,

$$\dot{\boldsymbol{x}}(t) = \boldsymbol{A}(t, \varepsilon)\boldsymbol{x}(t), \tag{2.7}$$

the state and the system matrix are written as,

$$\boldsymbol{x}(t) = \boldsymbol{x}_0(t) + \varepsilon\boldsymbol{x}_1(t) + \cdots = \sum_{n=0}^{N} \varepsilon^n \boldsymbol{x}_n(t), \tag{2.8}$$

$$\boldsymbol{A}(t) = \boldsymbol{A}_0(t) + \varepsilon\boldsymbol{A}_1(t) + \cdots = \sum_{n=0}^{N} \varepsilon^n \boldsymbol{A}_n(t). \tag{2.9}$$

Inserting these series the system equation (2.7) can be divided into,

$$\varepsilon^0: \quad \dot{\boldsymbol{x}}_0(t) = \boldsymbol{A}_0(t)\boldsymbol{x}_0(t), \tag{2.10a}$$

$$\varepsilon^1: \quad \dot{\boldsymbol{x}}_1(t) = \boldsymbol{A}_0(t)\boldsymbol{x}_1(t) + \boldsymbol{A}_1(t)\boldsymbol{x}_0(t), \tag{2.10b}$$

$$\varepsilon^2: \quad \ldots$$

where the first equation corresponds to the unperturbed system ($\varepsilon = 0$). The equations can be solved in an iterative matter, where the solutions of the preceding equations act as forcing terms for the current equation. In this way

the solution (2.8) is expanded with one power for each equation. The systematic way of approximating a solution make perturbation methods well suited for implementation using symbolic math software. One problem when using perturbation theory is the radius of convergence of the approximated solution, which can be hand to establish. When using a perturbation theory to find periodic solutions of a differential equation, as in the case of the open-loop system, Poincaré-Lindstedt method can be applied [16]. The idea is to chose the integrations constants in the solution of (2.10) to avoid so-called secular terms, i.e. terms which are unbounded.

In Paper B the Poincaré-Lindstedt meehod is used to approximate a familty of stable closed-loop periodic solutions. Since the control algorithm includes two parameters the methods is expanded to include two perturbation quantities. In Paper C the stability of the closed-loop periodic solutions is investigated, by approximating the characteristic multipliers using a perturbation method [54, 55].

2.2   Control strategies

The underactuated nature of the system introduces some challenges with respect to the control design, actually it prevents the creation and thereby the stabilization, of an equilibrium point in state space. It is therefore a common strategy to stabilize the attitude motion in a periodic trajectory. The zeros in the input function also introduce some difficulties when classical control methods are used. Furthermore, the time-periodic nature of the system caused the need for Floquet analysis to evaluate the stability properties of the system. Paper [A] stabilizes the open-loop equilibria using a passivity-based control law. The stabilization of periodic solutions is investigated in [B] and [C] also using a passivity-based method.

2.2.1   Passivity-based control

The motivation for using a passivity-based control approach is the existence of zeros in the input function of the model (2.5). These zeros give problems for many classical methods, for example all the methods investigated in [29]. The problem is that the system, or a part of the system, is unactuated when a zero occurs. The way most classical approaches, like feedback linearization, handles variations in the input function is to divide with a similar quantity which cancel out these variations. This strategy can, however, introduce singularities in the

control law if a change of sign occurs in the input function. To avoid these singularities one could, switch to alternative controllers when the system state is in the proximity of such a singularity. This was done for the TSS in [68]. The use of a passivity-based method can, however, offer a more elegant solution. Another reason for investigating passivity-based approaches for the system is that the equations of motion are given using an energy based formulation. In this case we can utilize the energy function of the system as a storage function in the passivity formulation. The energy function provide a single value function which encapsulate the system behavior, both regarding stationary and dynamical properties. for this reason an energy-based approach can be advantageous especially when dealing with complex systems [40].

The basis for the passivity-based control investigated during this project is the port-controlled Hamiltonian (PCH) formulation [41, 52]. The port-controlled Hamiltonian formulation offers directly an energy based method to model physical systems, considering the energy flow between system components, dissipation, and energy supplied through input signals. The classical Hamiltonian formulation is expanded to include damping and an output. In the following, this will be presented for a general system with state vector $\boldsymbol{x} \in \mathbb{R}^n$, input $\boldsymbol{u} \in \mathbb{R}^m$, and output $\boldsymbol{y} \in \mathbb{R}^m$,

$$\dot{\boldsymbol{x}} = (\mathcal{J}(t, \boldsymbol{x}) - \mathcal{R}(t, \boldsymbol{x})) \ \frac{\partial \mathcal{H}(t, \boldsymbol{x})}{\partial \boldsymbol{x}} + \mathcal{G}(t, \boldsymbol{x}) \, \boldsymbol{u}, \qquad (2.11)$$

$$\boldsymbol{y} = \mathcal{G}^T(t, \boldsymbol{x}) \frac{\partial \mathcal{H}(t, \boldsymbol{x})}{\partial \boldsymbol{x}}. \qquad (2.12)$$

In this general formulation the damping matrix $\mathcal{R} \in \mathbb{R}^{n \times n}$ is positive semi-definite $\mathcal{R} \geq 0$. The matrix $\mathcal{J} \in \mathbb{R}^{n \times n}$ is called the interconnection matrix and fulfills $\mathcal{J} = -\mathcal{J}^T$. Both matrices can be both time and state dependent, which is also the case for the Hamiltonian $\mathcal{H} \in \mathbb{R}$. The formulations offers a passive input-output connection in case the Hamiltonian H is bounded from below.

The description of the attitude dynamics (2.5) can be put into the port-controlled Hamiltonian form, by creating the artificial one-dimensional output,

$$y = \boldsymbol{g}^T(\nu, \theta, \varphi, i) \frac{\partial H}{\partial \boldsymbol{x}}. \qquad (2.13)$$

The output is characterized as artificial since it is not a quantity which can be directly measured from the system. The output is formed by an assumed complete state measurement, together with knowledge of the orbit position ν.

2.2.2 Time-periodic systems

The TSS is described by a time-periodic system equation, the solutions of which can be investigated using Floquet theory [16]. Floquet theory deals with the solutions of linear systems with time-periodic system matrices,

$$\dot{\boldsymbol{x}} = \boldsymbol{A}(t)\boldsymbol{x}, \tag{2.14}$$

where $\boldsymbol{A}(t) = \boldsymbol{A}(t+T)$ and T is the period. One of the main results, regarding stability of the solution of (2.14), is the following relation between the fundamental matrices $\boldsymbol{\Phi}(t)$ and $\boldsymbol{\Phi}(t+T)$,

$$\boldsymbol{\Phi}(t+T) = \boldsymbol{\Phi}(t)\boldsymbol{M}. \tag{2.15}$$

The matrix $\boldsymbol{M}$ is time-invariant and is called the monodromy matrix. The stability of (2.14) can be investigated by considering the eigenvalues of $\boldsymbol{M}$, which are called the characteristic multipliers of the system. The stability properties of the system can be summarized as (see [61]):

- The system is unstable if one multiplier is placed outside the unit circle.

- The system is asymptotically stable if all multipliers are situated inside the unit circle.

- The system is stable if non of the multipliers are placed outside the unit circle and if the multipliers on the unit circle have multiplicity one.

Unfortunately, there is no general analytically method for finding the monodromy matrix. A numerically solution is based on the fact that the fundamental matrix fulfills (2.14),

$$\dot{\boldsymbol{\Phi}} = \boldsymbol{A}(t)\boldsymbol{\Phi}. \tag{2.16}$$

Solving this system numerically with an initial condition of an identity matrix $\boldsymbol{\Phi}(0) = \boldsymbol{I}$, it is seen from (2.15) that the monodromy matrix can be found as $\boldsymbol{M} = \boldsymbol{\Phi}(T)$.

The stability of periodic solutions can be found by investigating the variational equation, which is a dynamical equation for the deviation from the periodic solution. This equation will be time-periodic, both in the case where a periodic solution of an autonomous system is considered and in the case where the periodic solution is enforced. Using the linear system,

$$\dot{\boldsymbol{x}} = \boldsymbol{A}(t)\boldsymbol{x} + \boldsymbol{b}(t) \tag{2.17}$$

as an example on the latter case, the deviation from the periodic solution $\boldsymbol{x}_p$ can be written as $\boldsymbol{\eta} = \boldsymbol{x} - \boldsymbol{x}_p$. Since both $\boldsymbol{x}$ and $\boldsymbol{x}_p$ are solutions of (2.17) the linear system describing $\boldsymbol{\eta}$ can be found as,

$$\dot{\boldsymbol{\eta}} = \boldsymbol{A}(t)\boldsymbol{\eta}, \tag{2.18}$$

which can be investigated using Floquet theory.

2.3   Summary of papers

Paper A, *Control by damping injection of electrodynamic tether system in an inclined orbit.* This paper treats the special case where the open-loop equilibrium of the TSS is stabilized. The work is based on the port-controlled Hamiltonian formulation (2.5) and uses the passive input-output connection introduced in (2.13).

The control strategy simply connects the output to the input, using a negative proportional gain. A prerequisite for this control strategy is that the system is zero state detectable. To investigate if this is the case the zeros of the input function are analyzed, since the input function is an important part of the output, in the port-controlled Hamiltonian formulation. It is concluded that both time, states, and orbit inclination induces zeros in the input function. The zeros induced by time do not affect the zero state detectability, since they are countable. The same conclusion is drawn regarding the zeros induced by the states, based on the argumentation that the open-loop equilibrium is the only equilibrium in the region of interest. The orbit inclination only induced zeros for equatorial and polar orbits, these zeros will, however, prevent zero state detectability and the control strategy would fail in these special cases. The closed-loop system can be written as a Hamiltonian system with damping. Seen in a PCH context the control strategy adds a damping matrix to the open-loop formulation, hence the term damping injection is used to characterize the strategy. Both the interconnection matrix and the Hamiltonian of the system are unchanged by the feedback controller. The unchanged Hamiltonian shows that the location of the equilibria of the system are unaffected by the controller, hence only their stability properties are changed.

The performance of the controller is investigated by finding the characteristic multipliers of the system. It is shown that there exists a finite controller gain, which minimize the absolute value of the largest multiplier, and thereby leads to the fastest convergence. The paper also includes some simulations of the closed-loop system. The special cases of equatorial and polar orbits are briefly treated, and it is shown that the stabilization fails in these case, due to unactuated out-of-plane and in-plane dynamics.

Paper B, *Stabilization of periodic solutions in a tethered satellite system by damping injection.* This paper investigates stabilization of the open-loop periodic solutions of the TSS. The stabilizing control law is an expansion of the one introduced in [A], and based on the same model. The control law is expanded by a bias term, which drives the system trajectory away from the open-loop equilibrium stabilized in [A].

The motivation for the control law is found by considering the perturbation method used to approximate the open-loop periodic solution. These are found by perturbing the unforced system with a constant current, and in that way drive the system trajectory away from the marginally stable equilibrium at the origin. The periodic solutions can be seen as evolving from this equilibrium, when the constant current is added. The periodic solutions are weakly unstable, i.e. marginally stable in a linear approximation, for small currents, and it is observed that the change in stability during the evolution of the periodic solutions only occur due to nonlinearities. One could expect that there is a connection between the stability of the equilibrium the periodic solutions originate from, and the stability of the solutions themself. This assumed connection is the motivation behind the proposed control law.

Using Floquet theory, it is shown that the control law actually creates a family of periodic solutions, which are asymptotically stable for some combinations of control parameters. The magnitude of the stability deciding multiplier, i.e. the numerically largest of the characteristic multipliers, are found in this parameter plane to establish a region in which stable solutions exist. The shape of the solutions is found using a perturbation method and through simulations. The solutions are symmetric which is a property induced by the symmetry of the dipole used to model the magnetic field. The investigation is concluded with simulations, comparing the convergence of the system, with the characteristic multipliers.

Paper C, *Passivity-based control of a rigid electrodynamic tether.* This paper expands the investigation of the control laws introduced in [A] and [B].

The investigation of the control law, which stabilize the open-loop equilibrium, is expanded by an analysis of the region of attraction (ROA) of the controller. Using the fact that equilibrium positions have not been changed by the controller and that the energy level is guaranteed not to increase, a ROA is stated based on the Hamiltonian. Furthermore, a ROA based on simulations is found. An additional analysis of the energy flow is also presented, based on the eigenvalues of the damping matrix and simulations. The analysis focuses on the limitation of the energy flow and the conditions to be fulfilled for the energy to flow out of the system. These conditions are connected to the zeros of the input functions. Using simulations, it is investigated how the energy flow is affected by perturbation in the magnetic field, or rather a mismatch between real field and the model used in the control algorithm. The mismatch is introduced by using a non-tilted and a tilted dipole, respectively, in the control algorithm and the system model

In connection with stabilization of periodic solutions the work is expanded with an argument that a stabilization of an equilibrium point is not possible, when only controlling the tether current, except in some special cases as for example the open-loop equilibria. The argument is based on the feasibility of finding a input signal that creates such general equilibrium points. The investigation of the approximations of the periodic solutions is expanded with an analysis of the accuracy of the approximations based on simulations of the nonlinear closed-loop system. The stabilization of the periodic solutions is briefly investigated when using a perturbed magnetic field. It is seen that, since the control uses no information about the solution to stabilize, the solutions are governed by the magnetic field and its periodic changes. It is demonstrated that the controller can still stabilize a set of perturbed periodic solutions.

Tethered Satellite Formations

The research in the area of tethered satellite formations has mainly focused on modeling the attitude motion of the system. The main objective is to obtain a model describing several formation structures. This is achieved by using a graph theoretical description of the formation, from which the Lagrangian of the system is formulated. From the Lagrangian the equations of motion are found using Lagrange's equation. The modeling is treated in detail in Paper D. Another objective is to investigate the use of electrodynamic tethers in connection with formation control. To maintain the generic structure of the system description, the modeling of the electrical circuit formed by the tethers is also based on graph theory. The control of the generic formation is treated in Paper E with the focus on obtaining a generic and decentralized control algorithm. The control law is limited to consider the in-plane motion of the system. This limitation is introduced to avoid an underactuated system, like the single tether system.

3.1 Modeling

The modeling of tethered satellite formations aim to provide a model of the basic dynamics of the formations, hence point masses are used to model the satellites and the tethers are modeled as constant-length rigid rods. The motion is described around the center of mass, which is assumed to follow a circular orbit. The formations are modeled as a static formation, where the equilibrium

positions are induced by the gravity gradient. The tethers are connected to the satellites such that they can move on a sphere, i.e. the connections of the tethers are modelled as spherical joints. The main assumption of the modeled formations, is that they form tree structures. A tree structure is a structure not containing cycles. This limitation simplifies the deduction of the equations of motion since each tether can move freely around its connection point and the degrees of freedom (DOF) of the model will be solely determined by the number of tethers. Each tether will represent two DOF in the general case, and one DOF in the case where only the in-plane motion is considered. In case cycles were present in the formation, the equations of motion should be found taking the algebraic constraint around each loop into account. These constraints are basically describing that the net distance around a cycle must be zero. Seen from a graph theoretical point of view the tree structure has the advantage that the path along the tethers between two arbitrary satellites is unique. This is utilized in the modeling.

3.1.1 Graph theory

Graph theory is a branch of mathematics used heavily in engineering and computer science, and has found many different applications [6, 14]. In connection with control theory it is often used to describe communication structures e.g. in connection with multi-agent systems. The motivation of using graph theory in connection with tethered satellite formations, is to describe the dynamics of different formations using the same framework. Furthermore, there is a great resemblance between a tethered formation and a graph. The satellites and tethers can easily be seen as the nodes and edges in a corresponding graph, and it is natural to utilize the mathematical formulation and theorems offered by graph theory in the description and the modeling process of the formations. In this work it has been advantageous to use directed graphs in the description.

A graph consists of a set of nodes or vertices v_i for $i = 1, \ldots, n$ and a set of edges e_j for $j = 1, \ldots, m$. Each edge connects two and only two nodes. In case a direction is associated with each edge, the graph is called a directed graph and in this case initial and terminal nodes are introduced such that an edge e_j is directed from its initial to its terminal node. The topology of the graph can be described by the incidence matrix $\boldsymbol{B} \in \mathbb{R}^{n \times n}$, with the elements B_{ij} defined as,

$$B_{ij} = \begin{cases} 1 & \text{if } v_i \text{ is the initial node of } e_j \\ -1 & \text{if } v_i \text{ is the terminal node of } e_j \\ 0 & \text{if } e_j \text{ is not incident with } v_i \end{cases} \quad (3.1)$$

The rank of the incidence matrix is $r = n - c$, where c is the number of disjoint

components, i.e. groups of nodes and edges, in the graph. The number r is also referred to as the rank of the graph. The nullity of $\boldsymbol{B}$ is $b = m - r$, which is also the nullity of the graph. A path in a graph can be seen as an ordered set of successive edges connecting two nodes, and the path can be assigned a direction according to the ordering. The direction of the path does not necessarily agree with the direction of the edges along the path, hence an edge can be included in a path either along or opposite the direction of the path. A cycle in a graph is a path of distinct edges from a node back to the same node. Like a path, a cycle is assigned an orientation, and the edges can again be included along or opposite the orientation of the cycle. The number of independent cycles in a graph is determined by the nullity of the graph.

A connected graph without any cycles is called a tree or a directed tree in case of a directed graph. The special case of a graph describing a tree structure has been heavily used in this work, hence some of the properties of such a structure will be mentioned here. The connection between the number of nodes and edges in a tree structure is given as $n = m + 1$, since a tree structure is assumed to be connected. Consequently the rank of a tree is $r = m$ and the nullity is $b = 0$, which is in agreement with the assumed lack of cycles. A rooted tree is a tree where there exist one and only one node not being the initial node of any edges. This node is called the root of the tree. In case the direction of the edges can be chosen freely, all nodes can constitute the root for a certain choice of directions. A path between two nodes is unique in a tree structure. The path from the nodes v_i for $i = 1, \ldots, m$ to the node v_{m+1} can be described by a single matrix quantity $\boldsymbol{P} \in \mathbb{R}^{m \times m}$ called the path matrix. This path is described by the elements P_{ji} defined as,

$$
P_{ji} = \begin{cases} 1 & \text{if } e_j \text{ is included along the direction of the path} \\ -1 & \text{if } e_j \text{ is included opposite the direction of the path} \\ 0 & \text{if } e_j \text{ is not included in the path} \end{cases} \tag{3.2}
$$

The path matrix can be found with respect to an arbitrary node in the tree, which is obvious since no specific ordering on the nodes is given. There is a simple relation between the path matrix and the incidence matrix $\boldsymbol{B}$. Consider the incidence matrix where row k is omitted. This matrix $\boldsymbol{A} \in \mathbb{R}^{m \times m}$ called the reduced incidence matrix is square due to the tree structure and has full rank. The path matrix $\boldsymbol{P}$ with respect to the node v_k can be written from the reduced incidence matrix $\boldsymbol{A}$ with respect to the same node,

$$
\boldsymbol{P} = \boldsymbol{A}^{-1}. \tag{3.3}
$$

3.1.2   Circuit theory

Besides using graph theory describing the formation structure, it is also applied to describe the equivalent electrical circuit, formed by the electrodynamic tethers. The basis for such description is briefly treated here, for circuits containing only impedances and voltage sources. Further treatment is given in [6, Chap. 2]. In Paper E the framework is used for networks only containing resistances and voltage sources, but expanded to consider nonlinear current-voltage relations.

The main idea in the modeling is to use a graph describing the interconnection of electric elements. The nodes of the graph represents the junctions in the electrical network and the edges represents the branches. The currents along the branches are collected in a vector $\boldsymbol{i} \in \mathbb{R}^m$ and are defined positive in the direction of the edge representing the branch. The potential differences along the branches are defined positive between the initial and the terminal node of the edges representing the branch. This means that a positive current along a resistor, will give rise to a positive voltage difference over the same resistor. These potentials are collected in the vector $\boldsymbol{v} \in \mathbb{R}^m$. The impedances are collected in the diagonal matrix $\boldsymbol{Z} \in \mathbb{R}^{m \times m}$.

To be able to formulate Kirchhoff's voltage law a description of the loops in the network is needed. The loops of the electrical network equals the cycles of the graph. These cycles are described by the matrix $\boldsymbol{Q}$ introduced with elements Q_{kj},

$$
Q_{kj} = \begin{cases} 1 & \text{if } e_j \text{ is included in the cycle } k \text{ along the orientation of the cycle} \\ -1 & \text{if } e_j \text{ is included in the cycle } k \text{ opposite the orientation of the cycle} \\ 0 & \text{if } e_j \text{ is not included in cycle } k \end{cases}
$$

$$(3.4)$$

A complete set of the linear independent cycles $\boldsymbol{Q} \in \mathbb{R}^{b \times m}$ can be found as the null space of the incidence matrix,

$$\boldsymbol{B}\boldsymbol{Q}^T = \boldsymbol{0}_{n \times b}. \tag{3.5}$$

Using the graph theoretical quantities, Kirchhoff's current and voltage law can be written as,

$$\boldsymbol{B}\boldsymbol{i} = \boldsymbol{0}, \tag{3.6a}$$
$$\boldsymbol{Q}\boldsymbol{v} = \boldsymbol{0}. \tag{3.6b}$$

Furthermore, the potential differences along the branches can be written using Ohm's law,

$$\boldsymbol{v} = \boldsymbol{Z}\boldsymbol{i} + \boldsymbol{u}, \tag{3.7}$$

where $\boldsymbol{u}$ is a vector of voltage sources along the branches. If there does not exist a source along a branch the corresponding element of $\boldsymbol{u}$ vanishes. The current along a branch can be seen as consisting of a current for each loop in which the branch is included. This can be written as,

$$\boldsymbol{i} = \boldsymbol{Q}^T \boldsymbol{i}_m, \tag{3.8}$$

where $\boldsymbol{i}_m \in \mathbb{R}^b$ is the loop currents. If a branch is only included in a single loop, the loop current equals the current along the branch with sign determined by the way the branch is included in the loop. Inserting this into (3.7), multiplying from the left by $\boldsymbol{Q}$, and using (3.6b) leads to the equation,

$$\boldsymbol{Z}_m \boldsymbol{i}_m = \boldsymbol{u}_m, \tag{3.9}$$

where $\boldsymbol{Z}_m = \boldsymbol{Q}\boldsymbol{Z}\boldsymbol{Q}^T$ is the loop impedance and $\boldsymbol{u}_m = -\boldsymbol{Q}\boldsymbol{u}$ is the loop voltage sources. This formulation is called the loop system formulation, since it is based on the voltage differences around each loop in the network.

3.2 Summary of papers

Paper D, *Modeling of tethered satellite formations using graph theory.* This paper investigates the unforced dynamics of the considered tethered satellite formations. The derivation of the dynamics is based on the path matrix (3.2) from which the positions and velocities of all the masses in the formation, relative to the CM, can be written. Using the positions and velocities, the Lagrangian can be written, including the kinetic energy and orbital energy. Since the system is described in the moving orbit frame, the centrifugal and Coriolis potentials are also included. From the Lagrangian the equations of motion can be found using Lagrange's equation, and the total system description is written in a matrix formulation. An notable feature of the formulation is that all parameters and the description of the formation structure are collected in a single matrix. The derivation is treated in detail for the in-plane dynamics, while the equations of motion for the combined in-plane and out-of-plane dynamics are stated in the appendix. The derivations goes along the same steps, and only the degrees of freedom and the complexity differ in the two cases.

Based on the equations of motion the stationary configurations situated in the orbit plane are investigated. The configurations are found from a chosen set, containing rods fixed in a vertical position, i.e. parallel to the gravity force. Based on this set, a new graph is formed where the edges corresponding to the vertically fixed rods are removed. By considering this new graph the equilibrium position of the non-vertical rods can be determined. It is found that only the

neighboring rods of the vertically fixed rod can have an inclined equilibrium position, all remaining rods will have a horizontal equilibrium position. An upper limit on the number of possible stationary configurations is found, based on the number of different ways the set of vertical rods can be chosen.

Paper E, *Decentralized control of tethered satellite formations using electro-dynamic tethers.* In this paper the use of electrodynamic tethers to actuate a tethered satellite formation is proposed. To avoid an underactuated system the investigation is limited to the in-plane motion. The paper expand the model from [D] with a model of the electrodynamic forces occurring when currents are lead through the tethers and interacts with the magnetic field. These currents are controlled using adjustable voltage sources situated at the satellites, and the modeling is based on an equivalent circuit described by graph theoretical quantities. Due to the use of graph theory the generic structure of the dynamical model is maintained when modeling the electrical circuit. The circuit is closed through phantom loops in the ionosphere, meaning that the satellites are capable of exchanging electrons with the ionosphere. These connections to the ionosphere are modeled by equivalent resistances with nonlinear current-voltage characteristics. The graph describing the circuit is a minor expansion of the structure graph, since the resistance of the ionosphere can be ignored. Consequently, the graph is expanded by a single node, such that the satellites and the ionosphere constitute the junctions of the circuit.

The second part of the paper treats a decentralized control design for the system. The control strategy is decentralized in the sense that each satellite applies the control action based on local observations. The control law is found in two steps. The first step stabilizes the tether currents at a desired level using the voltage sources, and it is shown that the currents will converge asymptotically towards this level. The second step is a linear feedback control law for the attitude motion. The feedback gains are subject to some constraints, to ensure that the control algorithm can be implemented in a decentralized way. Both parts of the control law are based on the graph description of the system, hence the resulting control strategy is generic for all formations included in the model description. In particular the incidence matrix is used to transfer measurements connected with the tethers to quantities associated with the satellites where the control actions are applied. The paper is concluded by an example illustrating the controller operating the system around one of the stationary configurations found in [D].

Conclusions and perspectives

This thesis have investigated the use of electrodynamic tethers in connection with space missions. The emphasis has been on the modeling and control of the attitude motion of such systems. The thesis considered single tether systems and tethered satellite formations.

The control problem of a single tether system focused on the general case of an inclined orbit. In this case the system was actuated through a time-periodic input function. For this case the thesis described the system using an energy function and utilized a passivity-based control strategy, first for stabilizing the open-loop equilibrium, and second, for stabilizing periodic trajectories of the system. The energy-based approach was shown to be advantageous in connection with handling the time-varying nature of the system, and for providing an energy function which made basis for investigations of stability and regions of attraction of the closed-loop system. The passivity-based control approach was treated in the Papers A, B, and C.

The main objective of the work regarding tethered satellite formations was to create a framework where several formation structures could be handled collectively. This objective was reached by describing the topology of the formations using graph theory, and utilizing this description in both the modeling and the control design. The formations under consideration was limited to tree structures, and the satellites and tethers were modeled as point masses and massless rods, respectively. The low level of detail made the model manageable and suitable for investigating basic properties, like natural frequencies and stationary

configurations of the system. The model of the attitude motion was derived in Paper D and the stationary configurations situated in the orbit plane were found. In Paper E the use of electrodynamic tethers for actuating the attitude motion was investigated, and a decentralized control design was developed based on the graph theoretical description of the system. The actuation of the system was based on an equivalent electric circuit of the network formed by the electrodynamic tethers. The design was able to stabilize the tethered formation and handle nonlinearities in the equivalent resistance between plasma and electron collectors/emitters of the system.

The main contribution of this thesis in the area of single tether system, was the passivity-based approach to the control problem. This enabled a stabilization of the open-loop equilibrium and a stabilization of periodic solution without any reference or delayed feedback signals. In the area of tethered satellite formations the main contributions were the use of graph theory to describe the formations and the introduction of electrodynamic tethers for formation control.

There are several directions where the work presented in this thesis could be expanded. The use of electrodynamic tethers will lead to changes in the orbit of the system. These changes need to be explored when using the attitude control strategy developed in this thesis. This is important both when using EDT's for orbit corrections and when using them to control the attitude motion. The use of electrodynamic tethers as the sole control device of a spacecraft, introduce some problems due to the limitations in the magnitude and direction of the control action. The use of additional actuators in combination with electrodynamic tethers are therefore an interesting research topic. Flexibility of the tethers could also be taken into account and the first step would be to investigate and further develop the control strategies to ensure that the tethers are in tension.

Seen in a larger perspective, the physical electrodynamic tether technology also need further evolution. First of all additional missions are needed to obtain more knowledge of the fundamental dynamical and electrical properties of the system when in space. The exchange of electrons with the ionosphere need to be further enhanced, in order to increase the collection of electrons to obtain higher electric currents. This could potentially lead to the use of shorter tethers, resulting in a reduced collision risk.

Bibliography

[1] J. Ballance and L. Johnson. Propulsive Small Expendable Deployer System (ProSEDS). In M. S. El-Genk, editor, *Space Technology and Applications International Forum*, volume 552 of *AIP Conference Proceedings*, pages 419–424. American Institute of Physics, 2001. ISBN 1-56396-980-7.

[2] V. V. Beletsky and E. M. Levin. *Dynamics of space tether systems*, volume 83 of *Advances in the astronautical sciences*. American Astronautical society, 1993.

[3] C. Bombardelli, E. C. Lorenzini, and M. B. Quadrelli. Retargeting dynamics of a linear tethered interferometer. *Journal of Guidance, Control, and Dynamics*, 27(6):1061–1067, nov-dec 2004. ISSN 0731-5090.

[4] M. P. Cartmell and D. J. McKenzie. A review of space tether research. *Progress in Aerospace Sciences*, 44(1):1–21, 2008. ISSN 0376-0421. doi: 10.1016/j.paerosci.2007.08.002.

[5] A. Celletti and V. Sidorenko. Some properties of the dumbbell satellite attitude dynamics. *Celestial Mechanics & Dynamical Astronomy*, 101(1-2):105–126, MAY 2008. ISSN 0923-2958. doi: 10.1007/s10569-008-9122-0.

[6] W. K. Chen. *Graph theory and its engineering applications*, volume 5 of *Advanced Series in Electrical and Computer Engineering*. World Scientific, 1996. ISBN 980-02-1859-1.

[7] S.-J. Chung and D. W. Miller. Propellant-free control of tethered formation flight, part 1: Linear control and experimentation. *Journal of Guidance, Control, and Dynamics*, 31(3):571–584, may-jun 2008. ISSN 0731-5090.

[8] S.-J. Chung, J.-J. E. Slotine, and D. W. Miller. Propellant-free control of tethered formation flight, part 2: Nonlinear underactuated control. *Journal of Guidance, Control, and Dynamics*, 31(5):1437–1446, sep-oct 2008. ISSN 0731-5090. doi: 10.2514/1.32189.

[9] J. Corsi and L. Iess. Stability and control of electrodynamic tethers for de-orbiting applications. *Acta Astronautica*, 48(5-12):491–501, 2001. ISSN 0094-5765.

[10] M. L. Cosmo and E. C. Lorenzini, editors. *Tethers in space handbook*. NASA Marshall Space Flight Center, 3rd edition, 1997.

[11] A. B. DeCou. Attitude and Tether Vibration Control in Spinning Tethered Triangles for Orbiting Interferometry. *Journal of the Astronautical Sciences*, 41(3):373–398, jul-sep 1993. ISSN 0021-9142.

[12] F. Dignath and W. Schiehlen. Control of the vibrations of a tethered satellite system. *Journal of Applied Mathematics and Mechanics*, 64(5): 715–722, 2000. ISSN 0021-8928.

[13] R. L. Forward, R. P. Hoyt, and C. W. Uphoff. Terminator Tether (TM): A spacecraft deorbit device. *Journal of Spacecraft And Rockets*, 37(2):187–196, mar-apr 2000. ISSN 0022-4650.

[14] L. R. Foulds. *Graph Theory Applications*. Universitext. Springer-Verlag, 1992. ISBN 3-540-97599-3.

[15] K. R. Fuhrhop, G. B. E., S. G. Bilén, and N. Voronka. System analysis of the expected electrodynamic tether performance for the proseds mission. In *39th AIAA/ASME/ASEE Joint Propulsion Conference*, Huntsville, AL, 20-23 July 2003. AIAA-2003-5096.

[16] R. Grimshaw. *Nonlinear Ordinary Differential Equations*. Blackwell Scientific Publications, 1990.

[17] A. Guerman. Spatial equilibria of multibody chain in a circular orbit. *Acta Astronautica*, 58(1):1–14, jan 2006. ISSN 0094-5765. doi: 10.1016/j. actaastro.2005.05.002.

[18] A. D. Guerman. Equilibria of multibody chain in orbit plane. *Journal of Guidance, Control, and Dynamics*, 26(6):942–948, nov-dec 2003. ISSN 0731-5090.

[19] R. P. Hoyt. Stabilization of electrodynamic space tethers. Technical report, Tethers Unlimited, Inc., 2001.

[20] L. Iess, C. Bruno, C. Ulivieri, U. Ponzi, M. Parisse, G. Laneve, M. Dobrowolny, F. De Venuto, B. Bertotti, L. Anselmo, and G. Vannaroni. Satellite de-orbiting by means of electrodynamic tethers part I: General concepts and requirements. *Acta Astronautica*, 50(7):399–406, 2002. ISSN 0094-5765.

[21] L. Iess, C. Bruno, C. Ulivieri, and G. Vannaroni. Satellite de-orbiting by means of electrodynamic tethers - part II: System configuration and performance. *Acta Astronautica*, 50(7):407–416, apr 2002. ISSN 0094-5765.

[22] L. Johnson and M. Herrmann. Internation space station electrodynamic tether reboost study. Technical memorandum NASA/TM-1998-208538, NASA, Mashall Space Flight Center, July 1998.

[23] I. Katz, J. R. Lilley Jr., A. Greb, J. E. McCoy, J. Galofaro, and D. C. Ferguson. Plasma turbulence enhanced current collection: Results from the plasma motor generator electrodynamic tether flight. *Journal Of Geophysical Research-Space Physics*, 100(A2):1687–1690, feb 1995. ISSN 0148-0227.

[24] S. Kawamoto, T. Makida, F. Sasaki, Y. Okawa, and S. Nishida. Precise numerical simulations of electrodynamic tethers for an active debris removal system. *Acta Astronautica*, 59(1-5):139–148, jul-sep 2006. ISSN 0094-5765. doi: 10.1016/j.actaastro.2006.02.035. 56th Congress of the International-Astronautical-Federation, Fukuoka, Japan, oct 17-21, 2005.

[25] M. Keshmiri, A. K. Misra, and V. J. Modi. General formulation for n-body tethered satellite system dynamics. *Journal of Guidance, Control, and Dynamics*, 19(1):75–83, jan-feb 1996. ISSN 0731-5090.

[26] M. Kruijff and M. Stelzer. YES2 post flight analysis summary. Technical Report TN0113, ESA, 2007. URL `http://www.yes2.info/files/TN0113v2.pdf`.

[27] K. D. Kumar. Review of dynamics and control of nonelectrodynamic tethered satellite systems. *Journal of Spacecraft and Rockets*, 43(4):705–720, 2006. ISSN 0022-4650.

[28] E. L. M. Lanoix, A. K. Misra, V. J. Modi, and G. Tyc. Effect of electrodynamic forces on the orbital dynamics of tethered satellites. *Journal of Guidance, Control, and Dynamics*, 28(6):1309–1315, 2005. ISSN 0731-5090.

[29] M. B. Larsen and M. Blanke. Nonlinear control of electrodynamic tether in equatorial or somewhat inclined orbits. In *Proc. Mediterranean Conference on Control & Automation MED '07*, pages 1–6, 2007. doi: 10.1109/MED. 2007.4433876.

[30] D. Leisawitz, J. C. Mather, S. H. Moseley, and X. L. Zhang. The submillimeter probe of the evolution of cosmic structure (SPECS). *Astrophysics and Space Science*, 269:563–567, 1999. ISSN 0004-640X.

[31] E. Lorenzini and J. Sanmartin. Electrodynamic tethers in space. *Scientific American*, 291(2):50–57, AUG 2004. ISSN 0036-8733.

[32] E. C. Lorenzini, M. Cosmo, S. Vetrella, and A. Moccia. Dynamics and control of the tether elevator/crawler system. *Journal of Guidance, Control, and Dynamics*, 12(3):404–411, may-jun 1989. ISSN 0731-5090.

[33] S. Macmillan and S. Maus. International geomagnetic reference field - the tenth generation. *Earth, Planets and Space*, 57(12):1135–1140, 2005. ISSN 1343-8832. doi: 10.1029/2005EO160006.

[34] K. K. Mankala and S. K. Agrawal. Equilibrium-to-equilibrium maneuvers of rigid electrodynamic tethers. *Journal of Guidance, Control, and Dynamics*, 28(3):541–545, 2005. ISSN 0731-5090.

[35] A. K. Misra. Equilibrium configurations of tethered three-body systems and their stability. *Journal of The Astronautical Sciences*, 50(3):241–253, jul-sep 2002. ISSN 0021-9142. AAS/AIAA 11th Space Flight Mechanics Meeting, Santa Barbara, California, feb 11-15, 2001.

[36] A. K. Misra and V. J. Modi. Three-dimensional dynamics and control of tether-connected n-body systems. *Acta Astronautica*, 26(2):77–84, 1992. ISSN 0094-5765.

[37] A. K. Misra, Z. Amier, and V. J. Modi. Attitude dynamics of three-boby tethred systems. *Acta Astronautica*, 17(10):1059–1068, 1988. ISSN 0094-5765.

[38] A. K. Misra, M. S. Nixon, and V. J. Modi. Nonlinear dynamics of two-body tethered satellite systems: Constant length case. *Journal of the Astronautical Sciences*, 49(2):219–236, apr-jun 2001. ISSN 0021-9142.

[39] B. Musetti, B. Cibrario, and P. Martella. Tethered satellite system reflight mission attitude dynamics and control: On-flight results. In *3rd ESA International Conference Spacecraft Guidance, Navigation and Control Systems*, pages 379–386. European Space Agency, November 1996.

[40] R. Ortega, A. v. d. Schaft, I. Mareels, and B. Maschke. Putting energy back in control. *IEEE Control Systems Magazine*, 21(2):18–33, 2001. ISSN 0272-1708.

[41] R. Ortega, A. v. d. Schaft, B. Maschke, and G. Escobar. Interconnection and damping assignment passivity-based control of port-controlled hamiltonian systems. *Automatica*, 38(4):585–596, 2002. ISSN 0005-1098.

[42] D. A. Padgett and A. P. Mazzoleni. Nullcline analysis as an analytical tethered satellite mission design tool. *Journal of Guidance, Control, and Dynamics*, 30(3):741–752, may-jun 2007. ISSN 0731-5090. doi: 10.2514/1.20946.

[43] C. Pardini, T. Hanada, P. H. Krisko, L. Anselmo, and H. Hirayama. Are de-orbiting missions possible using electrodynamic tethers? task review from the space debris perspective. *Acta Astronautica*, 60(10-11):916 – 929, 2007. ISSN 0094-5765. doi: 10.1016/j.actaastro.2006.11.001.

[44] J. Peláez. Self balanced electrodynamic tethers. *Collection of Technical Papers - AIAA/AAS Astrodynamics Specialist Conference*, 3:1392–1405, 2004.

[45] J. Peláez and M. Lara. Periodic solutions in electrodynamic tethers on inclined orbits. *Journal of Guidance, Control, and Dynamics*, 26(3):395–406, 2003. ISSN 0731-5090.

[46] J. Peláez and E. C. Lorenzini. Libration control of electrodynamic tethers in inclined orbit. *Journal of Guidance, Control, and Dynamics*, 28(2):269–279, 2005. ISSN 0731-5090.

[47] J. Peláez, E. C. Lorenzini, O. López-Rebollal, and M. Ruiz. A new kind of dynamic instability in electrodynamic tethers. *Journal of the Astronautical Sciences*, 48(4):449–476, 2000. ISSN 0021-9142.

[48] A. Pizarro-Chong and A. K. Misra. Dynamics of multi-tethered satellite formations containing a parent body. *Acta Astronautica*, 63(11-12):1188–1202, dec 2008. ISSN 0094-5765. doi: 10.1016/j.actaastro.2008.06.021.

[49] W. Purdy, S. Coffey, W. Barnds, B. Kelm, and M. Davis. Tips: Results of a tethered satellite experiment. In *Astrodynamics 1997*, volume 97 of *Advances In The Astronautical Sciences*, pages 3–23, 1998. ISBN 0-87703-441-9. AAS/AIAA Astrodynamics Conference, Sun Valley, Idaho, aug 04-07, 1997.

[50] M. Ruiz, O. López-Rebollal, E. C. Lorenzini, and J. Peláez. Modal analysis of the stability of periodic solutions in electrodynamic tethers. *Advances in the Astronautical Sciences*, 109 II:1553–1570, 2002. ISSN 0065-3438.

[51] J. R. Sanmartin, M. Martinezsanchez, and E. Ahedo. Bare wire anodes for electrodynamic tethers. *Journal of Propulsion and Power*, 9(3):353–360, may-jun 1993. ISSN 0748-4658.

[52] A. v. d. Schaft. L_2-*Gain and Passivity in Nonlinear Control*. Communications and Control Engineering. Springer-Verlag New York, Inc., Secaucus, NJ, USA, second edition, 2000. ISBN 1-85233-073-2.

[53] R. J. Sedwick and S. A. Schweighart. Propellantless spin-up of tethered or electromagnetically coupled sparse apertures. In H. A. MacEwen, editor, *Highly Innovative Space Telescope Concepts*, volume 4849 of *Proceedings of the Society of Photo-Optical Instrumentation Engineers (SPIE)*, pages

193–204. SPIE-International Society for Optical Engineering, 2002. ISBN 0-8194-4628-9.

[54] A. P. Seyranian. Sensitivity analysis of multiple-eigenvalues. *Mechanics of structures and machines*, 21(2):261–284, 1993. ISSN 0890-5452.

[55] A. P. Seyranian, F. Solem, and P. Pedersen. Stability analysis for multi-parameter linear periodic systems. *Archive of applied mechanics*, 69(3): 160–180, APR 1999. ISSN 0939-1533.

[56] L. Somenzi, L. Iess, and J. Peláez. Linear stability analysis of electrodynamic tethers. *Journal of Guidance, Control, and Dynamics*, 28(5):843–849, sep-oct 2005. ISSN 0731-5090. AIAA/AAS Astrodynamics Specialists Conference, Big Sky, Montana, aug 03-07, 2003.

[57] K. F. Sorensen. Conceptual design and analysis of an mxer tether boost station. Technical report, American Institute of Aeronautics and Astronautics, Propulsion Research Center / TD40, NASA Marshall Space Flight Center, AL 35812, 2001.

[58] W. Steiner, J. Zemann, A. Steindl, and H. Troger. Numerical study of large amplitude oscillations of a two-satellite continuous tether system with a varying length. *Acta Astronautica*, 35(9-11):607–621, 1995. ISSN 0094-5765.

[59] S. G. Tragesser and H. San. Orbital maneuvering with electrodynamic tethers. *Journal of Guidance, Control, and Dynamics*, 26(5):805–810, 2003. ISSN 0731-5090.

[60] S. G. Tragesser and A. Tuncay. Orbital design of earth-oriented tethered satellite formations. *Journal of the Astronautical Sciences*, 53(1):51–64, jan-mar 2005. ISSN 0021-9142.

[61] F. Verhulst. *Nonlinear Differential Equations and Dynamical Systems*. Universitext. Springer, 2nd edition, 1996.

[62] P. Williams. Optimal orbital transfer with electrodynamic tether. *Journal of Guidance, Control, and Dynamics*, 28(2):369–372, 2005. ISSN 0731-5090.

[63] P. Williams. Energy rate feedback for libration control of electrodynamic tethers. *Journal of Guidance, Control, and Dynamics*, 29(1):221–223, 2006. ISSN 0731-5090.

[64] P. Williams. Simple approach to orbital control using spinning electrodynamic tethers. *Journal of Spacecraft and Rockets*, 43(1):253–256, jan-feb 2006. ISSN 0022-4650.

[65] P. Williams. Libration control of electrodynamic tethers using predictive control with time-delayed feedback. *Journal of Guidance, Control, and Dynamics*, 32(4):1254–1268, 2009. ISSN 0731-5090. doi: 10.2514/1.41039.

[66] R. Wisniewski and M. Blanke. Fully magnetic attitude control for spacecraft subject to gravity gradient. *Automatica*, 35(7):1201–1214, jul 1999. ISSN 0005-1098.

[67] S. Yu. Periodic motion in the tethered satellite system. *Journal of Guidance, Control, and Dynamics*, 19(5):1195–1197, sep-oct 1996. ISSN 0731-5090.

[68] X. Zhou, J. Li, H. Baoyin, and V. Zakirov. Equilibrium control of electrodynamic tethered satellite systems in inclined orbits. *Journal of Guidance, Control, and Dynamics*, 29(6):1451–1454, 2006. ISSN 0731-5090. doi: 10.2514/1.21882.

Papers

Control by damping injection of electrodynamic tether system in an inclined orbit[1]

Abstract

Control of a satellite system with an electrodynamic tether as actuator is a time-periodic and underactuated control problem. This paper considers the tethered satellite in a Hamiltonian framework and determines a port-controlled Hamiltonian formulation that adequately describes the nonlinear dynamical system. Based on this model, a nonlinear controller is designed that will make the system asymptotically stable around its open-loop equilibrium. The control scheme handles the time-varying nature of the system in a suitable manner resulting in a large operational region. The performance of the closed loop system is treated using Floquet theory, investigating the closed loop properties for their dependency of the controller gain and orbit inclination.

I   Introduction

The principle of electrodynamic space tethers has been studied over the last couple of decades for its potential of providing cheap propulsion for spacecrafts (see [1] for the fundamentals and [2] for a survey of the literature). A tethered satellite system (TSS) consists of two or more spacecrafts tethered with cables, also known as space tethers. The current study will consider two satellites tethered with an electrodynamic tether. An electrodynamic tether is able to collect and release free electrons from/to the ionosphere, which makes a current flow along the tether. The current will interact with the magnetic field of the Earth and give rise to a Lorentz force acting along the tether. This force can be utilized to perform orbit maneuvers.

In this work a rigid tether model has been adopted and it is assumed that the current through the tether can be controlled without limitation. In general the model is time-varying, due to the periodic changes in the magnetic field along the orbit. This time-periodic nature gives rise to a family of unstable periodic solutions, which have been investigated in [3]. The special case of an equatorial orbit, which has the advantage of being time invariant, was investigated in [4].

In this paper, the focus will be on the case of an inclined orbit, which has been investigated by several others. One proposed control strategy is to stabilize the unstable periodic solution of the tether motion. In [5] two control schemes were proposed for such stabilization using two additional actuators. The first scheme used linear feedback of the difference between a reference trajectory and the current trajectory, the other used time-delayed autosynchronization. In [6], the unstable periodic solutions were stabilized using a current through the tether as actuator. The feedback law was designed using the energy variation along the orbit to synchronize the motion with a reference trajectory. In [7], a feedback linearisation control law was designed, using the current through the tether and the tether length as control inputs, to stabilize the open-loop equilibrium. This feedback law introduced two singularities along the orbit due to the unactuated out-of-plane dynamics, which was handled by switching to an additional control law.

The main contribution of this paper is to formulate the systems as a port-controlled Hamiltonian system to establish a passive connection between input and an output from which an asymptotically stable control law is designed to stabilize the open-loop equilibrium. From the port-controlled Hamiltonian formulation the controller is interpreted as damping injection for the conservative open-loop system. Traditionally the zeros of the input function can give rise to problems in connection with the control law (see [7]). However the paper shows that these are easily handled together with the time-varying nature of

the actuator due to the passive system formulation. The idea of using an energy based control method for the tether system is shown to be a natural choice since the dominating force on the system is the conservative gravity force and the perturbation force can be determined by the control input.

II   Model

In this section the tether model is deduced. The physical setup is first introduced. In the following sections the Lagrangian and the Hamiltonian of the system are stated and the generalized force arising from the Lorentz force will be derived. In the last section the system will be formulated as a port-controlled Hamiltonian system.

a)   Definitions and assumptions

The TSS under consideration consist of two satellites, the main-satellite and the sub-satellite, tethered with a rigid electrodynamic tether of length l and mass m_t. The satellites are modelled as point masses with mass m_B and m_A, respectively. The mass of the main-satellite is assumed the dominating mass of the system, $m_B \gg m_A + m_t$, from which it can be assumed that the center of mass of the TSS coincides with the center of mass of the main-satellite. It is assumed that the satellites are only subject to microgravity, while the tether in addition is affected by the Lorentz force. Since no perturbation forces are affecting the main-satellite, it will follow a unperturbed Keplerian orbit, which furthermore is assumed circular with semi-major axis R_o. The model is derived with the purpose of investigating the stability of the tether w.r.t. the orbital motion, thus it will only consider the influence of the Lorentz force on the attitude motion. The effect of the on the orbital motion was the subject of [8]. The motion of the tether is described in the orbit frame, defined with the $\boldsymbol{x}_o$-axis along the position vector from the Earth to the main-satellite, $\boldsymbol{y}_o$ along the velocity vector of the system and $\boldsymbol{z}_o$ normal to the orbit plane (see Fig. 1). Since the orbit is assumed circular the right ascension of the ascending node Ω, the orbit inclination i and the true anomaly ν will be adequate to describe the orbit frame w.r.t. to the inertia frame as seen in Fig. 1. The points along the tether are described using a unit vector $\boldsymbol{r}$ from the main- to the sub-satellite, from which the points along the tether can be written as $s\boldsymbol{r}$ with $s \in [0 \; l]$. The tether is assumed of constant length, hence the tether motion is restricted to a sphere and the system has $n = 2$ degrees of freedom. Spherical coordinates are introduced as the generalized coordinates $\boldsymbol{q} = [\theta \; \varphi]^T$, from which $\boldsymbol{r}$ can be
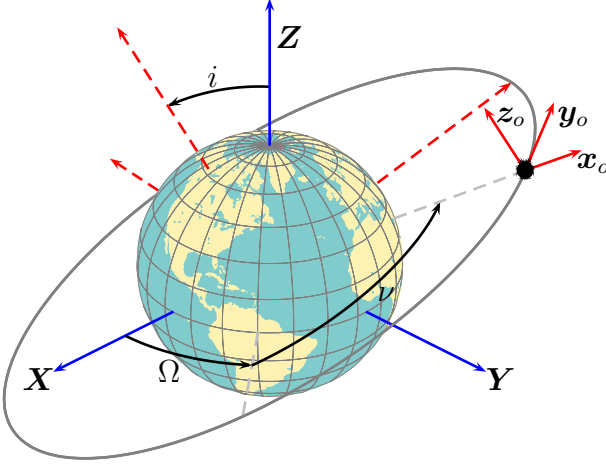
Figure 1: Orbit description. The orbit frame $(\boldsymbol{x}_o, \boldsymbol{y}_o, \boldsymbol{z}_o)$ occurs from an $\Omega \rightarrow i \rightarrow \nu$ rotation of the inertial frame $(\boldsymbol{X}, \boldsymbol{Y}, \boldsymbol{Z})$.
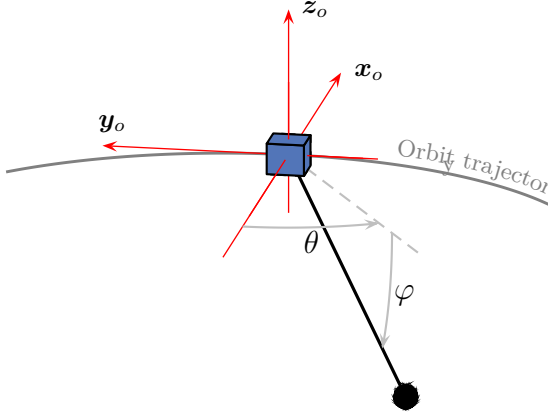
Figure 2: In- and out-of-plane angles described w.r.t. the orbit frame $(\boldsymbol{x}_o, \boldsymbol{y}_o, \boldsymbol{z}_o)$.

expressed in the orbit frame as,

$$\boldsymbol{r} = \begin{bmatrix} -\cos\theta\cos\varphi & -\sin\theta\cos\varphi & -\sin\varphi \end{bmatrix}^T, \tag{1}$$

where θ is the in-plane angle and φ the out-of-plane angle as seen in Fig. 2. The position of the main-satellite in the orbit is described by the true anomaly ν. The orbit is assumed circular thus ν is linearly increasing and it is evident to introduce ν as the non-dimensional time $\nu = \omega_o t$, which is subsequently used in

the model. The current I through the tether is seen as the control input and it is assumed to be controlled without limitations. When the tether is the only actuator the system is underactuated i.e. the number of inputs m is smaller than the degrees of freedom n.

b) Lagrangian

The Lagrangian of the system can be written as the difference between kinetic and potential energy,

$$L = K - V. \tag{2}$$

From the Lagrangian the equation of motion can be found from Lagrange's equation. Defining the Jacobian of a scalar function as a column vector this can be written as,

$$\frac{d}{dt}\left(\frac{\partial L}{\partial \dot{\boldsymbol{q}}}\right) - \frac{\partial L}{\partial \boldsymbol{q}} = \boldsymbol{\tau}, \tag{3}$$

where $\boldsymbol{\tau} = [\tau_\theta \ \tau_\varphi]^T$ represents the generalized force acting on the system. Since the motion relative to the orbit frame is of interest, the velocities are described relative to this frame, which introduces the centrifugal and the Coriolis potential. Since the system is orbiting the Earth the main effect of the gravitational field vanishes and V includes only the Tidal force. The Lagrangian L can be written (see e.g. [3]),

$$L(\boldsymbol{q}, \dot{\boldsymbol{q}}) = \frac{1}{2}\Lambda\left(\dot{\varphi}^2 + \cos^2\varphi\left((1+\dot{\theta})^2 + 3\cos^2\theta\right)\right), \tag{4}$$

where $(\dot{\ })$ denotes differentiation w.r.t. ν and $\Lambda = \frac{1}{3}\omega_o^2 l^2(3m_A + m_t)$. The term $2\dot{\theta}\cos^2\varphi$ represents the Coriolis potential and $\cos^2\varphi$ the centrifugal potential. From (3) it is seen that $\boldsymbol{\tau}$ can be scaled by Λ^{-1}, which leaves a parameterless Lagrangian.

c) Hamiltonian

The generalized momenta can be found as $\boldsymbol{p} = \frac{\partial L}{\partial \dot{\boldsymbol{q}}} = [p_\theta \ p_\varphi]^T$ from which,

$$p_\theta = \left(1+\dot{\theta}\right)\cos^2\varphi \tag{5a}$$

$$p_\varphi = \dot{\varphi}. \tag{5b}$$

The Hamiltonian H is given as,

$$H(\boldsymbol{q}, \boldsymbol{p}) = \boldsymbol{p}^T \dot{\boldsymbol{q}} - L(\boldsymbol{q}, \dot{\boldsymbol{q}}(\boldsymbol{p}, \boldsymbol{q})) \tag{6}$$

$$= \frac{1}{2} \left(p_\varphi^2 + \frac{p_\theta^2}{\cos^2 \varphi} - 2p_\theta - 3\cos^2 \theta \cos^2 \varphi \right) + 2. \tag{7}$$

The constant 2 is added, without loss of generality, to get a positive semi definite Hamiltonian. The singularities at $\varphi = \pm \frac{\pi}{2}$ are coursed by the use of spherical coordinates. Using H the equation of motion can be written using Hamilton's equation,

$$\dot{\boldsymbol{q}} = \frac{\partial H}{\partial \boldsymbol{p}}, \tag{8a}$$

$$\dot{\boldsymbol{p}} = -\frac{\partial H}{\partial \boldsymbol{q}} + \boldsymbol{Q}, \tag{8b}$$

where $\boldsymbol{Q} = \Lambda^{-1} \boldsymbol{\tau}$. The equations result in the following four coupled first order differential equations,

$$\dot{\theta} = \frac{p_\theta}{\cos^2 \varphi} - 1, \tag{9a}$$

$$\dot{\varphi} = p_\varphi, \tag{9b}$$

$$\dot{p}_\theta = -\frac{3}{2} \cos^2 \varphi \sin 2\theta + \tau_\theta, \tag{9c}$$

$$\dot{p}_\varphi = -\frac{p_\theta^2}{\cos^2 \varphi} \tan \varphi - \frac{3}{2} \cos^2 \theta \sin 2\varphi + \tau_\varphi. \tag{9d}$$

From Hamilton's equation (9) it is obvious that the equilibria of the unforced system ($\boldsymbol{Q} = \boldsymbol{0}$) is placed at the extrema of H. The open-loop equilibrium between the Earth and the main-satellite is described as $p_\theta^* = 1$ and $p_\varphi^* = \theta^* = \varphi^* = 0$.

d)   Generalized forces

The Lorentz force on a tether section of unit length is,

$$\bar{\boldsymbol{F}}_e = I\boldsymbol{r} \times \boldsymbol{B}, \tag{10}$$

where $\boldsymbol{B}$ is the magnetic field of the Earth. To find the generalized force $\boldsymbol{\tau}$ associated with the generalized coordinates, the Lorentz force per unit length is projected onto the generalized coordinates and integrated along the tether,

$$\tau_i = \int_0^l \bar{\boldsymbol{F}}_e \cdot \frac{\partial (s\boldsymbol{r})}{\partial q_i} \, ds, \quad \text{for } i = 1, 2. \tag{11}$$

A dipole model is a simple and widely used approximation of the magnetic field of the Earth. To avoid unnecessary complexity, the dipole moment is aligned with the rotational axis of the Earth. This results in a model independent of the rotation of the Earth. The B-field can be written in the orbit frame as,

$$\boldsymbol{B} = \frac{\mu_m}{R_o^3} \begin{bmatrix} -2\sin\nu\sin i \\ \cos\nu\sin i \\ \cos i \end{bmatrix}, \tag{12}$$

where μ_m is the strength of the B-field. Using (12) the generalized force is,

$$\boldsymbol{Q} = \boldsymbol{b}(\boldsymbol{q}, \nu)u, \tag{13}$$

where u is a dimensionless quantity proportional to the input current, which in turn can be written as,

$$u = \frac{3}{2} \frac{1}{3m_A + m_t} \frac{\mu_m}{\mu} I. \tag{14}$$

Here μ is the standard gravitational parameter of the Earth. The vector $\boldsymbol{b}(\boldsymbol{q}, \nu) = [b_\theta(\boldsymbol{q}, \nu)\ b_\varphi(\boldsymbol{q}, \nu)]^T$ will be denoted as the input function and is of great importance for the control design. It is essential for the controllability of the system and it will appear to be an important part of establishing a passive input-output connection for the system.

The input function can be written as,

$$b_\theta(\boldsymbol{q}, \nu) = \cos^2\varphi\tan\varphi\sin i\,(\cos\nu\sin\theta - 2\sin\nu\cos\theta) - \cos^2\varphi\cos i, \tag{15a}$$
$$b_\varphi(\boldsymbol{q}, \nu) = \sin i\,(\cos\theta\cos\nu + 2\sin\theta\sin\nu). \tag{15b}$$

$\boldsymbol{b}(\boldsymbol{q}, \nu)$ is in general quite complicated reflecting the fact that the magnetic field varies along the orbit (from which the time dependency occurs) and that the Lorentz force depends upon the tether orientation relative to the B-field. In the special case of an equatorial orbit ($i = 0°$) the input function becomes time invariant, but at the same time b_φ vanish and the out-of-plane motion will become unactuated. This case was treated in [4].

In the case of an inclined orbit $b_\varphi(\boldsymbol{q}, \nu)$ will have two zeros along the orbit, determined by $2\tan\theta = -\cot\nu$. For the open-loop equilibrium these are placed at $\nu = \pm\frac{\pi}{2}$. The zeros of $b_\theta(\boldsymbol{q}, \nu)$ occurs in a more complicated scheme. It can be seen from (15a) that for non-polar orbits ($i \neq 90°$) zeros cannot occur for small out-of-plane angels (more specifically for $2\,|\tan\varphi| < |\cot i|$), hence no zeros occur for the open-loop equilibrium or any other equilibrium in the orbit plane. For a polar orbit, b_θ vanish if $\sin 2\varphi = 0$ or $\cot\nu = 2\cos\theta$, i.e. the in-plane motion is unactuated at the open-loop equilibrium.

A critical situation where the system is uncontrollable can occur if $b_\theta = b_\varphi = 0$ for a period of time. This situation will occur if the tether and the magnetic

field are parallel, and no Lorentz force can be generated along the tether. We will not treat this situation in this work.

e) Port-controlled Hamiltonian system description

Introducing a state vector $\boldsymbol{x} = \begin{bmatrix} \boldsymbol{q}^T & \boldsymbol{p}^T \end{bmatrix}^T$ the system is rewritten as,

$$\dot{\boldsymbol{x}} = \boldsymbol{J}\frac{\partial H}{\partial \boldsymbol{x}} + \boldsymbol{g}(\boldsymbol{x}, \nu)u \tag{16a}$$

$$y = \boldsymbol{g}^T(\boldsymbol{x}, \nu)\frac{\partial H}{\partial \boldsymbol{x}}, \tag{16b}$$

where

$$\boldsymbol{J} = \begin{bmatrix} \boldsymbol{0} & \boldsymbol{I} \\ -\boldsymbol{I} & \boldsymbol{0} \end{bmatrix} \qquad \text{and} \qquad \boldsymbol{g} = \begin{bmatrix} \boldsymbol{0} \\ \boldsymbol{b}(\boldsymbol{q}, \nu) \end{bmatrix}. \tag{17}$$

This is a standard formulation of a mechanical system where only the momentum states are actuated. The output function (16b) is chosen to establish a passive input output connection. This formulation is called a port-controlled Hamiltonian description (see [9, p. 73]) and can, for single input systems, in general be written as,

$$\dot{\boldsymbol{x}} = (\boldsymbol{J}(\boldsymbol{x}, \nu) - \boldsymbol{R}(\boldsymbol{x}, \nu))\frac{\partial H}{\partial \boldsymbol{x}} + \boldsymbol{g}(\boldsymbol{x}, \nu)u \tag{18a}$$

$$y = \boldsymbol{g}^T(\boldsymbol{x}, \nu)\frac{\partial H}{\partial \boldsymbol{x}}, \tag{18b}$$

where $\boldsymbol{J} \in \mathbb{R}^{2n \times 2n}$ is the interconnection matrix and $\boldsymbol{R} \in \mathbb{R}^{2n \times 2n}$ is the damping matrix. It is assumed that the interconnection matrix is skew-symmetric $\boldsymbol{J} = -\boldsymbol{J}^T$ and that the damping matrix is symmetric and positive semi-definite, $\boldsymbol{R} = \boldsymbol{R}^T \geq 0$. Both the interconnection and the damping matrices can be state and time dependent. In the current case $\boldsymbol{R} = \boldsymbol{0}$ for the open-loop system since no damping forces are modelled.

III   Control Design

A controller based on the passivity property of the port-controlled Hamiltonian system will be designed in this section. Afterwards, the closed loop system will be investigated, using linear Floquet analysis, to find a controller gain k, which provides optimal stability properties.

a) Passivity based control design

A general stabilization of the system is a difficult task due to its time-varying and underactuated nature. In the port controlled Hamiltonian framework, this would require a feedback law, which reshapes the Hamiltonian of the closed loop system. An easier task would be to stabilize the open-loop equilibrium $\boldsymbol{x}^*$. The latter will be considered here. Since the Hamiltonian (which acts as storage function for the system) is positive definite, this task can be simply achieved by the feedback law $u = -ky$, where $k > 0$ (see [9, Corollary 3.3.1 p. 44]). An important condition for the control design is then that the system need be zero-state detectable, i.e. if $u = y = 0$ for $t > t_0$ the states should converge towards the equilibrium. The zero-state detectability of the system is closely related to the zeros of the input function.

The output can be written as,

$$y = \boldsymbol{g}^T(\boldsymbol{x}, \nu)\frac{\partial H}{\partial \boldsymbol{x}} = \boldsymbol{b}^T(\boldsymbol{q}, \nu)\frac{\partial H}{\partial \boldsymbol{p}}$$
$$= b_\theta(\boldsymbol{q}, \nu)\dot{\theta} + b_\varphi(\boldsymbol{q}, \nu)\dot{\varphi}, \tag{19}$$

where it has been used that $\dot{\boldsymbol{q}} = \frac{\partial H}{\partial \boldsymbol{p}}$. The zeros of the input function originating from time-periodicity have no influence on the zero-state detectability since they will be countable. The generalized coordinates can induce zeros in the input function as mentioned earlier, but in the case, where the generalized velocities are different from zero, they will only occur for countable instances of time. The case where the velocity is also zero, the state will have reached the equilibrium of interest, since this is the only open-loop equilibrium. The last variable to cause zeros in the input function is the orbit inclination i. In the case of a equatorial orbit ($i = 0°$) the second term of the output will be zero. If the in-plane dynamics at the same time has reached its equilibrium, the out-of-plane dynamics will by unobservable from the output and the system is therefore not zero-state detectable in this case. For a polar orbit ($i = 90°$) the situation is similar. The in-plane dynamics will be unobservable from the output in the case where the out-of-plane dynamics have reached its equilibrium position, hence the system is not zero-state detectable in the case of a polar orbit neither.

The stability of the closed loop system can by investigated using H as Lyapunov function candidate. The time derivative of H is,

$$\dot{H} = \left(\frac{\partial H}{\partial \boldsymbol{x}}\right)^T \boldsymbol{J}\frac{\partial H}{\partial \boldsymbol{x}} + \left(\frac{\partial H}{\partial \boldsymbol{x}}\right)^T \boldsymbol{g}(\boldsymbol{x}, \nu)u$$
$$= -k\left(\frac{\partial H}{\partial \boldsymbol{p}}\right)^T \boldsymbol{b}(\boldsymbol{q}, \nu)\boldsymbol{b}^T(\boldsymbol{q}, \nu)\frac{\partial H}{\partial \boldsymbol{p}}. \tag{20}$$

Due to the zero-state detectability, the derivative of this Lyapunov candidate is negative semi-definite, however LaSalle's theorem ensures asymptotically stability of $\boldsymbol{x}^*$.

The closed loop system can be written as a port-controlled Hamiltonian system as,

$$\dot{\boldsymbol{x}} = (\boldsymbol{J} - \boldsymbol{R}) \frac{\partial H}{\partial \boldsymbol{x}}, \tag{21}$$

where

$$\boldsymbol{R} = \boldsymbol{g}\boldsymbol{g}^T = \begin{bmatrix} \boldsymbol{0} & \boldsymbol{0} \\ \boldsymbol{0} & \boldsymbol{R}_2 \end{bmatrix}. \tag{22}$$

It is seen that the controller has added the damping matrix $\boldsymbol{R}_2 = \boldsymbol{b}\boldsymbol{b}^T$, hence the controller strategy is called damping injection. $\boldsymbol{R}_2$ will have one eigenvalue equal to zero, while the other will be positive except when $b_\theta = b_\varphi = 0$ in which case it will be zero. The lack of full rank of $\boldsymbol{R}_2$ is a consequence of the fact that the system is underactuated.

b)   Closed loop analysis

This section investigates the stability properties of the closed loop system, for different values of k, using Floquet analysis. A linearised version of the closed loop system can be written as,

$$\dot{\boldsymbol{x}} = \boldsymbol{A}(\nu)\boldsymbol{x}, \tag{23}$$

where $\boldsymbol{A}(\nu)$ is the $T = 2\pi$-periodic system matrix,

$$\boldsymbol{A}(\nu) = \begin{bmatrix} 0 & 0 & 1 & 0 \\ 0 & 0 & 0 & 1 \\ -3 & 0 & 0 & 0 \\ 0 & -4 & 0 & 0 \end{bmatrix}$$
$$- \frac{1}{2}k \begin{bmatrix} 0 & 0 & 0 & 0 \\ 0 & 0 & 0 & 0 \\ 0 & 0 & 2\cos^2 i & -\sin(2i)\cos\nu \\ 0 & 0 & -\sin(2i)\cos\nu & 2\sin^2 i \cos^2 \nu \end{bmatrix}. \tag{24}$$

The independent solutions of (23) can be written in a fundamental matrix $\boldsymbol{\Phi}(\nu)$ for which,

$$\dot{\boldsymbol{\Phi}}(\nu) = \boldsymbol{A}(\nu)\boldsymbol{\Phi}(\nu). \tag{25}$$

It is seen that $\boldsymbol{\Phi}(\nu + T)$ is also a fundamental matrix, hence the connection between $\boldsymbol{\Phi}(\nu)$ and $\boldsymbol{\Phi}(\nu + T)$ can be written,

$$\boldsymbol{\Phi}(\nu + T) = \boldsymbol{\Phi}(\nu)\boldsymbol{M}, \tag{26}$$

where $\boldsymbol{M}$ is the nonsingular monodromy matrix and the characteristic multipliers ρ_i can be found as the eigenvalues of $\boldsymbol{M}$. The stability of the system is determined from ρ_i (see [10]) and can be summarized as,

- If one characteristic multiplier is numerically lager than one $|\rho_i| > 1$, the system is unstable.

- If all characteristic multipliers are numerically less than one $|\rho_i| < 1$, the system is asymptotically stable.

- If the multipliers of unit length ($|\rho_i| = 1$) have equal algebraic and geometrical multiplicity and the remaining multipliers have $|\rho_i| < 1$ a periodic solution exist.

The general complex solution of (23) can, in the case where an eigenvalue of multiplicity m has m independent eigenvectors, be written as,

$$\boldsymbol{x}(\nu) = \sum_{i=1}^{2n} c_i \rho_i^{\frac{\nu}{T}} \boldsymbol{p}_i(\nu), \tag{27}$$

where $\boldsymbol{p}_i$ is a T-periodic function and c_i is a constant. From (27) it is clear the numerically largest multiplier will dominate the response as well as decide the stability (in agreement of the above scheme). This multiplier will determine the convergence of the solution. We will denote the numerically largest characteristic multiplier *the stability deciding multiplier*. In this work the characteristic multipliers are found numerically by solving (25) with the initial condition $\boldsymbol{\Phi}(0) = \boldsymbol{I}$. The monodromy matrix can then by found from (26) as $\boldsymbol{M} = \boldsymbol{\Phi}(T)$.

Fig. 3 shows the evolution of the characteristic multipliers in the complex plane for increasing controller gain. The absolute values are shown in Fig. 4. The inclination is $i = 45°$ in this case. For $k = 0$ the figures show that two periodic solutions exist with different frequencies corresponding to the natural frequencies of the in- and out-of-plane motions[1]. The in-plane motion has a natural frequency of $\sqrt{3}\omega_o$ corresponding to ρ_1 and ρ_2 while the out-of-plane natural frequency equals $2\omega_o$ corresponding to ρ_3 and ρ_4. $\rho_3 = \rho_4 = 1$ since the out-of-plane natural frequency is a multiple of the orbit rate, which corresponds to the frequency of the time variation of $\boldsymbol{A}(\nu)$. For increasing k the multipliers are moving towards the origin, reaching a minimum of the absolute value at $k \approx 3$. Afterwards three multipliers converge to one, while the last one converges to zero, resulting in an increasing stability deciding multiplier. It is seen that the system is asymptotically stable for all $k \neq 0$, which is in agreement with the stability proof of the previous section. Fig. 5 shows three simulations of the closed

---

[1]In the case $k = 0$ the eigenvalues can be found analytically and it can be checked the that geometric multiplicity of ρ_3 and ρ_4 equals two.
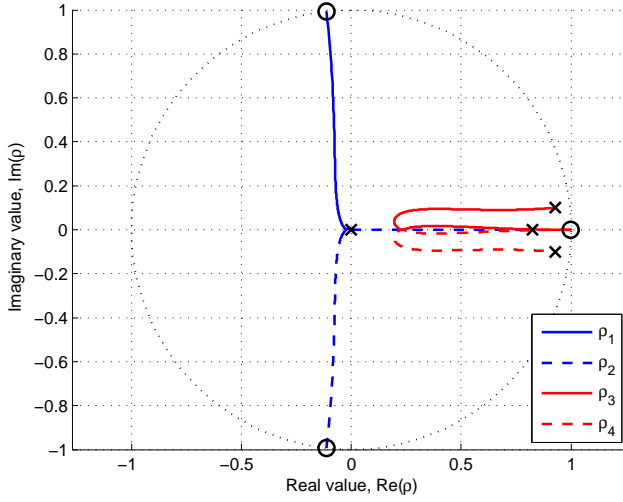
Figure 3: The characteristic multipliers shown in the complex plane. $k = 0$ is marked with ∘ and $k = 100$ is marked with ×.
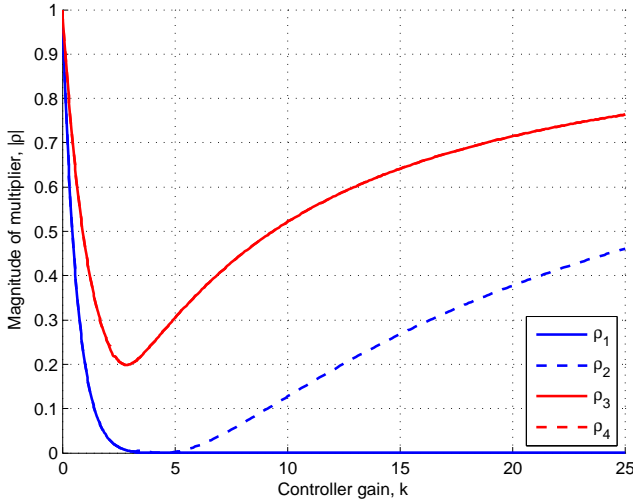
Figure 4: The absolute value of the characteristic multipliers as function of the controller gain k.

loop system for different controller gains. The gains are chosen to illustrate the influence of the deciding multiplier on the system response.
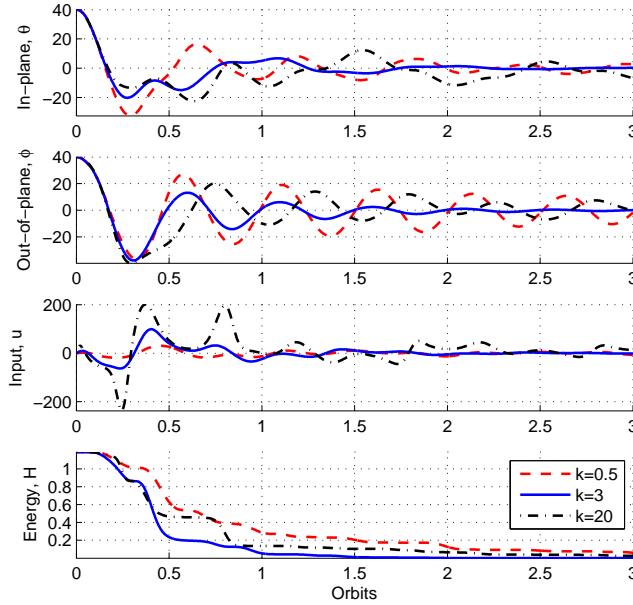
Figure 5: Simulation of nonlinear closed loop system for different gains k.

Due to the zeros of the input function the controller will only be stable in a certain range of orbit inclinations. Fig. 6 shows the stability deciding characteristic multiplier as function of the controller gain for different inclinations. In case of either an equatorial or a polar orbit, the characteristic multiplier is one for all k, and periodic solutions will occur. This is in agreement with the analysis of the zero-state detectability from the previous section. As already mentioned, the out-of-plane motion is unactuated in the equatorial case since $b_\varphi = 0$, hence in the linear approach, the out-of-plane motion will oscillate with its natural frequency. For polar orbits b_θ vanished in the linear approach, hence the motion is unactuated and similar to the equatorial orbit, the in-plane motion will oscillate with its natural frequency.

Fig. 7 shows simulation of the closed loop system for different inclinations. The figure shows that for the equatorial orbit the out-of-plane motion is poorly damped, while the in-plane motion is poorly damped for the polar orbit.
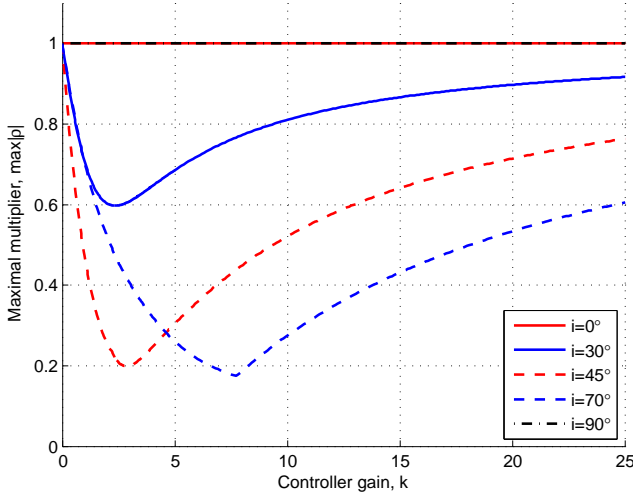
Figure 6: The absolute value of the deciding multiplier for different i.
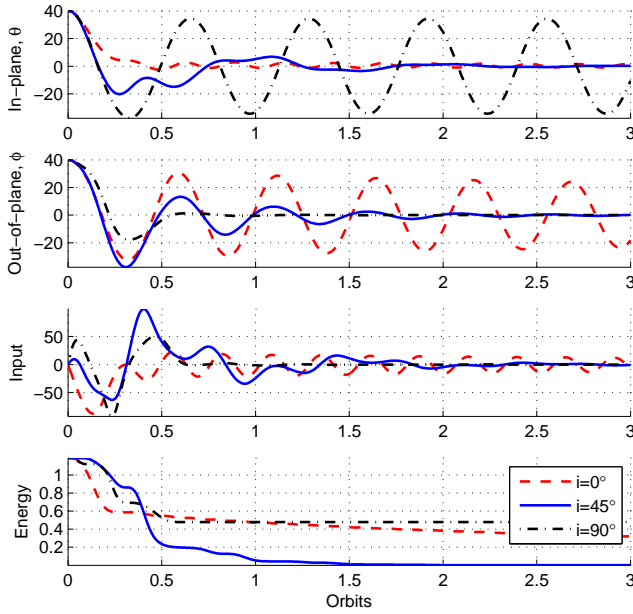
Figure 7: Simulation of nonlinear closed loop system for different orbit incli-
nation i. The controller gain is chosen as $k = 3$.

IV   Discussion

The controller designed in this paper has distinct advantages to other approaches. With this approach, the zeros of the input functions are not leading to singularities in the control law, which in turn gives to a large operational region. The approach is balancing the trade-off between performance and robustness in favour of the robustness of the control. This is a known property of a passivity based control design (see [11]). Robustness is quite important in a practical context, since the uncertainty in the magnetic field is quite large. The performance is limited by the minimum of the stability deciding multiplier, which lead to slow control action compared to other approaches.

Earlier papers have emphasized that the current which can be induced along the tether is limited (see e.g. [6]). This can prevent the choice of an optimal control gain, which will lead to a longer settling time for the controller However, it will not have any influence on the stability of the controller.

V   Conclusion

A controller that provides asymptotically stability for the open-loop equilibrium of a tethered satellite system was designed in this paper, using an electrodynamic tether as actuator. The design was based on a port-controlled Hamiltonian formulation of the system and stability was shown using the Hamiltonian as a Lyapunov function. The performance of the closed loop system was investigated using Floquet theory and a controller gain was found that minimize the settling time. The performance was investigated, primarily as a function of orbit inclination. As a salient feature, it was shown that damping was injected for all values of inclination, except when pure equatorial or polar orbits were considered. These orbits lead to nonactuated out-of-plane and in-plane dynamics, respectively, as should be expected.

References

[1] Vladimir V. Beletsky and Evgenii M. Levin. *Dynamics of space tether systems*, volume 83 of *Advances in the astronautical sciences*. American Astronautical society, 1993.

[2] M. P. Cartmell and D. J. McKenzie. A review of space tether research. *Progress in Aerospace Sciences*, 44(1):1–21, 2008.

[3] J. Peláez, E. C. Lorenzini, O. López-Rebollal, and M. Ruiz. A new kind of dynamic instability in electrodynamic tethers. *Journal of the Astronautical Sciences*, 48(4):449–476, 2000.

[4] M. B. Larsen and M. Blanke. Nonlinear control of electrodynamic tether in equatorial or somewhat inclined orbits. In *Proc. Mediterranean Conference on Control & Automation MED '07*, pages 1–6, 2007.

[5] J. Peláez and E. C. Lorenzini. Libration control of electrodynamic tethers in inclined orbit. *Journal of Guidance, Control, and Dynamics*, 28(2):269–279, 2005.

[6] Paul Williams. Energy rate feedback for libration control of electrodynamic tethers. *Journal of Guidance, Control, and Dynamics*, 29(1):221–223, 2006.

[7] Xiang Zhou, Junfeng Li, H. Baoyin, and Vadim Zakirov. Equilibrium control of electrodynamic tethered satellite systems in inclined orbits. *Journal of Guidance, Control, and Dynamics*, 29(6):1451–1454, 2006.

[8] Paul Williams. Optimal orbital transfer with electrodynamic tether. *Journal of Guidance, Control, and Dynamics*, 28(2):369–372, 2005.

[9] Arjan van der Schaft. L_2-*Gain and Passivity in Nonlinear Control*. Communications and Control Engineering. Springer-Verlag New York, Inc., Secaucus, NJ, USA, second edition, 2000.

[10] R. Grimshaw. *Nonlinear Ordinary Differential Equations*. Blackwell Scientific Publications, 1990.

[11] R. Ortega, Arjan van der Schaft, I. Mareels, and B. Maschke. Putting energy back in control. *IEEE Control Systems Magazine*, 21(2):18–33, 2001.

Stabilization of periodic solutions in a tethered satellite system by damping injection[1]

Abstract

A spacecraft with electrodynamic tether orbiting the Earth will be subject to a periodic forcing term induced by the variation of the magnetic field along the orbit. The periodic forcing term leads to a family of unstable periodic solutions for a tether carrying a constant current. This paper presents a control design for stabilizing these periodic solutions. The design consists of a control law for stabilizing the open-loop equilibrium and a bias term which forces the system trajectory away from the equilibrium. The tether needs to be positioned away from open-loop equilibrium for the tether to affect the orbit parameters. An approximation of the periodic solutions of the closed loop system is found as a series expansion in the parameter plane spanned by the controller gain and the bias term. The stability of the solutions is investigated using linear Floquet analysis of the variational equation and the region of stable periodic solutions in the parameter plane is found.

---

[1]In proceedings of *European Control Conference 2009*.

I   Introduction

An electrodynamic tether is an actuator for performing orbit maneuvers of satellites or spacecrafts in general, mainly proposed for deorbiting of obsoleted satellites. The actuator consists of a conducting wire connecting a sub-satellite to a main-satellite. Assuming the system is orbiting an environment with a magnetic field and free electrons (e.g. the ionosphere of a low Earth orbit), the magnetic field will induce a voltage along the tether and by collecting and emitting electrons from/to the environment a current will flow through the tether. The current will interact with the magnetic field and give rise to an electrodynamic force (the Lorentz force) acting on the tether. This force can be utilized to perform orbit maneuvers. See [1] for a basic mathematical treatment of the system and [2] for a survey of the literature.

In this paper the tether will be modelled as a rigid rod. For modelling the magnetic field of the Earth a dipole model with dipole moment along the rotational axis of the Earth is adopted. The tether motion is described with respect to the main-satellite, which makes the model useful for investigating the local stability of the tether system. The variation in the magnetic field along the orbit introduces time-variations in the model. Using the tether as the only actuator of the satellite, makes the system underactuated.

This type of model has been used in several articles both for investigating the stability of the tether system relative to the orbit and for control design. In [3] it was shown that the tethered satellite system contained a family of unstable periodic solutions when a constant current is applied through the tether. The periodic solutions occur from a periodic forcing term originating from the variations in the magnetic field. The time-varying and underactuated nature of the system makes it a difficult task to design stabilizing controllers for the system. The time-invariant special case of an equatorial orbit was addressed in [4], while stabilization of the origin in the time-varying case was treated in [5] and [6]. Another control strategy for the system is to stabilize the known unstable periodic solutions. This control strategy has been investigated in several papers and is also the subject of the present paper. In [7] two different control schemes was investigated using the difference between the open-loop periodic solution and the current trajectory as feedback signals. A linear feedback controller and a time-delayed autosynchronization controller was investigated. The control forces were assumed generated by some additional actuators. In [8] the energy variations along a unstable periodic solution was used to synchronize the system trajectory with the periodic solution.

The control design presented in this paper is based on [6] where the origin of the open-loop system was stabilized by use of damping injection. In this paper the

design is extended to create stable periodic solutions of the tether motion. The control design has the advantage compared to other designs that no reference solution is used, i.e. knowledge of the unstable open-loop periodic solution is not necessary. The price of this feature is that the shape of the orbit is perturbed compared to the open-loop solution.

The first section of the paper contains a brief review of the system model, while the second section will deduce the control design. The third section contain an analysis of the closed loop system, including an approximation of the periodic solutions and an investigation of their stability.

II   Model

The model derived in this section will describe the tether motion relative to the orbit frame, i.e. the attitude motion of the system. For a more elaborate derivation see [3] or [6]. It is assumed that a rigid tether of mass m_t connects two satellites, a main-satellite and a sub-satellite of mass m_B and m_A, respectively. Both satellites are modelled as point masses. It is assumed that the main-satellite follows an unperturbed Keplerian orbit, i.e. that the center of mass of the system is placed at the main-satellite. For simplicity the orbit is assumed circular with orbit rate ω_o. We will defined the orbit frame with the $\boldsymbol{x}_o$-axis along the position vector of the main-satellite relative to the center of the Earth. The $\boldsymbol{y}_o$-axis defines the velocity of the satellite and the $\boldsymbol{z}_o$-axis the normal to the orbit plane. In this coordinate system the open-loop system will have two stable equilibria, one on the positive part and one on the negative part of the $\boldsymbol{x}_o$-axis. Similar there will be two unstable equilibria along the $\boldsymbol{y}_o$-axis. We will consider a tether system operating around the equilibrium on the negative part of the $\boldsymbol{x}_o$-axis. The tether is assumed of constant length l, hence the motion is restricted to a sphere. This makes it natural to introduce spherical coordinates $\boldsymbol{q} = [\theta \; \varphi]^T$ to describe the $n = 2$ degrees of freedom. The in-plane angle θ will be defined as the angle in the orbit plane measured from the negative part of the $\boldsymbol{x}_o$-axis and the out-of-plane angle φ is the angle out of the orbit plane, (see Fig. 1). Using the generalized coordinates a unit vector along the tether can be written as,

$$\boldsymbol{r} = \begin{bmatrix} -\cos\theta\cos\varphi & -\sin\theta\cos\varphi & -\sin\varphi \end{bmatrix}^T. \tag{1}$$

With the assumption of a circular orbit it is natural to introduce the true anomaly ν as the (dimensionless) time variable of the model. This corresponds to scaling the time by the orbit rate, $\nu = \omega_o t$.
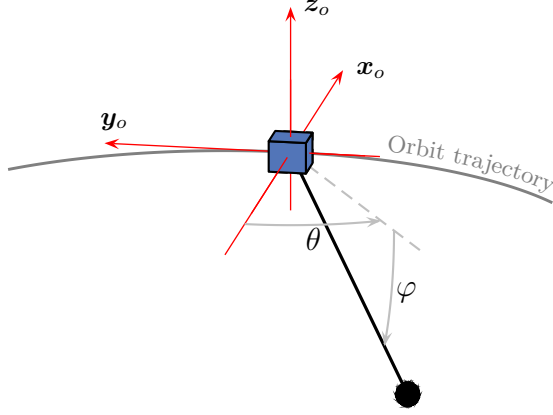
Figure 1: In- and out-of-plane angles described w.r.t. the orbit frame $(\boldsymbol{x}_o, \boldsymbol{y}_o, \boldsymbol{z}_o)$.

a) Energy functions

The Lagrangian of the system can be written as (see e.g. [3]),

$$L(\boldsymbol{q}, \dot{\boldsymbol{q}}) = \frac{1}{2}\Lambda \left(\dot{\varphi}^2 + \cos^2\varphi \left((1+\dot{\theta})^2 + 3\cos^2\theta \right) \right), \qquad (2)$$

where (˙) denotes differentiation w.r.t. ν and Λ is a constant determined from the mass and the orbit rate of the system as $\Lambda = \frac{1}{3}\omega_o^2 l^2 (3m_A + m_t)$. The kinetic energy is included in the terms $\dot{\theta}^2 \cos^2\varphi$ and $\dot{\varphi}^2$, while the potential originating from the tidal force is represented by $3\cos^2\theta \cos^2\varphi$. The terms $\cos^2\varphi$ and $2\dot{\theta}\cos^2\varphi$ includes the centrifugal and the Coriolis potential, respectively. Introducing the generalized momenta $\boldsymbol{p} = [p_\theta \ p_\varphi]$ as,

$$p_\theta = \frac{\dot{\theta}}{\cos^2\varphi} - 1, \qquad (3\text{a})$$

$$p_\varphi = \dot{\varphi}, \qquad (3\text{b})$$

the Hamiltonian of the system can be written as,

$$H(\boldsymbol{q}, \boldsymbol{p}) = \frac{1}{2}\left(p_\varphi^2 + \frac{p_\theta^2}{\cos^2\varphi} - 2p_\theta - 3\cos^2\theta \cos^2\varphi \right) + 2. \qquad (4)$$

The constant Λ has been left out, which corresponds to scaling the Hamiltonian with this quantity. This can be done remembering to scale the generalized force with Λ^{-1}. A constant has been added to the Hamiltonian without loss of generality to obtain a positive definite function. Using the Hamiltonian the

equation of motion can be written using Hamilton's equation,

$$\dot{\boldsymbol{q}} = \frac{\partial H}{\partial \boldsymbol{p}}, \tag{5a}$$

$$\dot{\boldsymbol{p}} = -\frac{\partial H}{\partial \boldsymbol{q}} + \boldsymbol{\tau}, \tag{5b}$$

where $\boldsymbol{\tau}$ is the (scaled) generalized force. We will define the Jacobians of the Hamiltonian as column vectors.

b) Generalized force

The system is actuated by leading a current I through the tether. The Lorentz force per unit length tether induced by the current can be written as,

$$\bar{\boldsymbol{F}}_e = I\boldsymbol{r} \times \boldsymbol{B}, \tag{6}$$

where $\boldsymbol{B}$ is the magnetic field of the Earth. The total generalized force can be found by projecting the force onto the generalized coordinates and integrating along the tether. By describing the points along the tether as $\bar{\boldsymbol{r}} = s\boldsymbol{r}$ for $s \in [0\ l]$ the generalized force $\boldsymbol{\tau} = [\tau_\theta\ \tau_\varphi]^T$ can be written,

$$\tau_\theta = \int_0^l \bar{\boldsymbol{F}}_e \cdot \frac{\partial \bar{\boldsymbol{r}}}{\partial \theta}\ ds, \tag{7a}$$

$$\tau_\varphi = \int_0^l \bar{\boldsymbol{F}}_e \cdot \frac{\partial \bar{\boldsymbol{r}}}{\partial \varphi}\ ds. \tag{7b}$$

A common way to model the magnetic field of the Earth is to use a dipole model with dipole moment along the rotational axis of the Earth. One advantage of this model is that it is independent of the rotation of the Earth. Along a circular orbit the magnetic field from such a dipole can be described in the local frame as,

$$\boldsymbol{B} = \frac{\mu_m}{R_o^3} \begin{bmatrix} -2\sin\nu\sin i & \cos\nu\sin i & \cos i \end{bmatrix}^T, \tag{8}$$

where μ_m is the strength of the dipole and R_o is the radius of the orbit. The orbit inclination i describes how much the orbit plane is tilted compared to the equatorial plane of the Earth. It is assumed that the magnetic field do not vary along the length of the tether. Inserting the B-field in (6) and (7) the generalized force can be written in the affine form,

$$\boldsymbol{\tau} = \boldsymbol{b}(\boldsymbol{q}, \nu)u, \tag{9}$$

where u is a dimensionless quantity proportional to the input current,

$$u = \frac{3}{2} \frac{1}{3m_A + m_t} \frac{\mu_m}{\mu} I. \tag{10}$$

The proportionality constant is merged by the constant terms from the Lagrangian, the B-field and the projection of the Lorentz force. For simplicity u will be used as control input to the system. The input function $\boldsymbol{b}(\nu, \boldsymbol{q}) = [b_\theta(\nu, \boldsymbol{q})\ b_\varphi(\nu, \boldsymbol{q})]^T$ can be written as,

$$b_\theta = \cos^2 \varphi \tan \varphi \sin i \left(\cos \nu \sin \theta - 2 \sin \nu \cos \theta\right) - \cos^2 \varphi \cos i, \tag{11a}$$

$$b_\varphi = \sin i \left(\cos \theta \cos \nu + 2 \sin \theta \sin \nu\right). \tag{11b}$$

In the case of an equatorial orbit $(i = 0°)$ the input function will be time invariant, for all other cases the input function is time-periodic. This periodicity is induced by the variations of the magnetic field along the orbit. For a constant input u the input function will act as a periodic forcing term in which case a family of periodic solutions occur. In [3] these solutions was investigated and found to be unstable. The total system description can be written as,

$$\dot{\boldsymbol{q}} = \frac{\partial H}{\partial \boldsymbol{p}}, \tag{12a}$$

$$\dot{\boldsymbol{p}} = -\frac{\partial H}{\partial \boldsymbol{q}} + \boldsymbol{b}(\nu, \boldsymbol{q})u. \tag{12b}$$

Introducing the state vector $\boldsymbol{x} = \begin{bmatrix} \boldsymbol{q}^T & \boldsymbol{p}^T \end{bmatrix}^T$ the equation can be written in the compact form,

$$\dot{\boldsymbol{x}} = \boldsymbol{J}\frac{\partial H}{\partial \boldsymbol{x}} + \boldsymbol{g}(\nu, \boldsymbol{q})u, \tag{13}$$

where the matrix $\boldsymbol{J}$ is defined using $n \times n$ unit matrices $\boldsymbol{I}$,

$$\boldsymbol{J} = \begin{bmatrix} \boldsymbol{0} & \boldsymbol{I} \\ -\boldsymbol{I} & \boldsymbol{0} \end{bmatrix}. \tag{14}$$

The input function can be written as,

$$\boldsymbol{g}(\nu, \boldsymbol{q}) = \begin{bmatrix} \boldsymbol{0} \\ \boldsymbol{b}(\nu, \boldsymbol{q}) \end{bmatrix}. \tag{15}$$

III   Control Design

The Lorentz force used to perform orbit maneuvers with the tether system is only generated for an input current different from zero $u \neq 0$, which will destroy the open-loop equilibrium. Ideally the control objective for the system should be to stabilize the tether away from the open-loop equilibrium. This is, however, a hard task due to the time-periodic and underactuated nature of the system. Instead one could try to stabilize the periodic solutions of the system.

The present control design used to stabilize the periodic solutions is based on the design presented in [6] for stabilizing the open-loop equilibrium. The first step in the design is to define an output for the system as,

$$y = \boldsymbol{b}^T (\nu, \boldsymbol{q}) \frac{\partial H}{\partial \boldsymbol{p}} = b_\theta \dot{\theta} + b_\varphi \dot{\varphi}. \tag{16}$$

Note that from Hamilton's equation (5) the partial derivative $\frac{\partial H}{\partial \boldsymbol{p}}$ is seen to be the generalized velocity $\dot{\boldsymbol{q}}$. The output is chosen to establish a passive input-output connection from which a stabilizing control can be designed as $u = -ky$, $k > 0$ (see [9]). The resulting closed loop system becomes,

$$\dot{\boldsymbol{x}} = (\boldsymbol{J} - k\boldsymbol{R}) \frac{\partial H}{\partial \boldsymbol{x}}, \tag{17}$$

where $\boldsymbol{R}$ is the positive semidefinite matrix,

$$\boldsymbol{R} = \begin{bmatrix} \boldsymbol{0} & \boldsymbol{0} \\ \boldsymbol{0} & \boldsymbol{R}_2 \end{bmatrix}, \qquad \boldsymbol{R}_2 = \begin{bmatrix} b_\theta^2 & b_\theta b_\varphi \\ b_\theta b_\varphi & b_\varphi^2 \end{bmatrix}. \tag{18}$$

Using H as a positive definite Lyapunov candidate the time derivative is,

$$\dot{H} = \left(\frac{\partial H}{\partial \boldsymbol{x}} \right)^T (\boldsymbol{J} - k\boldsymbol{R}) \frac{\partial H}{\partial \boldsymbol{x}}$$
$$= -k \left(\frac{\partial H}{\partial \boldsymbol{p}} \right)^T \boldsymbol{R}_2 \frac{\partial H}{\partial \boldsymbol{p}}. \tag{19}$$

From (19) and LaSalle's theorem [10, Theorem 4.4, p. 128] asymptotically stability can be stated for the origin of the closed loop system. Since the feedback connection is adding damping to the open-loop system the term $-ky$ will be referred to as damping injecting. To force the trajectory away from the open-loop equilibrium a bias term v is added to the control law to obtain the final feedback connection,

$$u = -ky + v. \tag{20}$$

The idea is to investigate the effect that damping injection will have on the already known unstable periodic solutions.

The control law will, as we will see in the next section, stabilize a family of periodic solutions. This family can be seen as the family found in [3] perturbed by the controller gain k. The control law is simple compared to some of the other approaches know to the authors, mainly since the approach does not need a reference trajectory of the orbit which is intended to be stabilized. One can argue that the stabilized periodic solutions is in fact another family of solutions compared to the open-loop solutions.

IV   Closed Loop Analysis

In this section the closed loop system will be investigated using mainly numerical tools. All the numerical investigations of the system are carried out using an orbit inclination of $i = 45°$.

a)   Series approximation of the periodic solutions

A common way to find periodic solutions in dynamical systems is to use a perturbation method called the Poincaré-Lindstedt method (see [11, Chap. 7]). Assuming that we know a solution for a certain parameter value ε_0 the basic idea is to expand the solution using a power series in terms of this parameters, obtaining solutions valid for small parameter variations of ε. For simplicity and without loss of generality we can assume that $\varepsilon_0 = 0$. To illustrate the method we consider a forced linear system,

$$\dot{\boldsymbol{x}}(t,\varepsilon) = \boldsymbol{A}(t,\varepsilon)\boldsymbol{x}(t,\varepsilon) + \boldsymbol{b}(t,\varepsilon), \tag{21}$$

where $\boldsymbol{A}$ and $\boldsymbol{b}$ are periodic in t. The solution $\boldsymbol{x}(t,\varepsilon)$, the system matrix $\boldsymbol{A}(t,\varepsilon)$ and the forcing term $\boldsymbol{b}(t,\varepsilon)$ can be written as power series of ε,

$$\boldsymbol{x}(t,\varepsilon) = \boldsymbol{x}_0(t) + \varepsilon\boldsymbol{x}_1(t) + \varepsilon^2\boldsymbol{x}_2(t) + \ldots \tag{22a}$$
$$\boldsymbol{A}(t,\varepsilon) = \boldsymbol{A}_0(t) + \varepsilon\boldsymbol{A}_1(t) + \varepsilon^2\boldsymbol{A}_2(t) + \ldots \tag{22b}$$
$$\boldsymbol{b}(t,\varepsilon) = \boldsymbol{b}_0(t) + \varepsilon\boldsymbol{b}_1(t) + \varepsilon^2\boldsymbol{b}_2(t) + \ldots \tag{22c}$$

Inserting these into the differential equation (21) and separating the equation for each power of ε the following equations occur,

$$\dot{\boldsymbol{x}}_0 = \boldsymbol{A}_0\boldsymbol{x}_0 + \boldsymbol{b}_0, \tag{23a}$$
$$\dot{\boldsymbol{x}}_1 = \boldsymbol{A}_0\boldsymbol{x}_1 + \boldsymbol{A}_1\boldsymbol{x}_0 + \boldsymbol{b}_1, \tag{23b}$$
$$\dot{\boldsymbol{x}}_2 = \boldsymbol{A}_0\boldsymbol{x}_2 + \boldsymbol{A}_1\boldsymbol{x}_1 + \boldsymbol{A}_2\boldsymbol{x}_0 + \boldsymbol{b}_2, \tag{23c}$$
$$\dot{\boldsymbol{x}}_3 = \qquad \ldots \tag{23d}$$
$$\vdots$$

where it is understood that all quantities are function of t. The first equation (23a) corresponds to the system equation for $\varepsilon = 0$, for which the solution $\boldsymbol{x}_0(t)$ is assumed known. The solution $\boldsymbol{x}_0(t)$ occurs in the forcing term for the equation of $\boldsymbol{x}_1(t)$, which has the same system matrix $\boldsymbol{A}_0$ as the known solution. The solutions $\boldsymbol{x}_0(t)$ and $\boldsymbol{x}_1(t)$ act as forcing terms of the $\boldsymbol{x}_2(t)$ equation and so on. In this way the solution $\boldsymbol{x}_m(t)$ can be found from knowledge of the solutions

$\boldsymbol{x}_0(t), \boldsymbol{x}_1(t), \ldots, \boldsymbol{x}_{m-1}(t)$. The constants of integration should be chosen to avoid terms which lead to unstable solutions in the higher order equations.

In the present study the method is expanded to include two parameters and the solutions is expanded in the kv parameter plane. Due to the periodic forcing term we will limit our attention to periodic solutions with the same period. Since the natural frequency of the out-of-plane motion is a multiple of the forcing frequency, all integration constants must be chosen as zero to avoid unstable terms. Using a linearised version of the state space equation the solutions of order three are found, where c_i and s_i are short notation for $\cos i$ and $\sin i$,

$$
\begin{aligned}
\theta(\nu) = & -\frac{c_i}{3}v + \frac{s_i^2}{3}\sin(2\nu)\,v^2 + \frac{c_i s_i^2}{6}\sin(2\nu)\,vk \\
& + \frac{2}{9}c_i s_i^2\left(\cos(2\nu) + \frac{1}{3}\right)v^3 \\
& + \frac{s_i^2}{3}\Big(\frac{s_i^2}{260}\cos(4\nu) + \\
& \quad \frac{7}{3}\left(c_i^2 - \frac{2}{35}s_i^2\right)\cos(2\nu) - \frac{1}{9}\left(c_i^2 + \frac{1}{4}s_i^2\right)\Big)v^2 k \\
& + \frac{c_i s_i^2}{13}\Big(\frac{s_i^2}{40}\cos(4\nu) + \\
& \quad \frac{13}{3}\left(c_i^2 + \frac{1}{30}s_i^2\right)\cos(2\nu) + \frac{13}{216}s_i^2\Big)vk^2 + \ldots
\end{aligned}
\tag{24a}
$$

$$
\begin{aligned}
\phi(\nu) = & \frac{s_i}{3}\cos(\nu)\,v - \frac{2c_i s_i}{9}\sin(\nu)\,v^2 \\
& + \frac{s_i^3}{36}\left(-\frac{3}{5}\sin(3\nu) + \sin(\nu)\right)vk \\
& + \frac{s_i^3}{9}\left(\frac{3}{5}\cos(3\nu) + \cos(\nu)\right)v^3 \\
& + \frac{c_i s_i^3}{9}\left(-\frac{2}{5}\cos(3\nu) + 2\cos(\nu)\right)v^2 k \\
& - \frac{s_i^3}{30}\Big(\frac{s_i^2}{56}\cos(5\nu) + \left(c_i^2 + \frac{13}{120}s_i^2\right)\cos(3\nu) - \\
& \quad\quad \frac{5}{3}\left(c_i^2 - \frac{1}{20}s_i^2\right)\cos(\nu)\Big)vk^2 + \ldots
\end{aligned}
\tag{24b}
$$

To obtain periodic solutions which matches the nonlinear system better, the method is extended to the take the nonlinearities in the system into account. This is done by expanding the nonlinearities into Taylor series. This leads to a more complicated solution scheme than shown in (23), but the basic solution (23a) and the feature that solutions act as forcing terms for the higher order equations, remains unchanged. From this method the following periodic

solutions are obtained,

$$\theta(\nu) = -\frac{c_i}{3}v + \frac{4s_i^2}{9}\sin(2\nu)v^2 + \frac{c_is_i^2}{6}\sin(2\nu)vk$$
$$+ \frac{c_i}{18}\left(\frac{23}{3}s_i^2\cos(2\nu) + \left(-\frac{4}{9}c_i^2 + s_i^2\right)\right)v^3$$
$$+ \frac{s_i^2}{18}\left(\frac{s_i^2}{65}\cos(4\nu) + \right.$$
$$\left.20\left(c_i^2 - \frac{7}{150}s_i^2\right)\cos(2\nu) - \frac{1}{3}s_i^2\right)v^2k$$
$$+ \frac{c_is_i^2}{13}\left(\frac{s_i^2}{40}\cos(4\nu) + \right.$$
$$\left.\frac{13}{3}\left(c_i^2 + \frac{1}{30}s_i^2\right)\cos(2\nu) + \frac{13}{216}s_i^2\right)vk^2 + \ldots \tag{25a}$$

$$\phi(\nu) = \frac{s_i}{3}\cos(\nu)v - \frac{2c_is_i}{9}\sin(\nu)v^2$$
$$+ \frac{s_i^3}{36}\left(-\frac{3}{5}\sin(3\nu) + \sin(\nu)\right)vk$$
$$+ \frac{s_i}{27}\left(\frac{58}{15}s_i^2\cos(3\nu) + \frac{1}{2}\left(c_i^2 + 4s_i^2\right)\cos(\nu)\right)v^3$$
$$+ \frac{c_is_i^3}{9}\left(-\frac{3}{5}\cos(3\nu) + \frac{5}{3}\cos(\nu)\right)v^2k$$
$$- \frac{s_i^3}{30}\left(\frac{s_i^2}{56}\cos(5\nu) + \left(c_i^2 + \frac{13}{120}s_i^2\right)\cos(3\nu) - \right.$$
$$\left.\frac{5}{3}\left(c_i^2 - \frac{1}{20}s_i^2\right)\cos(\nu)\right)vk^2 + \ldots \tag{25b}$$

Without damping injection $k = 0$ the solution coincides with the open-loop solution found in [3] and without the bias term $v = 0$ the periodic solution vanishes to the origin which is in agreement with the fact that the damping injection stabilizes the origin. The method of finding periodic solutions is implemented using MAPLE and the solutions shown in this paper are of order seven.

b)   Properties of periodic solutions

Fig. 2 shows the solution for $k = 0.5$ and $v = \pm 0.5$ along with a numerical simulations of the two sets of parameters. One problem of using a perturbation method is that the convergence of the solutions is only guaranteed for small changes of the parameters. The present solution appears to converge inside a unit circle of the parameter plane for $k > 0$. For the simulations shown in Fig. 2 it is seen that the simulation of $v = 0.5$ converges closer to the series approximation than the solution of $v = -0.5$.

The offset of the solutions along the θ-axis is determine by the sign of the bias term corresponding to the direction of the current. This sign determines if electrical energy is converted to orbital energy or vice versa. From (25) it is seen that $\theta(\nu)$ only consist of frequencies of even multiple of the orbit rate,
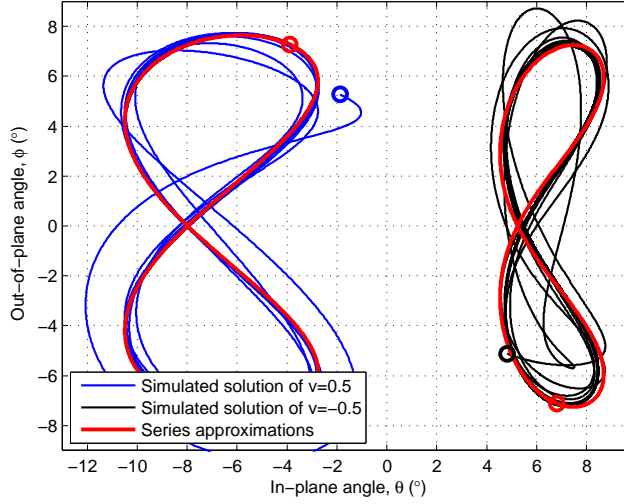
Figure 2: Series approximation of the periodic solutions with $k = 0.5$ and $v = \pm 0.5$. The solutions at $t = 0$ are marked with $\circ$.

while $\varphi(\nu)$ consist of frequencies of odd multiples. This is a consequence of the way the solutions are affecting each other through the forcing terms. This property implies that $\theta(\nu) = \theta(\nu + \pi)$ and $\varphi(\nu) = -\varphi(\nu + \pi)$. This corresponds to symmetric solutions around the θ-axis, which is also seen from the simulation in Fig. 2. Seen from a physical point of view, this symmetry is induced by the symmetry of the aligned dipole model approximating the magnetic field.

c) Region of stable periodic solutions

In this section Floquet theory is applied on a linearised version of the closed loop system to determine the stability of the periodic solutions. A linearisation of the system closed by the feedback loop $u = -ky + v$ can be written as,

$$\dot{\boldsymbol{x}} = \boldsymbol{A}_{cl}\left(\nu, k, v, i\right)\boldsymbol{x} + \boldsymbol{b}_{cl}\left(\nu, k, v, i\right), \qquad (26)$$

where $\boldsymbol{A}_{cl}$ and $\boldsymbol{b}_{cl}$ are $T = 2\pi$ periodic in ν and given as,

$$\boldsymbol{A}_{cl}\left(\nu, k, v, i\right) = \begin{bmatrix} 0 & 0 & 1 & 0 \\ 0 & 0 & 0 & 1 \\ -3 & -2vs_i\sin\nu & -kc_i^2 & kc_is_i\cos\nu \\ 2vs_i\sin\nu & -4 & kc_is_i\cos\nu & -ks_i^2\cos^2\nu \end{bmatrix}, \quad (27a)$$

$$\boldsymbol{b}_{cl}\left(\nu, k, v, i\right) = \begin{bmatrix} 0 & 0 & -c_i & s_i\cos\nu \end{bmatrix}^T. \qquad (27b)$$
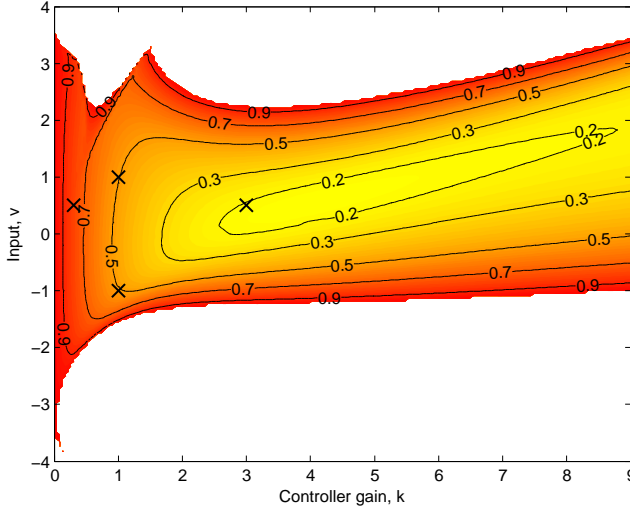
Figure 3: Stability region in the parameter plane. Simulations of the system are shown in fig. 4 for the points in the parameters plane marked with ×.

The deviation from the periodic solution $\boldsymbol{x}_p(\nu)$ can be found from the variational equation by writing the solution as $\boldsymbol{x}(\nu) = \boldsymbol{x}_p(\nu) + \boldsymbol{\eta}(\nu)$. The deviation $\boldsymbol{\eta}(\nu)$ obeys the differential equation,

$$\dot{\boldsymbol{\eta}}(\nu) = \boldsymbol{A}_{cl}\left(\nu, k, v, i\right)\boldsymbol{\eta}(\nu), \tag{28}$$

hence the stability of the periodic solutions can be found from a Floquet analysis of $\boldsymbol{A}_{cl}$. In this work the characteristic multipliers ρ_j are found from numerical integration of the system. Alternatively they could be found as power series similar to those describing the periodic solutions. One advantage of using the numerical method is that the limitations in the region of convergence for the series solution is avoided. Fig. 3 shows the magnitude of the stability deciding multiplier ρ, i.e. the multiplier of largest magnitude. For clarity the multiplier is only shown in the stable region, $|\rho| < 1$. The characteristic multiplier indicates how fast the deviation $\boldsymbol{\eta}(\nu)$ converges to zero, i.e. the settling time of the solution. Fig. 3 shows that a minimum exist of the multiplier. This can be seen as an analogy to a LTI system where an increasing damping coefficient eventually will lead to an overdamped system, hence the settling time will increase, resulting in a slower convergence. It was demonstrated by Peláez et al. [3] that the open-loop periodic solutions exhibit a weakly unstable behaviour (i.e. $|\rho| = 1$) up until a certain level v^* where the deciding multiplier moves outside the unit circle. The same is indicated in Fig. 3 where $v^* \approx \pm 3.5$, which is in agreement with [3].

(a) $k = 0.3$, $v = 0.5$, $\rho \approx 0.79$

(b) $k = 3$, $v = 0.5$, $\rho \approx 0.19$

(c) $k = 1$, $v = 1$, $\rho \approx 0.51$

(d) $k = 1$, $v = -1$, $\rho \approx 0.51$
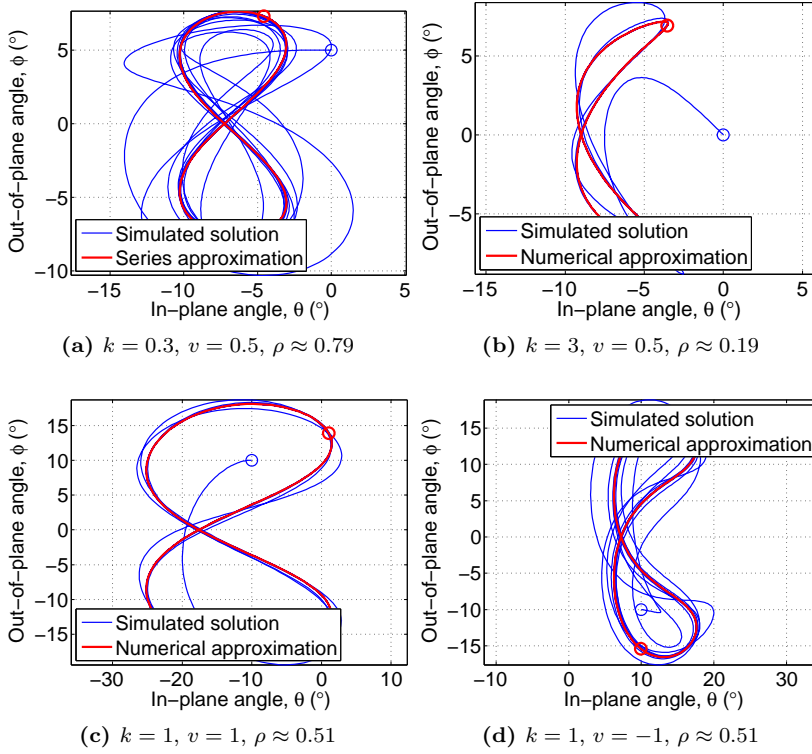
Figure 4: Simulations of closed loop system using four different parameter sets from the stable region.

Fig. 4 shows simulations using different parameters from the stable part of the parameter plane. In Fig. 4a the series solution is shown along with the simulation, and it is seen that the trajectory in fact converges towards this periodic solution. For the simulation in Figures 4b, 4c and 4d the reference trajectory is found from a numerical simulation, since the series solution do not converge in this part of the parameter plane. Consequently it is no surprise that the solution in these cases goes towards the periodic solution. The difference in convergence is clearly illustrated in Figures 4a and 4b, where the increase of controller gain has resulted in a larger damping of the deviation, hence a faster settling time. The simulations in Figures 4c and 4d have similar deciding multipliers, however, from the figures it seems that the solution in Fig. 4c has a faster convergence than the solution in Fig. 4d, despite the similar multiplier.

Using the characteristic multipliers the (complex) solution to the equation of

variation (28) can be written assuming distinct multipliers as,

$$\boldsymbol{\eta}(\nu) = \sum_{j=1}^{2n} c_j \rho_j^{\frac{\nu}{T}} \boldsymbol{\psi}_j(\nu), \tag{29}$$

where $\boldsymbol{\psi}_j(\nu)$ are a T-periodic functions and c_j are constant. Ignoring other than the term of the deciding multiplier the norm of the deviation can be written as,

$$\|\boldsymbol{\eta}(\nu)\| \approx c \, |\rho|^{\frac{\nu}{T}} \, \|\boldsymbol{\psi}(\nu)\| \,. \tag{30}$$

Since $\boldsymbol{\psi}(\nu)$ is a T-periodic function it is seen that the term $|\rho|^{\frac{\nu}{T}}$ will determine the convergence of the solution. Fig. 5 shows $\|\boldsymbol{\eta}(\nu)\|$ together with the convergence term $|\rho|^{\frac{\nu}{T}}$ and it is seen that the deviation follows the convergence term. The difference between the $\|\boldsymbol{\eta}(\nu)\|$ and the convergence term has three main reasons: the remaining multipliers which will have the most profound effect in the beginning of the simulation; the periodic function $\boldsymbol{\psi}(\nu)$ which effect will be averaged out over a period; and the nonlinearities in the system.

V   Discussion

One open question is how the stabilized periodic solutions can be utilized to create a strategy for performing orbit maneuvers. The main task in this connection would be to investigate what effect a tether following a periodic solution will have on the orbit parameters. The changes in the orbit parameters due to an electrical tether have been investigated in several papers (see [12]), but, to the knowledge of the authors, not for a tether following a periodic trajectory. In this connection one would expect that it do not matter if the open-loop periodic solutions or a perturbed version of these are stabilized. The region of attraction of each solution should also be investigated further, since it will influence the transition between two periodic solutions.

VI   Conclusion

A controller to stabilize periodic solutions of an electrodynamic tether system was investigated in this paper. The controller was based on a control design providing damping injection for the open-loop equilibrium. A series approximation of the solution was found in state space and the stability was investigated numerically in the parameter plane. It was shown that there exists a minimum of the stability deciding characteristic multiplier in the parameter plane

(a) $k = 0.3$, $v = 0.5$, $\rho \approx 0.79$

(b) $k = 3$, $v = 0.5$, $\rho \approx 0.19$

(c) $k = 1$, $v = 1$, $\rho \approx 0.51$

(d) $k = 1$, $v = -1$, $\rho \approx 0.51$
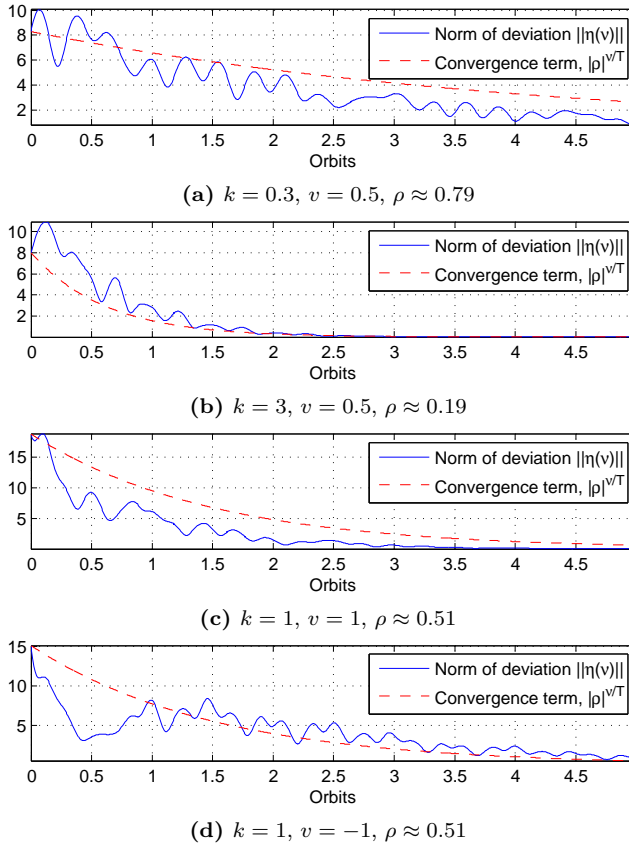
Figure 5: Convergence towards the periodic solutions, for the previously used parameters.

and that the convergence towards the periodic solutions was determined by the characteristic multipliers found from a linear Floquet analysis.

References

[1] Vladimir V. Beletsky and Evgenii M. Levin. *Dynamics of space tether systems*, volume 83 of *Advances in the astronautical sciences*. American Astronautical society, 1993.

[2] M. P. Cartmell and D. J. McKenzie. A review of space tether research.

Progress in Aerospace Sciences, 44(1):1–21, 2008. ISSN 0376-0421. doi: 10.1016/j.paerosci.2007.08.002.

[3] J. Peláez, E. C. Lorenzini, O. López-Rebollal, and M. Ruiz. A new kind of dynamic instability in electrodynamic tethers. *Journal of the Astronautical Sciences*, 48(4):449–476, 2000. ISSN 0021-9142.

[4] M. B. Larsen and M. Blanke. Nonlinear control of electrodynamic tether in equatorial or somewhat inclined orbits. In *Proc. Mediterranean Conference on Control & Automation MED '07*, pages 1–6, 2007. doi: 10.1109/MED. 2007.4433876.

[5] Xiang Zhou, Junfeng Li, H. Baoyin, and Vadim Zakirov. Equilibrium control of electrodynamic tethered satellite systems in inclined orbits. *Journal of Guidance, Control, and Dynamics*, 29(6):1451–1454, 2006. ISSN 0731-5090. doi: 10.2514/1.21882.

[6] M. B. Larsen and M. Blanke. Control by damping injection of electrodynamic tether system in an inclined orbit. In *Proc. ACC '09. American Control Conference*, pages 4824–4829, 2009. doi: 10.1109/ACC.2009.5159896.

[7] J. Peláez and E. C. Lorenzini. Libration control of electrodynamic tethers in inclined orbit. *Journal of Guidance, Control, and Dynamics*, 28(2):269–279, 2005. ISSN 0731-5090.

[8] Paul Williams. Energy rate feedback for libration control of electrodynamic tethers. *Journal of Guidance, Control, and Dynamics*, 29(1):221–223, 2006. ISSN 0731-5090.

[9] Arjan van der Schaft. L_2-*Gain and Passivity in Nonlinear Control*. Communications and Control Engineering. Springer-Verlag New York, Inc., Secaucus, NJ, USA, second edition, 2000. ISBN 1-85233-073-2.

[10] Hassan K. Khalil. *Nonlinear Systems*. Prentice Hall, third edition, 2002. ISBN 0130673897.

[11] R. Grimshaw. *Nonlinear Ordinary Differential Equations*. Blackwell Scientific Publications, 1990.

[12] Paul Williams. Optimal orbital transfer with electrodynamic tether. *Journal of Guidance, Control, and Dynamics*, 28(2):369–372, 2005. ISSN 0731-5090.

Passivity-based control of a rigid electrodynamic tether[1]

Abstract

Electrodynamic tethers provide actuation for performing orbit correction of spacecrafts. When an electrodynamic tether system is orbiting the Earth in an inclined orbit, periodic changes in the magnetic field result in a family of unstable periodic solutions in the attitude motion. This paper shows how these periodic solutions can be stabilized by controlling only the current through the tether. A port-controlled Hamiltonian formulation is employed to describe the tethered satellite system and a passive input-output connection is utilized in the control design. The control law consists of two parts, a feedback connection, which stabilizes the open-loop equilibrium, and a bias term, which is able to drive the system trajectory away from this equilibrium, a feature necessary to obtain orbit adjustment capabilities of the electrodynamic tether. It is then shown how the periodic solutions of the closed-loop system can be approximated by power series and a relation is found between control gain and perturbations around the open-loop solution. Stability properties of the system are investigated using Floquet analysis and the region of stability is found in the plane defined by the control parameters.

---

[1]Submitted to *Journal of Guidance, Control, and Dynamics.*

Nomenclature

$\boldsymbol{A}$	=	System matrix of open-loop system
$\boldsymbol{A}_k$	=	System matrix related to the feedback loop
$\boldsymbol{A}_v$	=	System matrix related to the bias term
$\boldsymbol{B}$	=	Magnetic field of the Earth, T
$\boldsymbol{B}_Z$	=	Aligned dipole approximation of $\boldsymbol{B}$, T
$\boldsymbol{b}$	=	Input function
c_i	=	Short notation for $\cos i$
$\boldsymbol{F}_e$	=	Lorentz force per unit length tether, N
$\boldsymbol{g}$	=	Input function in PCH framework
H	=	Non-dimensional Hamiltonian
$\mathcal{H}$	=	Hamiltonian, J
I	=	Current through tether, A
i	=	Orbit inclination, rad
$\boldsymbol{J}$	=	Interconnection matrix
k	=	Controller gain
k^*	=	Optimal controller gain
$\mathcal{L}$	=	Lagrangian, J
l	=	Length of tether, m
$\boldsymbol{M}$	=	Monodromy matrix
m_A	=	Mass of sub-satellite, kg
m_B	=	Mass of main satellite, kg
m_t	=	Mass of tether, kg
$\boldsymbol{p}$	=	Non-dimensional generalized momenta, $\boldsymbol{p} = [p_\theta \; p_\varphi]^T$
p_θ	=	Generalized momentum associated with θ
p_φ	=	Generalized momentum associated with φ
$\boldsymbol{Q}$	=	Non-dimensional generalized force
$\boldsymbol{q}$	=	Generalized coordinates $\boldsymbol{q} = [\theta \; \varphi]^T$, rad
$\boldsymbol{R}$	=	Damping matrix
$\boldsymbol{r}$	=	Unit vector along the tether
s_i	=	Short notation for $\sin i$
u	=	Control input
v	=	Bias term
$\boldsymbol{x}$	=	State vector
y	=	System output
θ	=	In-plane angle, rad
Λ	=	Collection of tether parameters, Nm
$\lambda_{\max}$	=	Largest eigenvalue of damping matrix
μ	=	Standard gravitation parameter of the Earth, $\mathrm{m}^3\mathrm{s}^{-2}$
μ_m	=	Strength of the magnetic field, Tm^3
ν	=	Argument of latitude (time variable), rad

$$
\begin{array}{lll}
\rho & = & \text{Stability-deciding characteristic multiplier} \\
\rho_j & = & \text{Characteristic multipliers} \\
\boldsymbol{\tau} & = & \text{Generalized force } \boldsymbol{\tau} = [\tau_\theta \ \tau_\varphi]^T, \text{ Nm} \\
\boldsymbol{\Phi} & = & \text{Fundamental matrix} \\
\varphi & = & \text{Out-of-plane angle, rad} \\
\Omega & = & \text{Right ascension of the ascending node, rad} \\
\omega & = & \text{Orbit rate, rad/s}
\end{array}
$$

I   Introduction

A tethered satellite system (TSS) is a system of two or more satellites connected with cables. TSS's have been proposed in connection with numerous different tasks and for several missions, and have therefore been the subject of much research over the last three decades (see [1, 2] for reviews). In this work we will consider a TSS consisting of two satellites, a main satellite and a sub-satellite, connected by an electrodynamic tether (EDT). An electrodynamic tether provides a means of performing orbit maneuvers using only electrical power. The system acts as an actuator for the orbit motion by generating an electrodynamic force (the Lorentz force) acting along the tether. By collecting electrons from the surrounding plasma and emitting them from dedicated electron emitters, a current can be led through the tether. Interaction of this current with the magnetic field of the Earth creates a Lorentz force that influences the trajectory of the satellite. This controllable force could be used to perform orbit adjustments, and electrodynamic tethers have been proposed for deorbiting obsolete satellites [3, 4], for altitude adjustment of the international space station [5] and for rebooting in connection with momentum exchange between satellites [6].

There are several control tasks associated with an electrodynamic tether system. Tether vibration control [7] damps vibration along a flexible tether; orbit control [8, 9] changes one or more of the orbit parameters; and attitude control deals with stabilizing libration of the satellite-tether system [10, 11]. This work treats the attitude problem. Control of the attitude motion is required in order to utilize the Lorentz force for the desired orbit corrections. The attitude control problem is difficult since control of current alone leaves the attitude dynamics under-actuated, and instantaneous forces are always perpendicular to the instantaneous B-field. This problem is also well known when dealing with attitude control using magnetic coils [12]. Common assumptions when dealing with the attitude control problem are to model the tether as a rigid rod and ignore the orbit changes caused by the Lorentz force. These assumptions will also be made in this study.

An electrodynamic tether system was investigated in [13] assuming a constant current was passed through the tether. In this case the Lorentz force, acting as a periodic forcing term, was shown to give rise to unstable periodic solutions of the attitude motion. When driven by a constant current, energy is pumped into the attitude motion and active current control is needed to stabilize the motion. Looking into the deorbiting problem, a simple switching control law was presented in [14], where the current was switched on and off depending on the level of a Lyapunov function. Ref. [15] showed that stabilization of the open-loop equilibrium of the TSS was possible using feedback linearization. Due to zeros in the input function, the primary control law contained singularities. This problem was handled by switching to a secondary control law in proximity of a singularity. Generation of a Lorentz force and ability to influence the orbit of a TSS is the prime purpose of an electrodynamic tether. This requires the tether to carry a non-zero current, but will also drive the attitude system away from its open-loop equilibrium. The ability to stabilize the attitude away from the equilibrium is therefore crucial. An commonly explored control strategy for the attitude dynamics is stabilization of open-loop periodic solutions. Two control laws were investigated by [10] with this purpose. The first approach used a feedback of the difference between the present trajectory and a reference trajectory. The second used time-delayed autosynchronization, where the difference between the present trajectory and a one-period-delayed trajectory was used in the feedback loop. Stabilization was obtained using additional actuators. Examining energy considerations, Williams [16] stabilized the periodic solutions by synchronization between the system energy and the energy of a reference trajectory. Considering the combined attitude and orbit control problem using Gauss's planetary equations for modeling the orbit changes, the recent work [11] used numerical predictive control and time-delayed feedback after having discretized the system dynamics.

This article suggests a solution to the attitude control problem for the tethered satellite system using a passivity-based control law, based on a port-controlled Hamiltonian (PCH) formulation of the dynamics. A control law that adds damping to the open-loop system is shown to make the open-loop equilibrium asymptotically stable. It is discussed how, by adding a bias term, open-loop periodic solutions can be stabilized. The proposed time-varying control law is shown to have the advantage of being static in the sense that no delayed signals or reference trajectories are used. Properties of the closed-loop periodic solutions are investigated and compared to the open-loop solutions. The work presented in this article is an extension of results presented in [17] and [18].

The outline of the article is as follows: Section II derives the equations of motion for the system and formulates it as a port-controlled Hamiltonian system such that a passive input-output connection is created. Sections III and IV consider the control design for stabilization of the open-loop equilibrium and the open-

loop periodic solutions, and bounds are provided for the region of convergence for the time-varying controller. Finally section VI offers conclusions.

a) Notation

The notation $\boldsymbol{r}^T$ and $\boldsymbol{A}^T$ will be used to denote the transpose of a vector $\boldsymbol{r}$ or a matrix $\boldsymbol{A}$. The derivative of a scalar or a vector function (H or $\boldsymbol{x}$) with respect to the argument of latitude will be denoted $\dot{H}$ or $\dot{\boldsymbol{x}}$. The Jacobian of a scalar function will be defined as a column vector, hence $\frac{\partial H}{\partial \boldsymbol{x}}$ is a column vector. Identity matrices are denoted $\boldsymbol{I}$, where dimensions should be clear from the context.

II   Model

Consider a TSS consisting of a main satellite and a sub-satellite connected by an electrodynamic tether. The satellites have masses m_B and m_A and are treated as point masses. The tether has mass m_t and length l. The system will not be considered during the deployment and retrieval phases, hence the length of the tether is assumed constant. For simplicity it is assumed that the mass of the main satellite comprises the main contribution to the total mass $m_B \gg m_A + m_t$, and the center of mass (CM) of the system can therefore be assumed to coincide with that of the main satellite. Only the effect of the EDT on the attitude motion is modeled, and no additional orbit-perturbing forces are included, hence the CM follows a Keplerian orbit. Further, the system is orbiting the Earth in an assumed circular orbit. The orbit plane of the circular orbit can be described by two of the orbit parameters, the right ascension of the ascending node Ω and the inclination i, illustrated in Fig. 1. The orbit position is described by the argument of latitude in this paper, where the orbit is circular with nonzero inclination. The argument of latitude is denoted ν, which is measured from the direction of the ascending node. In case the inclination was zero, the true longitude would be used instead. The orbit rate $\omega = \frac{d\nu}{dt}$ is constant and ν is therefore adopted as the independent variable of the model. The attitude motion is described in the orbit frame spanned by the x, y, and z axes. The x-axis is placed along a vector from the Earth to the CM, the y-axis is directed along the orbit velocity, and the z-axis is normal to the orbit plane. The orbit frame can be found from an Euler rotation of the inertial frame using the angles Ω, i and ν as indicated in Fig. 1. The inertial frame does not rotate with the Earth and is defined by the X, Y and Z axes. The X-axis is in the direction of the vernal point, and the Z-axis coincides with the rotational axis
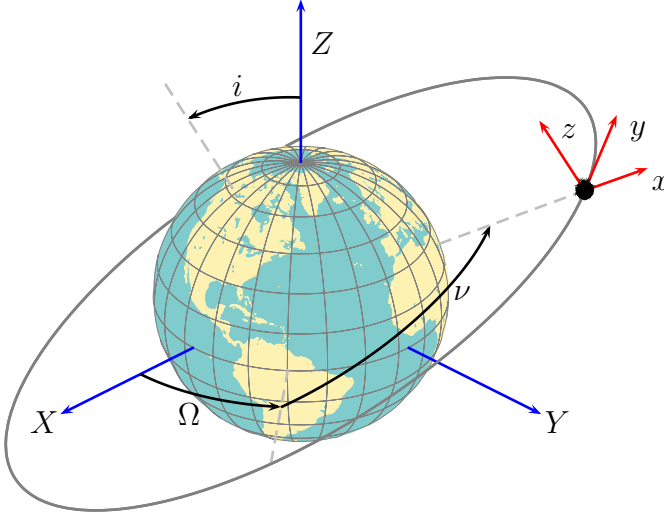
Figure 1: Orbit description of a circular orbit and the orbit frame.

of the Earth. The attitude of the TSS is described by a unit vector $\boldsymbol{r}$ from the main satellite to the sub-satellite. The system has two stable equilibria due to the gravity gradient. They occur when $\boldsymbol{r}$ coincides with the x-axis of the orbit frame. In this article the system is described around the equilibrium along the negative x-axis and this equilibrium is referred to as the open-loop equilibrium, even though there are several. The choice of working point is, however, of no importance due to the symmetry of the gravitational potential. Since the tether is of constant length, the tether motion is restricted to a sphere of radius l in the orbit frame. This sphere is described by an in-plane angle θ and an out-of-plane angle φ, which are adopted as the generalized coordinates of the system, $\boldsymbol{q} = [\theta \ \varphi]^T$. The in-plane and the out-of-plane angles are illustrated in Fig. 2. The in-plane angle is the angle between the negative part of the x-axis and the tether projection onto the orbit plane. The out-of-plane angle is the angle between the projection and the actual tether position. Using the generalized coordinates, the vector along the tether can be written as,

$$\boldsymbol{r} = \begin{bmatrix} -\cos\theta\cos\varphi \\ -\sin\theta\cos\varphi \\ -\sin\varphi \end{bmatrix}. \tag{1}$$
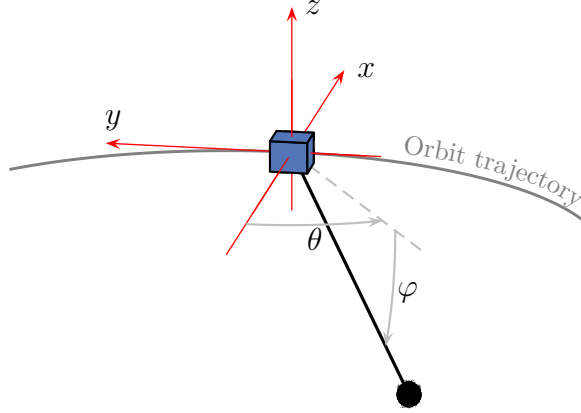
Figure 2: Definition of the in-plane and the out-of-plane angle in the orbit frame.

a) Equations of motion

The Lagrangian of the system has been derived in several previous articles (see e.g. [13]) and can be expressed as,

$$\mathcal{L}(\boldsymbol{q}, \dot{\boldsymbol{q}}) = \frac{1}{2}\Lambda\left(\dot{\varphi}^2 + \cos^2\varphi\left(\left(1+\dot{\theta}\right)^2 + 3\cos^2\theta\right)\right),\tag{2}$$

where $\Lambda = \frac{1}{3}\omega^2 l^2(3m_A + m_t)$ is a constant formed by the parameters of the system. Besides the kinetic energy, the Lagrangian includes the gravitational potential, the Coriolis potential and the centrifugal potential, represented by the terms $\frac{3}{2}\Lambda\cos^2\theta\cos^2\varphi$, $\Lambda\dot{\theta}\cos^2\varphi$, and $\frac{1}{2}\Lambda\cos^2\varphi$, respectively. In a Hamiltonian description of the system, the states representing the generalized velocities are replaced by the generalized momenta $\hat{\boldsymbol{p}} = [\hat{p}_\theta\ \hat{p}\varphi]^T = \frac{\partial\mathcal{L}}{\partial\dot{\boldsymbol{q}}}$. From (2) these are given by,

$$\hat{p}_\theta = \Lambda\left(1+\dot{\theta}\right)\cos^2\varphi,\tag{3a}$$

$$\hat{p}_\varphi = \Lambda\dot{\varphi}.\tag{3b}$$

Using the generalized momenta, the Hamiltonian $\mathcal{H}$ of the system is $\mathcal{H}(\boldsymbol{q}, \hat{\boldsymbol{p}}) = \dot{\boldsymbol{q}}^T\hat{\boldsymbol{p}} - \mathcal{L}(\boldsymbol{q}, \dot{\boldsymbol{q}}(\boldsymbol{q}, \hat{\boldsymbol{p}}))$,

$$\mathcal{H}(\boldsymbol{q}, \hat{\boldsymbol{p}}) = \frac{1}{2\Lambda}\left(\hat{p}_\varphi^2 + \frac{\hat{p}_\theta^2}{\cos^2\varphi} - 2\Lambda\hat{p}_\theta - 3\Lambda^2\cos^2\theta\cos^2\varphi\right).\tag{4}$$

To simplify the Hamiltonian, it is scaled by Λ^{-1}. Furthermore, the generalized momenta are scaled and shifted such that

$$p_\theta = \frac{\hat{p}_\theta}{\Lambda} - 1, \tag{5a}$$

$$p_\varphi = \frac{\hat{p}_\varphi}{\Lambda}. \tag{5b}$$

The shift of $\hat{p}_\theta$ is introduced to place the open-loop equilibrium at the origin of the state space. Using these coordinates, the equations of motion are then expressed using Hamilton's equation,

$$\dot{q} = \frac{\partial H}{\partial p}, \tag{6a}$$

$$\dot{p} = -\frac{\partial H}{\partial q} + Q, \tag{6b}$$

where p is introduced as $p = [p_\theta \; p_\varphi]^T$ and $Q = \frac{\tau}{\Lambda}$ is a non-dimensional version of the generalized force. The Hamiltonian is dimensionless and independent of the system parameters,

$$H(q, p) = \frac{1}{2} \left(p_\varphi^2 + \frac{(p_\theta + 1)^2}{\cos^2 \varphi} - 2p_\theta - 3\cos^2 \theta \cos^2 \varphi \right) + 1. \tag{7}$$

Here, a constant $+1$ is added, without loss of generality, to create a positive definite Hamiltonian around the origin. Inserting in (6) the equations of motion are,

$$\dot{\theta} = \frac{p_\theta + 1}{\cos^2 \varphi} - 1, \tag{8a}$$

$$\dot{\varphi} = p_\varphi, \tag{8b}$$

$$\dot{p}_\theta = -\frac{3}{2}\cos^2 \varphi \sin 2\theta + Q_\theta \tag{8c}$$

$$\dot{p}_\varphi = \frac{p_\theta + 1}{\cos^2 \varphi} \tan \varphi - \frac{3}{2}\cos^2 \theta \sin 2\varphi + Q_\varphi \tag{8d}$$

The unforced system $(Q = 0)$ has four equilibria, which can be determined from the critical points of the Hamiltonian. All equilibria are situated in the orbit plane $(\varphi^* = 0)$ and have zero momenta $p^* = 0$. The system has two stable equilibria placed at $\theta^* = 0$ and $\theta^* = \pi$. The remaining two $\theta^* = \pm\frac{\pi}{2}$ are saddle nodes and are unstable.

b)   Actuation

The system is actuated by a current through the tether. The current interacts with the magnetic field of Earth and gives rise to a mechanical force acting along

the tether. An essential part of the actuator model is the modeling of the B-field of the Earth. The B-field can be modeled using a spherical harmonic expansion (see [19, 20]). A dipole model is a spherical harmonic expansion of degree 1 and is commonly employed for analytical derivations to avoid the complexity of a higher order spherical harmonic expansion. The dipole model can be written as the sum of three components, each of which are dipoles directed along the axes in an Earth-fix coordinate system,

$$\boldsymbol{B} = \boldsymbol{B}_X + \boldsymbol{B}_Y + \boldsymbol{B}_Z. \tag{9}$$

The main contribution to the B-field comes from the dipole $\boldsymbol{B}_Z$ aligned with the rotational axis of the Earth. The remaining dipoles cause $\boldsymbol{B}$ to be tilted from the rotational axis of the Earth. This reflects the fact that the magnetic north pole of the Earth does not coincide with the geographical north pole. An upper limit for the magnitude of perturbations caused by $\boldsymbol{B}_X$ and $\boldsymbol{B}_Y$ was provided in [21]. It is common to use $\boldsymbol{B}_Z$ to model the B-field, since this choice leads to a model independent of the rotation of the Earth. This study also adopts $\boldsymbol{B}_Z$ as the B-field model, but $\boldsymbol{B}$ will be used in simulations to investigate the influence of perturbations to the B-field. By evaluating the dipole model at the origin of the orbit frame, the dipole $\boldsymbol{B}_Z$ is expressed in the orbit frame,

$$\boldsymbol{B}_Z = \frac{\mu_m}{R^3} \begin{bmatrix} -2\sin\nu\sin i \\ \cos\nu\sin i \\ \cos i \end{bmatrix}, \tag{10}$$

where μ_m is the strength of the dipole and R is the radius of the orbit. The electrodynamic force acting on the tether is the Lorentz force, which is proportional to the cross product between a tangent vector to the tether and the B-field vector. Since the tether is assumed to be rigid, the position vector $\boldsymbol{r}$ forms a tangent vector at every point along the tether and the Lorentz force per unit length tether becomes,

$$\boldsymbol{F}_e = I\boldsymbol{r} \times \boldsymbol{B}, \tag{11}$$

where I is the current through the tether. In the sequel, it is assumed that I can be controlled without limitations and the B-field is constant over the length of the tether. To find the generalized force $\boldsymbol{\tau} = [\tau_\theta \ \tau_\varphi]^T$ caused by the Lorentz force, Eq. (11) is projected onto the generalized coordinates. Inclusion of the contribution from the entire tether requires integration along the tether,

$$\tau_\theta = \int_0^l \boldsymbol{F}_e^T \frac{\partial(s\boldsymbol{r})}{\partial\theta} \ ds, \tag{12a}$$

$$\tau_\varphi = \int_0^l \boldsymbol{F}_e^T \frac{\partial(s\boldsymbol{r})}{\partial\varphi} \ ds. \tag{12b}$$

Using (12), the non-dimensional generalized force has the affine form,

$$\boldsymbol{Q} = \boldsymbol{b}(\nu, \boldsymbol{q})u. \tag{13}$$

The input u is a dimensionless quantity proportional to the current through the tether,

$$u = \frac{3}{2} \frac{1}{3m_A + m_t} \frac{\mu_m}{\mu} I, \tag{14}$$

where μ is the standard gravitation parameter of the Earth. Considering $\boldsymbol{b}(\boldsymbol{q}, \nu) = [b_\theta \; b_\varphi]^T$ as input function to the system,

$$b_\theta(\nu, \boldsymbol{q}) = \cos\varphi \sin\varphi \sin i \, (\cos\nu \sin\theta - 2\sin\nu \cos\theta) - \cos^2\varphi \cos i, \tag{15a}$$
$$b_\varphi(\nu, \boldsymbol{q}) = \sin i \, (\cos\theta \cos\nu + 2\sin\theta \sin\nu) . \tag{15b}$$

The zeros of the input function are important for the actuation and control design of the system. The input function was analyzed and conditions for zeros were stated in [17].

The model is under-actuated since it has two degrees of freedom (DOF) and only one control input. Consequently, the magnitude of the Lorentz force can be controlled by the current, but the direction is determined by the states and the direction of the magnetic field. The system description is time-periodic, since the TSS is orbiting through the static magnetic field. Using a more advanced model of the magnetic field, the system description would still be time-periodic, but the period would be a combination of the orbit period and the period of the rotation of the Earth. It is observed that the Hamiltonian of the system is time-invariant when the orbit is circular.

c)   Passive input-output description

The control design presented in this paper is based on a passive input-output connection, which is the subject of this section. The equations of motion (6) can be written in a compact form as,

$$\dot{\boldsymbol{x}} = \boldsymbol{J} \frac{\partial H}{\partial \boldsymbol{x}} + \boldsymbol{g}\,(\nu, \boldsymbol{q})\, u, \tag{16}$$

where $\boldsymbol{x} = [\boldsymbol{q}^T \; \boldsymbol{p}^T]^T$ is the state vector and $\boldsymbol{g}\,(\nu, \boldsymbol{q}) = [\boldsymbol{0}^T \; \boldsymbol{b}^T\,(\nu, \boldsymbol{q})]^T$. The square matrix $\boldsymbol{J}$ is the symplectic identity ,

$$\boldsymbol{J} = \begin{bmatrix} \boldsymbol{0} & \boldsymbol{I} \\ -\boldsymbol{I} & \boldsymbol{0} \end{bmatrix}. \tag{17}$$

In a general context, the formulation can be expanded to include damping and

an output y,

$$\dot{\boldsymbol{x}} = (\boldsymbol{J} - \boldsymbol{R}) \frac{\partial H}{\partial \boldsymbol{x}} + \boldsymbol{g}\left(\nu, \boldsymbol{q}\right) u, \tag{18a}$$

$$y = \boldsymbol{g}^T\left(\nu, \boldsymbol{q}\right) \frac{\partial H}{\partial \boldsymbol{x}}. \tag{18b}$$

The matrix $\boldsymbol{J} = -\boldsymbol{J}^T$ is called the interconnection matrix and $\boldsymbol{R} = \boldsymbol{R}^T \geq 0$ is the damping matrix. Both matrices can be functions of state variables and time. The matrix $\boldsymbol{J}$ describes how the system is interconnected which in case of a mechanical system like the electrodynamic tethers is given as (17), and $\boldsymbol{R}$ describes the damping in the system. In the present model damping e.g. air drag is not taken into account, but the matrix will occur later to describe the damping added in the closed-loop system. This system formulation is called a port-controlled Hamiltonian (see [22]) and a salient feature is that the input-output connection is passive. The input u and the output y is called the port power variables. The product yu describe instantaneous power flow of the system due to the control action. This can be seen from the time derivative of the Hamiltonian which are,

$$\dot{H} = -\left(\frac{\partial H}{\partial \boldsymbol{x}}\right)^T \boldsymbol{R}\frac{\partial H}{\partial \boldsymbol{x}} + uy. \tag{19}$$

The first term describe the power flow due to the damping. From (19) it is also seen that u and y forms a passive input-output connection, if the Hamiltonian has a lower bound. This section has presented the system for a single input, but it is similar for the multi-input case.

III Stabilization of open-loop equilibrium

Having formulated the system with a passive input-output relation, the stabilization of the origin can be obtained under conditions described below, by the simple feedback law (see [22, Corollary 3.3.1, p. 44]),

$$u = -ky, \qquad k > 0. \tag{20}$$

This can be seen by using the Hamiltonian H as a Lyapunov function. The quantity H has been defined as a positive definite function around the open-loop equilibrium and its derivative with respect to ν is,

$$\dot{H} = \left(\frac{\partial H}{\partial \boldsymbol{x}}\right)^T \boldsymbol{J}\frac{\partial H}{\partial \boldsymbol{x}} + \left(\frac{\partial H}{\partial \boldsymbol{x}}\right)^T \boldsymbol{g}\left(\nu, \boldsymbol{q}\right) u$$
$$= -ky^2. \tag{21}$$

Hence, the derivative of H is negative semi-definite. The first term vanishes due to the structure of the interconnection matrix. If the system is zero-state observable, the derivative will be negative definite and asymptotic stability is guaranteed. The zero-state observability condition can be relaxed to zero-state detectability, following [22]. Zero state observability can be formulated as: A lasting zero in the output ($y = 0$) of the unforced dynamics ($u = 0$) implies that the system is at the zero state $\boldsymbol{x} = \boldsymbol{0}$. Due to the definition of y, the zeros of the input function (15) are essential to fulfill the zero-state observability condition. The zeros induced by the time-varying input have no influence on the zero-state observability since these are countable. The zeros induced by the generalized coordinates have no influence either, which is best seen by writing the output as,

$$y = \boldsymbol{b}^T(\nu, \boldsymbol{q})\dot{\boldsymbol{q}} = b_\theta(\nu, \boldsymbol{q})\dot{\theta} + b_\varphi(\nu, \boldsymbol{q})\dot{\varphi}. \tag{22}$$

If $\boldsymbol{q}$ induces a zero in the input function when $\dot{\boldsymbol{q}} \neq \boldsymbol{0}$, the open-loop dynamics will lead the system trajectory away from this point, since the origin is the only equilibrium in the region of interest. This also shows that $\dot{\boldsymbol{q}} = \boldsymbol{0}$ cannot induce a lasting zero, except for the open-loop equilibria. The inclination i can also cause a zero in b_θ and b_φ for equatorial ($i = 0°$) or polar orbits ($i = 90°$), respectively. These situations are hard to handle since either the in-plane or the out-of-plane dynamics are unactuated. However, these conditions are not of great practical importance since they occur as an effect of simplifying the model of the magnetic field. Using the control law (20), the closed-loop dynamics can be written as a Hamiltonian system with additional damping using the open-loop Hamiltonian H,

$$\dot{\boldsymbol{x}} = (\boldsymbol{J} - k\boldsymbol{R})\frac{\partial H}{\partial \boldsymbol{x}}. \tag{23}$$

Here, the positive semi-definite damping matrix can be written as,

$$\boldsymbol{R} = \boldsymbol{g}(\nu, \boldsymbol{x})\boldsymbol{g}^T(\nu, \boldsymbol{x}) = \begin{bmatrix} \boldsymbol{0} & \boldsymbol{0} \\ \boldsymbol{0} & \boldsymbol{D} \end{bmatrix}. \tag{24}$$

The matrix $\boldsymbol{D} = \boldsymbol{b}(\nu, \boldsymbol{q})\boldsymbol{b}^T(\nu, \boldsymbol{q})$ describes damping added by the controller to the system. The matrix $\boldsymbol{D}$ has one positive eigenvalue $\lambda_{\max}$ and one equal to zero, except in the case where $\boldsymbol{b} = \boldsymbol{0}$. The lack of full of rank of $\boldsymbol{D}$ is a consequence of the system being under-actuated. The energy flow of the closed-loop system becomes,

$$\begin{aligned} \dot{H} &= \left(\frac{\partial H}{\partial \boldsymbol{x}}\right)^T (\boldsymbol{J} - k\boldsymbol{R})\frac{\partial H}{\partial \boldsymbol{x}} \\ &= -k\left(\frac{\partial H}{\partial \boldsymbol{p}}\right)^T \boldsymbol{D}\frac{\partial H}{\partial \boldsymbol{p}} \\ &= -k\dot{\boldsymbol{q}}^T \boldsymbol{D}\dot{\boldsymbol{q}} \ \geq \ -k\lambda_{\max}\|\dot{\boldsymbol{q}}\|^2. \end{aligned} \tag{25}$$

The energy flow is non-positive and has a lower bound determined from the non-zero eigenvalue of $\boldsymbol{D}$.

One of the advantages of the control law in Eq. (20) is that the zeros in the input function do not lead to singularities in the control. This could potentially lead to a large region of attraction (ROA) for the closed-loop system.

a)   Closed-loop analysis

The closed-loop description of the system will be time-periodic due to the periodic changes in the input function. To investigate the stability and performance of such a system, Floquet analysis can be used if the system is linear. Linearizing the closed-loop system around the origin leads to the description,

$$\dot{\boldsymbol{x}} = \boldsymbol{A}_1(\nu)\boldsymbol{x}, \tag{26}$$

where the system matrix $\boldsymbol{A}_1(\nu)$ is a $T = 2\pi$ periodic function. The system matrix can be written as,

$$\boldsymbol{A}_1(\nu) = \boldsymbol{A} - k\boldsymbol{A}_k(\nu), \tag{27}$$

where $\boldsymbol{A}$ is the open-loop system matrix and $\boldsymbol{A}_k(\nu)$ is the part originating from the feedback loop,

$$\boldsymbol{A} = \begin{bmatrix} 0 & 0 & 1 & 0 \\ 0 & 0 & 0 & 1 \\ -3 & 0 & 0 & 0 \\ 0 & -4 & 0 & 0 \end{bmatrix}, \tag{28}$$

$$\boldsymbol{A}_k(\nu) = \begin{bmatrix} 0 & 0 & 0 & 0 \\ 0 & 0 & 0 & 0 \\ 0 & 0 & \cos^2 i & -\frac{1}{2}\sin(2i)\cos\nu \\ 0 & 0 & -\frac{1}{2}\sin(2i)\cos\nu & \sin^2 i\cos^2\nu \end{bmatrix}. \tag{29}$$

According to Floquet theory, a fundamental matrix $\boldsymbol{\Phi}(\nu)$ of (26) fulfills,

$$\boldsymbol{\Phi}(\nu + T) = \boldsymbol{\Phi}(\nu)\boldsymbol{M}, \tag{30}$$

where the monodromy matrix $\boldsymbol{M}$ can be written as

$$\boldsymbol{M} = \boldsymbol{\Phi}^{-1}(0)\boldsymbol{\Phi}(T). \tag{31}$$

The stability of the system can be determined from the eigenvalues ρ_i of $\boldsymbol{M}$, which are referred to as the characteristic multipliers. The system (26) is asymptotically stable if all ρ_i are placed inside the unit circle. The multiplier $\rho = \rho_j$

where $j = \arg\max_i |\rho_i|$ is denoted the stability-deciding multiplier. Remembering that the fundamental matrix fulfills the differential equation,

$$\dot{\boldsymbol{\Phi}}(\nu) = \boldsymbol{A}_1(\nu)\,\boldsymbol{\Phi}(\nu), \qquad (32)$$

it is seen from (31) that the monodromy matrix can be found from an integration of (32) over one period of time from the initial conditions $\boldsymbol{\Phi}(0) = \boldsymbol{I}$. The multipliers can be expanded in a power series around a value of k where the multipliers are known [23, 24]. In this case around $k = 0$, where the system equals the unforced open-loop system. To do this, the monodromy matrix is expanded in a power series as well. The open-loop system is time-invariant and the multipliers and the monodromy matrix are therefore easily found for $k = 0$. The expansions of ρ_3 and ρ_4 are difficult to find since they are equal for $k = 0$. The geometric multiplicity equals two, hence in this case there are two independent eigenvectors corresponding to the eigenvalues $\rho_3 = \rho_4 = 1$. The expansion becomes even more complicated since the eigenvalues do not cross at $k = 0$ but only share a tangent. This means that the expansions of ρ_3 and ρ_4 are equal in a linear approximation. The expansion of the characteristic multipliers becomes,

$$\rho_{1,2} = e^{\pm 2\sqrt{3}\pi j}\left(1 - \pi c_i^2 k + \tfrac{\pi}{12}c_i^2\left(6\pi c_i^2 \mp j\sqrt{3}\right)k^2\right) + \dots, \qquad (33a)$$

$$\rho_{3,4} = 1 - \tfrac{\pi}{2}s_i^2 k + \tfrac{s_i^4}{96}\left(12\pi^2 \pm j5\pi\right)k^2 + \dots, \qquad (33b)$$

where j is the imaginary unit and c_i and s_i are short notation for $\cos i$ and $\sin i$, respectively. The multipliers $\rho_{1,2}$ and $\rho_{3,4}$ are associated with the in-plane and the out-of-plane motion, respectively, and their magnitude can be written as

$$|\rho_{1,2}| = 1 - c_i^2\pi k + c_i^4\tfrac{\pi^2}{2}k^2 + \dots, \qquad (34a)$$

$$|\rho_{3,4}| = 1 - s_i^2\tfrac{\pi}{2}k + s_i^4\tfrac{\pi^2}{8}k^2 + \dots. \qquad (34b)$$

It is seen that the system is asymptotically stable for small $k > 0$. One problem of the expansion is that the radius of convergence is limited. Another problem is that it can be hard to find higher order terms due to difficulties of finding the higher order terms of the monodromy matrix.

An alternative way of finding the characteristic multipliers is to use numerical integration to determine the monodromy matrix from (31). Figure 3 shows the characteristic multipliers ρ_i found numerically for increasing controller gain k plotted in the complex plane. The corresponding magnitudes are shown in Fig. 4. The solutions placed on the unit circle for $k = 0$ correspond to the open-loop solutions where the in-plane and the out-of-plane dynamics have a natural frequency of $\sqrt{3}$ and 2 as indicated by the eigenvalues of $\boldsymbol{A}$ in (28). It is seen that there exists an optimal controller gain k^* which minimizes $|\rho|$. The existence of k^* is also indicated by (34). For $k > k^*$ the stability-deciding
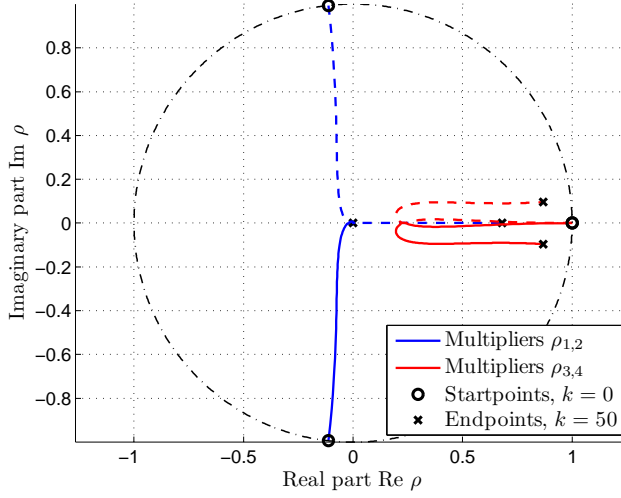
Figure 3: Characteristic multipliers ρ_i as function of k for a fix inclination of $i = 45°$.
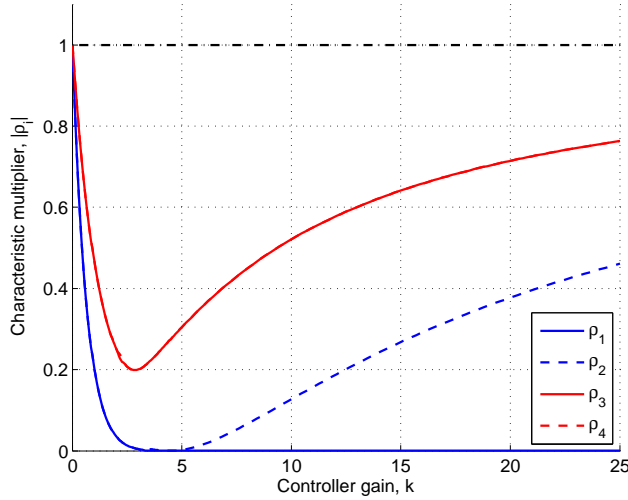
Figure 4: Absolute value of ρ_i as function of k for a fix inclination of $i = 45°$.

multiplier is seen to converges towards the unit circle. It is noted that ρ stays inside the unit circle for all $k > 0$, hence the system is asymptotically stable for all $k > 0$, which is in agreement with the result found using H as a Lyapunov function.

Figure 5 shows the stability-deciding multiplier as a function of the controller gain for different inclinations. The qualitative behavior of the multiplier shown
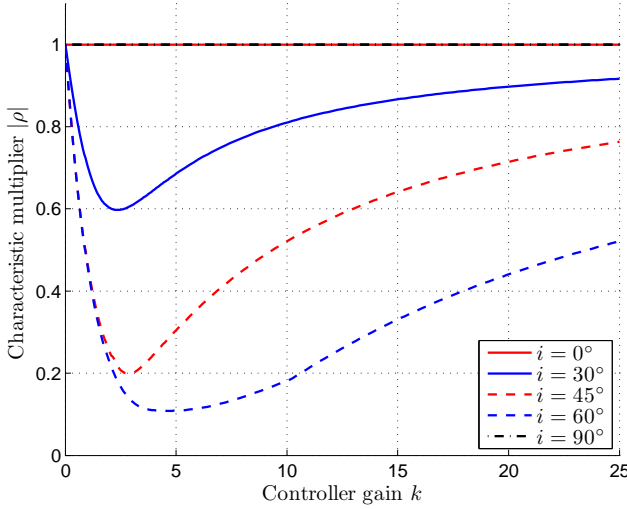
Figure 5: Absolute value of the stability-deciding multiplier for different inclinations.

in Fig. 5 follows the behaviour seen in Fig. 4, with the exception of a polar or an equatorial orbit. In these cases the stability-deciding multiplier lies on the unit circle for all k as a consequence of the unactuated in-plane and out-of-plane dynamics, respectively. This is also confirmed from the expansion (34) where higher order terms of the in-plane and the out-of-plane multipliers are multiplied by a factor $\cos^2 i$ and $\sin^2 i$, respectively.

The proposed control law preserves all four open-loop equilibria, so the closed-loop system can only be asymptotically stable, global asymptotical stability can not be obtained. An estimation of the region of attraction (ROA), the range of initial conditions $\boldsymbol{x}_0$ for which the system will converge to the origin, is therefore crucial in the evaluation of the control design. In this connection it is important to observe that the control law is the same for the two stable equilibria. It is therefore expected that the state space is divided equally between the regions of attraction around the two stable equilibria.

An obvious way to estimate the ROA is to use the Hamiltonian of the system. If the trajectory gets trapped in the potential well around the origin, the non-increasing energy level guaranteed by the controller will lead the trajectory to the origin. To be able to escape the potential well, the energy level must be greater than the energy level H^* of the separatrices in state space. The energy

level can be found from the energy at the saddle nodes that divides the potential wells of the stable equilibria (see Fig. 6). All initial conditions $(\boldsymbol{q}_0, \boldsymbol{p}_0)$ around
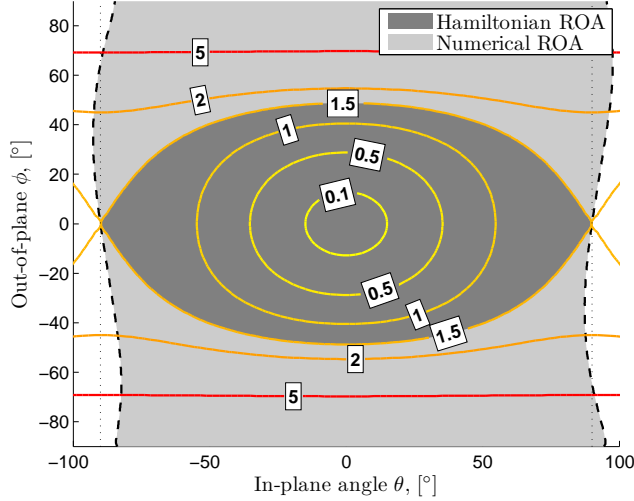
Figure 6: Region of attraction shown in the configuration space for $\dot{\boldsymbol{q}} = \boldsymbol{0}$.

the equilibrium with $H(\boldsymbol{q}_0, \boldsymbol{p}_0) < H^*$ lie in the region of attraction for the equilibrium. Since the Hamiltonian is independent of the orbit inclination, the estimation of the ROA will be independent of inclination as well. Figure 6 shows the estimate of the ROA in the configuration space for $\dot{\boldsymbol{q}} = \boldsymbol{0}$ along with the level curves of H.

Figure 6 also shows the ROA found numerically for the initial time $\nu_0 = 0$. The shape of the numerically determined ROA is similar for other initial times. The region of attraction more or less equals the lower hemisphere of the configuration space. The configuration space is divided equally between the region of attraction of the upper and the lower equilibrium, as expected.

Figure 7 shows two simulations of the convergence towards the energy minimum for different initial times. The initial state is set to $\boldsymbol{q}_0 = [\frac{\pi}{6} \ \frac{\pi}{6}]^T$ and $\dot{\boldsymbol{q}}_0 = \boldsymbol{0}$. The dashed curves in the Figure show simulations using the non-aligned dipole to model the B-field, with different initial positions of the perturbation dipoles. It is seen that the perturbation of the B-field results in energy levels slightly perturbed compared to the nominal model, but the converges is unaffected by the perturbation.

The control strategy can handle even more complicated models of the magnetic field, provided that sufficient information on the model is available to the con-
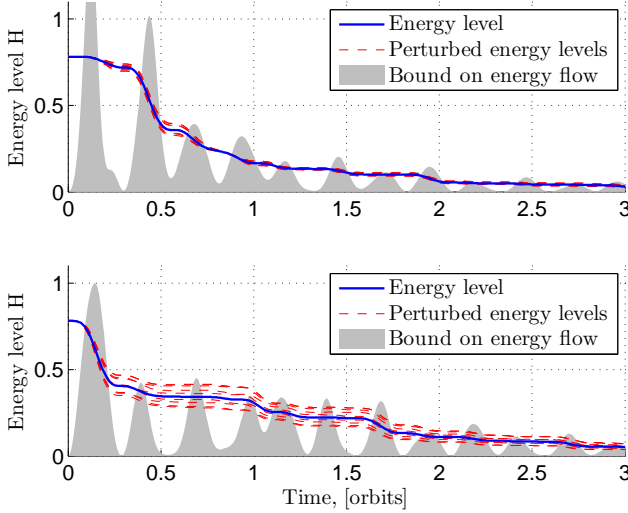
Figure 7: Simulated energy flow for $\nu_0 = 0$ and $\nu_0 = \frac{\pi}{2}$.

troller. The bound on the energy flow shown in Fig. 7 equals $\lambda_{\max} \|\dot{\boldsymbol{q}}\|^2$, which is a scaled version of the lower bound given in (25). It is seen that the energy level of the system is only decreasing when the limit on the energy flow is larger than zero.

IV Stabilization of periodic solutions

Since it is necessary to lead a non-zero current through the tether to generate a Lorentz force on the system, and this current will force the system away from its open-loop equilibrium, it is necessary to find a closed-loop solution that can stabilize the attitude motion with a non-zero tether current. Stabilization about an arbitrary point in the configuration space is not possible due to the under-actuated nature of the system. Only the control signal $u = 0$ will lead to equilibria in the equations of motion. Any other control signal will lead to time variations in either the in-plane or the out-of-plane momentum. Since the closed-loop system describes a continuous vector field, the system trajectory cannot converge to points other than the equilibria. An alternative to a stabilization of a point in the configuration space is to stabilize a periodic trajectory. The periodic open-loop solutions found in [13] are obvious candidates for such trajectories. This strategy was investigated in several articles [10, 11, 16].

To lead the trajectory away from the open-loop equilibrium and stabilize the

open-loop periodic solutions, a bias term v is added to the control law (20),

$$u = -ky + v, \qquad k > 0. \tag{35}$$

This control law is motivated by the creation of the open-loop periodic solutions when $k = 0$. The unstable open-loop periodic solutions were seen to evolve from the marginally stable open-loop equilibrium when the system was perturbed by a constant input. The intention of the control law is then to create similar periodic solutions from the asymptotically stable closed-loop equilibrium. One could expect that the periodic solutions would inherit the stability properties of the closed-loop equilibrium. However, stable periodic solutions only exist for some combinations of the controller gain k and the bias term v. The reason is that the two variables will influence the energy flow to the system, and thereby the stability, in different directions.

a)   Closed-loop analysis

Using the control law (35), the linear approximation of the closed-loop system becomes,

$$\dot{\boldsymbol{x}} = \boldsymbol{A}_2\left(\nu\right)\boldsymbol{x} + \boldsymbol{b}_2\left(\nu\right)v, \tag{36}$$

where $\boldsymbol{b}_2(\nu)$ is a $T = 2\pi$ periodic forcing term originating from the bias,

$$\boldsymbol{b}_2(\nu) = \begin{bmatrix} 0 \\ 0 \\ -\cos i \\ \sin i \cos \nu \end{bmatrix}. \tag{37}$$

The system matrix $\boldsymbol{A}_2(\nu)$ is also $T = 2\pi$ periodic and can be written as,

$$\boldsymbol{A}_2(\nu) = \boldsymbol{A} - k\boldsymbol{A}_k(\nu) + v\boldsymbol{A}_v(\nu), \tag{38}$$

where $\boldsymbol{A}$ and $\boldsymbol{A}_k(\nu)$ are given in (28) and (29), respectively, and $\boldsymbol{A}_v(\nu)$ is given as,

$$\boldsymbol{A}_v(\nu) = \begin{bmatrix} 0 & 0 & 0 & 0 \\ 0 & 0 & 0 & 0 \\ 0 & -2\sin i \sin \nu & 0 & 0 \\ 2\sin i \sin \nu & 0 & 0 & 0 \end{bmatrix}. \tag{39}$$

The periodic solutions $\boldsymbol{x}_p$ can be approximated by a power series in the parameters k and v using a perturbation method. The solutions for small k and v are approximated around the known solution for $k = v = 0$. This is obtained by writing the system matrices and the solution as power series in the parameters.

The resulting differential equation is split according to each power and solved, based on the known solution. This approach is a trivial extension of the method presented in [25]. The expansions of the solutions are, to the third order,

$$
\begin{aligned}
\theta(\nu) = & -\tfrac{c_i}{3}v + \tfrac{s_i^2}{3}\sin(2\nu)\,v^2 + \tfrac{c_i s_i^2}{6}\sin(2\nu)\,vk \\
& + \tfrac{2}{9}c_i s_i^2\left(\cos(2\nu)+\tfrac{1}{3}\right)v^3 \\
& + \tfrac{s_i^2}{3}\left(\tfrac{s_i^2}{260}\cos(4\nu)+\right. \\
& \quad \left.\tfrac{7}{3}\left(c_i^2-\tfrac{2}{35}s_i^2\right)\cos(2\nu)-\tfrac{1}{9}\left(c_i^2+\tfrac{1}{4}s_i^2\right)\right)v^2 k \\
& + \tfrac{c_i s_i^2}{13}\left(\tfrac{s_i^2}{40}\cos(4\nu)+\right. \\
& \quad \left.\tfrac{13}{3}\left(c_i^2+\tfrac{1}{30}s_i^2\right)\cos(2\nu)+\tfrac{13}{216}s_i^2\right)vk^2, \tag{40a} \\
\phi(\nu) = & \tfrac{s_i}{3}\cos(\nu)\,v - \tfrac{2c_i s_i}{9}\sin(\nu)\,v^2 \\
& + \tfrac{s_i^3}{36}\left(-\tfrac{3}{5}\sin(3\nu)+\sin(\nu)\right)vk \\
& + \tfrac{s_i^3}{9}\left(\tfrac{3}{5}\cos(3\nu)+\cos(\nu)\right)v^3 \\
& + \tfrac{c_i s_i^3}{9}\left(-\tfrac{2}{5}\cos(3\nu)+2\cos(\nu)\right)v^2 k \\
& - \tfrac{s_i^3}{30}\left(\tfrac{s_i^2}{56}\cos(5\nu)+\left(c_i^2+\tfrac{13}{120}s_i^2\right)\cos(3\nu)-\right. \\
& \quad \left.\tfrac{5}{3}\left(c_i^2-\tfrac{1}{20}s_i^2\right)\cos(\nu)\right)vk^2. \tag{40b}
\end{aligned}
$$

When no damping is added to the system ($k = 0$), the solutions (40) coincide with the open-loop periodic solutions found by Peláez et al. [13]. The solutions can be approximated with higher precision by taking the non-linearities into account. This is done by replacing the non-linearities with their Taylor expansions and again writing the solution as a power series. The improved solutions are given as,

$$
\begin{aligned}
\theta(\nu) = & -\tfrac{c_i}{3}v + \tfrac{4s_i^2}{9}\sin(2\nu)\,v^2 + \tfrac{c_i s_i^2}{6}\sin(2\nu)\,vk \\
& + \tfrac{c_i}{18}\left(\tfrac{23}{3}s_i^2\cos(2\nu)+\left(-\tfrac{4}{9}c_i^2+s_i^2\right)\right)v^3 \\
& + \tfrac{s_i^2}{18}\left(\tfrac{s_i^2}{65}\cos(4\nu)+\right. \\
& \quad \left.20\left(c_i^2-\tfrac{7}{150}s_i^2\right)\cos(2\nu)-\tfrac{1}{3}s_i^2\right)v^2 k \\
& + \tfrac{c_i s_i^2}{13}\left(\tfrac{s_i^2}{40}\cos(4\nu)+\right. \\
& \quad \left.\tfrac{13}{3}\left(c_i^2+\tfrac{1}{30}s_i^2\right)\cos(2\nu)+\tfrac{13}{216}s_i^2\right)vk^2, \tag{41a}
\end{aligned}
$$

$$\phi(\nu) = \frac{s_i}{3} \cos(\nu) v - \frac{2c_i s_i}{9} \sin(\nu) v^2$$
$$+ \frac{s_i^3}{36} \left(-\frac{3}{5} \sin(3\nu) + \sin(\nu) \right) vk$$
$$+ \frac{s_i}{27} \left(\frac{58}{15} s_i^2 \cos(3\nu) + \frac{1}{2} \left(c_i^2 + 4s_i^2 \right) \cos(\nu) \right) v^3$$
$$+ \frac{c_i s_i^3}{9} \left(-\frac{3}{5} \cos(3\nu) + \frac{5}{3} \cos(\nu) \right) v^2 k$$
$$- \frac{s_i^3}{30} \left(\frac{s_i^2}{56} \cos(5\nu) + \left(c_i^2 + \frac{13}{120} s_i^2 \right) \cos(3\nu) - \right.$$
$$\left. \frac{5}{3} \left(c_i^2 - \frac{1}{20} s_i^2 \right) \cos(\nu) \right) vk^2. \tag{41b}$$

The solutions (41) agree with the one found in [13] for $k = 0$, which illustrates that the closed-loop solutions are perturbed by the controller gain k compared to the open-loop solutions. Note that the in-plane solutions only consist of even multiples of the basic frequency, while the out-of-plane only consists of odd multiples. Consequently, $\theta(\nu) = \theta(\nu + \pi)$ and $\varphi(\nu) = -\varphi(\nu + \pi)$, which geometrically means that the solutions are mirrored in the θ-axis. The solutions are seen to collapse to a point on the θ-axis for an equatorial orbit ($i = 0°$). The approximations of the periodic solutions are found as an eight order power series, which is used when referring to a series approximation.

The solutions (40) and (41) are only valid for small values of k and v due to the convergence properties of the power series. Periodic solutions exist, however, for larger values as well. These solutions can be found by numerical simulations. To investigate the stability of the solutions, the variable $\boldsymbol{\eta}(\nu) = \boldsymbol{x}(\nu) - \boldsymbol{x}_p(\nu)$ is introduced to describe a deviation from a periodic solution. Inserting in (36) it is seen that $\boldsymbol{\eta}(\nu)$ obeys the differential equation,

$$\dot{\boldsymbol{\eta}} = \boldsymbol{A}_2(\nu)\boldsymbol{\eta}. \tag{42}$$

The equation can be investigated by means of Floquet analysis, which is carried out in the same manner as in the previous section. Using a power series the multipliers become,

$$\rho_{1,2} = e^{\pm 2\sqrt{3}\pi j}$$
$$\left(1 - \pi c_i^2 k + \frac{\pi}{12} c_i^2 \left(6\pi c_i^2 \mp j\sqrt{3} \right) k^2 \pm j s_i^2 c_i \frac{\pi\sqrt{3}}{3} kv \right) + \dots, \tag{43a}$$
$$\rho_{3,4} = 1 - s_i^2 \frac{\pi}{2} k + \frac{s_i^4}{96} \left(12\pi^2 \pm j5\pi \right) k^2 \pm j s_i^2 c_i \frac{7\pi}{12} kv \pm j s_i^2 \frac{\pi}{6} v^2 + \dots. \tag{43b}$$

The magnitudes of the multipliers are,

$$|\rho_{1,2}| = 1 - c_i^2 \pi k + c_i^4 \frac{\pi^2}{2} k^2 + \dots, \tag{44a}$$
$$|\rho_{3,4}| = 1 - s_i^2 \frac{\pi}{2} k + s_i^4 \frac{\pi^2}{8} k^2 + \dots. \tag{44b}$$

The magnitudes are unchanged compared to (34) by the bias in the second order approximation. This shows that the periodic solutions are asymptotically stable

for small $k > 0$ and small v. The region of stable periodic solutions ($|\rho| < 1$) is shown in the parameter plane defined by k and v in Fig. 8. The Figure is based
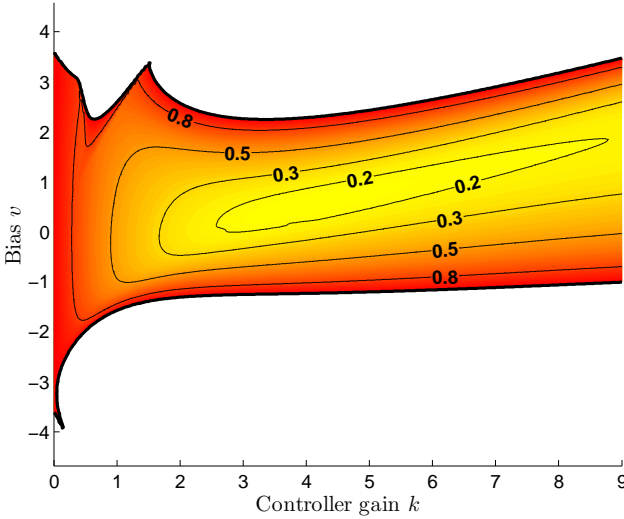
Figure 8: Stable region in the parameter space for $i = 45°$.

on stability-deciding multipliers found numerically. Stable periodic solutions are seen to exist in a region in the parameter plane and, in agreement with the result from the previous section, the line $v = 0$ is included in this region. For each controller gain the bias term has lower and upper limits, which are related to energy flow into the system. However, the relations are quite complex and further scrutiny is not within the scope of this paper.

The approximating series are convenient to show the existence and basic properties of the periodic solutions, as well as to determine initial conditions for simulations. To investigate how well the power series approximates the periodic solution, the error ε is introduced,

$$\varepsilon = \frac{1}{2\pi} \int_0^{2\pi} \|\widehat{\boldsymbol{x}}(\nu) - \widetilde{\boldsymbol{x}}_p(\nu)\|^2 \ d\nu, \tag{45}$$

where $\widetilde{\boldsymbol{x}}_p$ is the series approximation. The solution $\widehat{\boldsymbol{x}}$ is found from a nonlinear simulation that has converged to a periodic solution. The error is shown for different parameter values for a third and an eighth order approximation in Figures 9 and 10. In the case $v = 0$, where the solution collapses to the origin, the approximation is exact. The investigation of accuracy of the approximating series requires that the solution is stable and also that the parameters are in the region of converge of the series. Another obstacle is that for k close to zero, convergence of the solution is so slow that computational efforts makes it
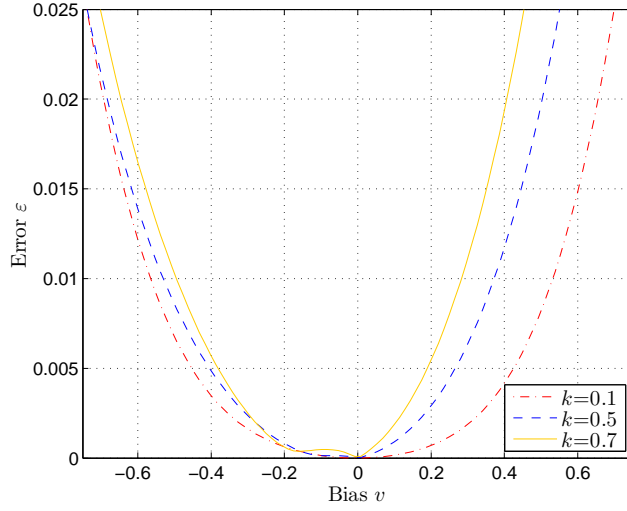
Figure 9: Error associated with the third order approximation.
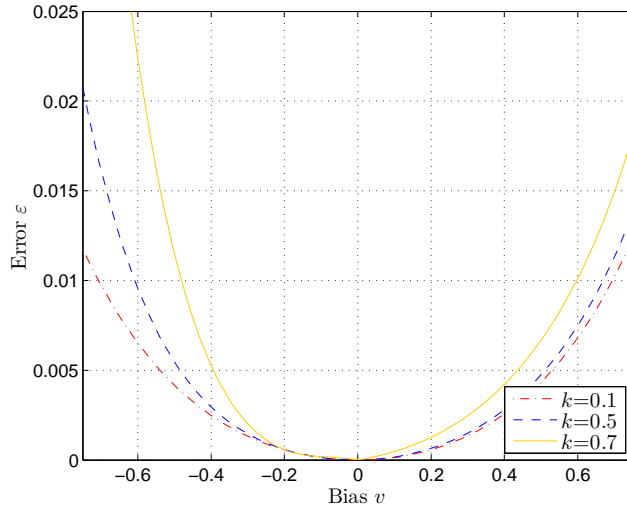
Figure 10: Error associated with the eighth order approximation.

impractical to determine the magnitude of error. Apart from these limitations, Figures 9 and 10 show that the approximating series can be used with reasonable accuracy for parameter ranges shown. It is noted that the limitations associated with the approximating series do not limit the general investigation in this paper as the general results were based on full simulations of the nonlinear system.

Figures 11 to 14 show simulations of the system for $v = 1$, and an inclination of $i = 45°$. Figure 11 illustrates a simulation of the open-loop system ($k = 0$)
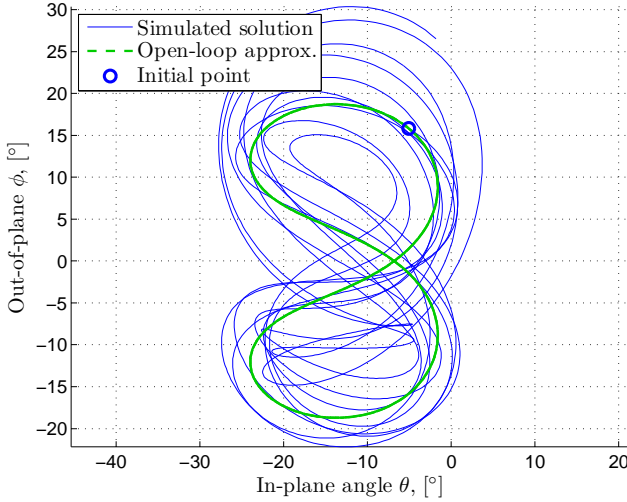
Figure 11: Open-loop simulation of unstable periodic solution for $k = 0$ and $v = 1$.

with an initial value found from the approximated periodic solution. It is seen that this open-loop periodic solution is unstable, even though the instability evolves quite slowly. Figures 12 and 13 shows a simulation of the closed loop system with $k = \frac{1}{2}$, illustrated in the configuration space and as function of time, respectively. It is seen that the system trajectory converges towards a periodic solution, which resembles the solution approximated by the power series. The stabilized solution is perturbed from the open-loop solution due to the damping injection. Figure 14 shows a simulation of a periodic solution for $k = \frac{1}{2}$ using tilted and non-tilted dipole models of the magnetic field of the Earth. Focus on the periodic solution is obtained by removing an initial transient. To avoid a quasi-periodic solution, the simulation was carried out for a satellite with an orbit period of 90 min, hence the periodicity of the system is increased from 2π to 32π, due to the rotation of the Earth. The simulations verify that the controller is able to stabilize a periodic solution with the new period, which is bounded in a region around the unperturbed solution. Since the controller contains no information of a reference solution, the solution is given entirely by the variation in the magnetic field. The mismatch between the B-field model used in the controller and the actual one has no significant influence on the stability of the solution.
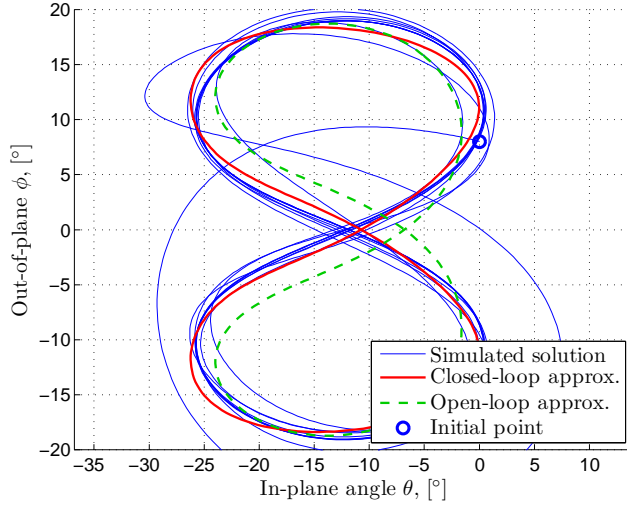
Figure 12: Converges towards periodic solution for $k = \frac{1}{2}$ in the configuration space.
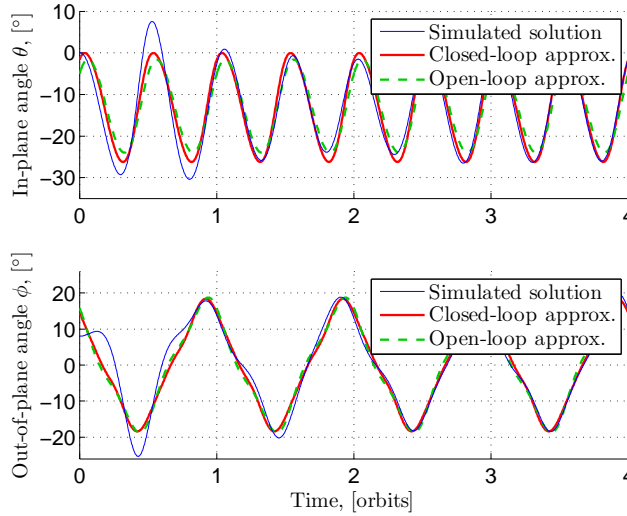
Figure 13: Converges towards periodic solution for $k = \frac{1}{2}$.

V   Conclusion

This paper developed a control law for stabilizing periodic solutions in the attitude of an electrodynamic tether system. The time-varying control law was
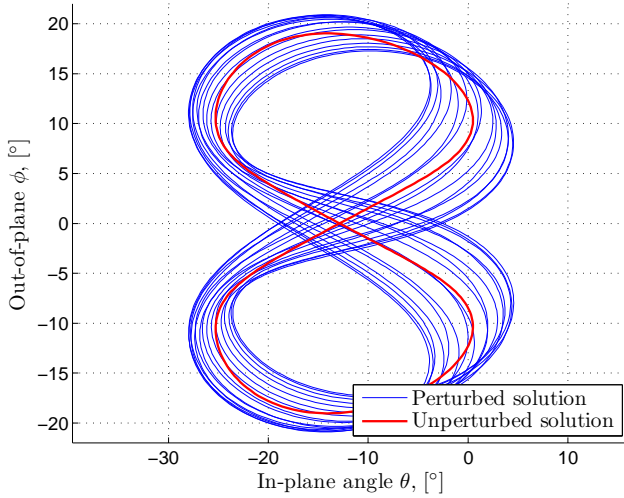
Figure 14: Periodic solution using different models of the magnetic field.

shown to stabilize a family of periodic solutions, which were found to be perturbed versions of a known family of unstable open-loop periodic solutions. The control design was based on a passive input-output connection obtained by formulating the equations of motion as a port-controlled Hamiltonian system. The passivity-based formulation allowed zeros in the input function to be handled in a simple manner, without introducing singularities in the control law. The first part of the control law gave stabilization of the open-loop equilibrium. A large region of attraction was demonstrated for this control law, and it was shown that an optimal control gain exists, providing the fastest convergence towards the equilibrium. An attractive feature of the total control law was shown to be its independence of reference signal and delayed signals. The shapes of the stabilized periodic solutions were investigated using series approximations and numerical simulations. The periodic solutions were found to form symmetric curves around points in the orbit plane, whose distances to the origin were increasing with a bias term in the controller. Stability properties of the controller were investigated by Floquet analysis and the allowable parameter range for stable solutions was determined. The work assumed a simple model of the magnetic field, but the sensitivity to perturbations in the magnetic field was briefly studied. The control law was shown to give an asymptotically stable closed-loop system for all relevant orbits.

References

[1] K. D. Kumar. Review of dynamics and control of nonelectrodynamic tethered satellite systems. *Journal of Spacecraft and Rockets*, 43(4):705–720, 2006. ISSN 0022-4650.

[2] M. P. Cartmell and D. J. McKenzie. A review of space tether research. *Progress in Aerospace Sciences*, 44(1):1–21, 2008. ISSN 0376-0421. doi: 10.1016/j.paerosci.2007.08.002.

[3] L. Iess, C. Bruno, C. Ulivieri, U. Ponzi, M. Parisse, G. Laneve, M. Dobrowolny, F. De Venuto, B. Bertotti, L. Anselmo, and Giuliano Vannaroni. Satellite de-orbiting by means of electrodynamic tethers part I: General concepts and requirements. *Acta Astronautica*, 50(7):399–406, 2002. ISSN 0094-5765.

[4] Carmen Pardini, Toshiya Hanada, Paula H. Krisko, Luciano Anselmo, and Hiroshi Hirayama. Are de-orbiting missions possible using electrodynamic tethers? task review from the space debris perspective. *Acta Astronautica*, 60(10-11):916 – 929, 2007. ISSN 0094-5765. doi: 10.1016/j.actaastro.2006.11.001.

[5] L. Johnson and M. Herrmann. Internation space station electrodynamic tether reboost study. Technical memorandum NASA/TM-1998-208538, NASA, Mashall Space Flight Center, July 1998.

[6] Kirk F. Sorensen. Conceptual design and analysis of an mxer tether boost station. Technical report, American Institute of Aeronautics and Astronautics, Propulsion Research Center / TD40, NASA Marshall Space Flight Center, AL 35812, 2001.

[7] Monica Pasca. Nonlinear control of tethered satellite system oscillations. *Nonlinear Analysis*, 30(6):3867–3878, 1997. ISSN 0362-546x.

[8] S. G. Tragesser and H. San. Orbital maneuvering with electrodynamic tethers. *Journal of Guidance, Control, and Dynamics*, 26(5):805–810, 2003. ISSN 0731-5090.

[9] Paul Williams. Optimal orbital transfer with electrodynamic tether. *Journal of Guidance, Control, and Dynamics*, 28(2):369–372, 2005. ISSN 0731-5090.

[10] J. Peláez and E. C. Lorenzini. Libration control of electrodynamic tethers in inclined orbit. *Journal of Guidance, Control, and Dynamics*, 28(2):269–279, 2005. ISSN 0731-5090.

[11] Paul Williams. Libration control of electrodynamic tethers using predictive control with time-delayed feedback. *Journal of Guidance, Control, and Dynamics*, 32(4):1254–1268, 2009. ISSN 0731-5090. doi: 10.2514/1.41039.

[12] R Wisniewski and M Blanke. Fully magnetic attitude control for spacecraft subject to gravity gradient. *Automatica*, 35(7):1201–1214, jul 1999. ISSN 0005-1098.

[13] J. Peláez, E. C. Lorenzini, O. López-Rebollal, and M. Ruiz. A new kind of dynamic instability in electrodynamic tethers. *Journal of the Astronautical Sciences*, 48(4):449–476, 2000. ISSN 0021-9142.

[14] J. Corsi and L. Iess. Stability and control of electrodynamic tethers for de-orbiting applications. *Acta Astronautica*, 48(5-12):491–501, 2001. ISSN 0094-5765.

[15] Xiang Zhou, Junfeng Li, H. Baoyin, and Vadim Zakirov. Equilibrium control of electrodynamic tethered satellite systems in inclined orbits. *Journal of Guidance, Control, and Dynamics*, 29(6):1451–1454, 2006. ISSN 0731-5090. doi: 10.2514/1.21882.

[16] Paul Williams. Energy rate feedback for libration control of electrodynamic tethers. *Journal of Guidance, Control, and Dynamics*, 29(1):221–223, 2006. ISSN 0731-5090.

[17] M. B. Larsen and M. Blanke. Control by damping injection of electrodynamic tether system in an inclined orbit. In *Proc. ACC '09. American Control Conference*, pages 4824–4829, 2009. doi: 10.1109/ACC.2009.5159896.

[18] M. B. Larsen and M. Blanke. Stabilization of periodic solutions in a tethered satellite system by damping injection. In *European Control Conference*, pages 2169–2174, 2009.

[19] S. Macmillan and S. Maus. International geomagnetic reference field - the tenth generation. *Earth, Planets and Space*, 57(12):1135–1140, 2005. ISSN 1343-8832. doi: 10.1029/2005EO160006.

[20] J. R. Wertz. *Spacecraft Attitude Determination and Control*. D. Reidel Publishing Co., 1978. ISBN 90-277-0959-9.

[21] M. B. Larsen and M. Blanke. Nonlinear control of electrodynamic tether in equatorial or somewhat inclined orbits. In *Proc. Mediterranean Conference on Control & Automation MED '07*, pages 1–6, 2007. doi: 10.1109/MED. 2007.4433876.

[22] Arjan van der Schaft. L_2-*Gain and Passivity in Nonlinear Control*. Communications and Control Engineering. Springer-Verlag New York, Inc., Secaucus, NJ, USA, second edition, 2000. ISBN 1-85233-073-2.

[23] A. P. Seyranian. Sensitivity analysis of multiple-eigenvalues. *Mechanics of structures and machines*, 21(2):261–284, 1993. ISSN 0890-5452.

[24] A. P Seyranian, F. Solem, and P. Pedersen. Stability analysis for multi-parameter linear periodic systems. *Archive of applied mechanics*, 69(3): 160–180, APR 1999. ISSN 0939-1533.

[25] R. Grimshaw. *Nonlinear Ordinary Differential Equations*. Blackwell Scientific Publications, 1990.

Modeling of tethered satellite formations using graph theory[1]

Abstract

Tethered satellite formations have recently gained increasing attention due to future mission proposals. Several different formations have been investigated for their dynamic properties and control schemes have been suggested. Formulating the equations of motion and investigation which geometries could form stable formations in space are cumbersome when done at a case to case basis, and a common framework providing a basic model of the dynamics of tethered satellite formations can therefore be advantageous. This paper suggests the use of graph theoretical quantities to describe a tethered satellite formation and propose a method to deduce the equations of motion for the attitude dynamics of the formation in a compact form. The use of graph theory and Lagrange mechanics together allows a broad class of formations to be described using the same framework, and the manual element in the modeling is significantly alleviated. A method is stated for finding stationary configurations and an upper limit of their number is determined. The method is shown to be valid for general tethered satellite formations that form a tree structure.

---

[1]Submitted to *Acta Astronautica.*

I   Introduction

Tethered satellite formations have been proposed in several contexts, especially in relation to remote sensing and space stations [1]. Several potential applications have been investigated in the literature. An elevator system for a space station using tethers was investigated in [2]. In connection with remote sensing, tether systems have been investigated as atmospheric probes [3] and interferometers [4]. The dynamic properties of several different types of formations have been investigated. Chain structures were studied by [5, 6], ring structures by [7], hub-and-spoke structures by [8, 9] and anchored structures, the latter also refereed to as double pyramid formations, by [8, 10]. Ref. [8] investigated hub-and-spoke and closed-hub-and-spoke formations. A hub-and-spoke formation consists of a main satellite and a number of sub-satellites tethered to the main one. In a closed-hub-and-spoke formation, the sub-satellites are further connected to each other. The closed-hub-and-spoke formation was found to be unstable, but was shown to be stabilizable by tethering an anchor satellite to each side of the formation, such that the formation resembled a double pyramid. Ref. [10] considered a double pyramid formation in connection with a multi-sensor network. The formation was assumed to rotate around the axis through the anchor satellites. The stability region was stated as function of the system parameters and a condition was found to ensure that the tethers of the formation were kept in tension. A chain structure is probably the kind of formation which has received the greatest attention. Both chains with a fixed number of satellites like three or four [11, 12], and a general N-body chain [5, 6] have been investigated. The research on two tethered satellites is a very mature area and it is not in the scope of this article to give an overview of this field. The equations of motion for an N-body structure were deduced in [5] for both in-plane and out-of-plane dynamics and a simple relation was found between the natural frequency of the in-plane and the out-plane motions. The model was expanded in [13] to consider a varying tether length, flexibility of the tether and a non-circular orbit. The stationary configurations situated in the orbit plane of an N-body chain were found in [6] through an investigation of the stationary points of the potential energy and an upper limit on total number of stationary points was found. The investigation of the stationary configurations was further expanded in [14] to also include the out-of-plane dimension of the configuration space.

This work considers tethered satellite formations forming a tree structure, a topology of tethers where there are no cycles. The main contributions of this article are a description of the structure using graph theoretical quantities, a derivation of the equations of motion in generic form using the graph description of the formation topology, and an investigation of the stationary configurations of formations based on this description. The structure of a formation is described

using a matrix describing the path along the tethers from each satellite to a main satellite of the formation. The equations of motion are deduced for a formation with constant-length tethers using the path matrix as a parameter. The dynamics are stated both for the motion in the orbit plane, and for the general motion in three dimensions. A method to determine the stationary configurations in the orbit plane is described. The proposed method follows the steps presented in [6], but extends the method by expanding the scope to a general tree structured formation.

The outline of the remaining part of the article is as follows. Means for a graph theoretical description of the tethered satellite formation are first introduced. Two matrices, describing the interconnection of satellites and the paths around the formation, are defined along with useful sets of edges and nodes. Section III treats the derivation of the equations of motion for the motion in the orbit plane. Stationary configurations in the orbit plane are dealt with in Section IV where a method of finding the configurations is stated and the configurations are classified according to the number of vertical tethers in a configuration. Section V uses a Y-formation with four tethers to exemplify the investigation of stationary configurations. Section VI offers conclusions of the work. A expands the equations of motion to out-of-plane motion and B provides proofs of the properties used in Section IV.

II   Graph description of formations

Consider a tethered satellite formation consisting of massless tethers connecting satellites in a tree structure. The limitation to a tree structure is introduced to simplify the equations of motion by avoiding algebraic constraints associated with cycles within a formation. In a tree structure with $n+1$ satellites there are n tethers, with each tether connecting two satellites. Each satellite is modeled as a point mass m_i for $i = 0, \ldots, n$ and tethers are modeled as rigid rods of constant length l_j for $j = 1, \ldots, n$. The total mass of the system is denoted $m = \sum_{i=0}^{n} m_i$ and the relative mass of each satellite is $\mu_i = \frac{m_i}{m}$ for $i = 0, \ldots, n$. The relative masses and the length of the rods are collected in the diagonal matrices $\boldsymbol{\Lambda} \in \mathbb{R}^{(n+1) \times (n+1)}$ and $\boldsymbol{L} \in \mathbb{R}^{n \times n}$,

$$
\boldsymbol{\Lambda} = \begin{bmatrix} \mu_0 & 0 & \ldots & 0 \\ 0 & \mu_1 & \ldots & 0 \\ \vdots & \vdots & \ddots & \vdots \\ 0 & 0 & \ldots & \mu_n \end{bmatrix} \tag{1}
$$

$$
\boldsymbol{L} = \begin{bmatrix} l_1 & 0 & \dots & 0 \\ 0 & l_2 & \dots & 0 \\ \vdots & \vdots & \ddots & \vdots \\ 0 & 0 & \dots & l_n \end{bmatrix}. \tag{2}
$$

The formation is described by a connected, directed graph representing masses as nodes and rods as edges. The notation m_i and l_j is reused to denote the nodes and the edges of the graph. The graph forms a rooted tree where the node m_0 represents the root. The root of the tree can be chosen arbitrarily. It is assumed, without loss of generality, that each edge is directed away from the root and that the edge l_k is connected to and directed towards m_k. The formation topology can then be described by the incidence matrix $\boldsymbol{B} \in \mathbb{R}^{(n+1) \times n}$ where each row represents a node and each column an edge. The incidence matrix $\boldsymbol{B}$ with elements B_{ij} is defined as,

$$
B_{ij} = \begin{cases} 1 & \text{if } l_j \text{ is connected to and pointing away from } m_i \\ -1 & \text{if } l_j \text{ is connected to and pointing towards } m_i \\ 0 & \text{if } l_j \text{ is not connected to } m_i \end{cases} . \tag{3}
$$

Due to the assumption of a tree structure, the incidence matrix $\boldsymbol{B}$ has full rank and by removing one row from $\boldsymbol{B}$ a square matrix of full rank is formed. This square matrix is called the basic incidence matrix or the reduced incidence matrix with respect to the node corresponding to the removed row. The basic incidence matrix $\boldsymbol{A} \in \mathbb{R}^{n \times n}$ describes the structure with respect to the root, that is the sub-matrix of $\boldsymbol{B}$ which excludes the first row. The path from a node m_i to the root is unique and can be described as a column of the path matrix $\boldsymbol{P} \in \mathbb{R}^{n \times n}$. The ith column represents the directed path from m_i to m_0 such that,

$$
P_{ji} = \begin{cases} 1 & \text{if } l_j \text{ is in the path from } m_i \text{ to } m_0 \text{ directed towards } m_0 \\ -1 & \text{if } l_j \text{ is in the path from } m_i \text{ to } m_0 \text{ directed towards } m_i \\ 0 & \text{if } l_j \text{ is not in the path from } m_i \text{ to } m_0 \end{cases} . \tag{4}
$$

All non-zero elements of $\boldsymbol{P}$ are negative due to the definition of the direction of the edges. The basic incidence matrix and the path matrix are related as each others inverse,

$$
\boldsymbol{P} = \boldsymbol{A}^{-1}, \tag{5}
$$

according to [15, Theorem 2.10, pp. 55-56].

Some sets connected to the graph are introduced in the following. These sets are used in connection of the determination of the stationary configuration of the formation. The set T_j comprise the nodes in a sub-tree rooted at m_j. The

sub-tree occurs when the graph is divided into two disjoint connected graphs by removing the edge l_j. After introducing T_j, the path matrix can be written as,

$$P_{ji} = \begin{cases} -1 & \text{for } i \in T_j \\ 0 & \text{for } i \notin T_j \end{cases}. \tag{6}$$

Definition (4) is valid for a tree structure with arbitrary directed edges, while (6) is only valid assuming edges are directed away from the root.

The set J includes an arbitrary combination of edges. The set can be decomposed into sets J_k for $k = 1, \ldots, \ell$ each describing a connected structure. It is assumed that the elements of the set J_k are not connected to elements in J_p for $k \neq p$, this means the decomposition is minimal in the sense that ℓ is as small as possible. The complement of the set J is denoted $\bar{J}$ and the cardinality of these sets are denoted $|J|$ and $|\bar{J}|$, respectively. The set of neighboring edges of l_j is denoted N_j, meaning that the edge l_k is included in N_j if one of the two nodes incident with l_j is also incident with l_k. The notation $N_J = \cup_{i \in J} N_i \setminus J$ is used for the neighboring edges of J. To illustrate the notation, an example of

Figure 1: Graph of a rooted tree.

a tree structure is shown in Figure 1. The corresponding incidence matrix and path matrix are,

$$\boldsymbol{B} = \begin{bmatrix} 1 & 0 & 0 & 0 & 0 & 0 & 1 & 0 & 0 \\ -1 & 1 & 0 & 1 & 0 & 0 & 0 & 0 & 0 \\ 0 & -1 & 1 & 0 & 0 & 0 & 0 & 0 & 0 \\ 0 & 0 & -1 & 0 & 0 & 0 & 0 & 0 & 0 \\ 0 & 0 & 0 & -1 & 1 & 1 & 0 & 0 & 0 \\ 0 & 0 & 0 & 0 & -1 & 0 & 0 & 0 & 0 \\ 0 & 0 & 0 & 0 & 0 & -1 & 0 & 0 & 0 \\ 0 & 0 & 0 & 0 & 0 & 0 & -1 & 1 & 1 \\ 0 & 0 & 0 & 0 & 0 & 0 & 0 & -1 & 0 \\ 0 & 0 & 0 & 0 & 0 & 0 & 0 & 0 & -1 \end{bmatrix}, \tag{7}$$

$$\boldsymbol{P} = \begin{bmatrix} -1 & -1 & -1 & -1 & -1 & -1 & 0 & 0 & 0 \\ 0 & -1 & -1 & 0 & 0 & 0 & 0 & 0 & 0 \\ 0 & 0 & -1 & 0 & 0 & 0 & 0 & 0 & 0 \\ 0 & 0 & 0 & -1 & -1 & -1 & 0 & 0 & 0 \\ 0 & 0 & 0 & 0 & -1 & 0 & 0 & 0 & 0 \\ 0 & 0 & 0 & 0 & 0 & -1 & 0 & 0 & 0 \\ 0 & 0 & 0 & 0 & 0 & 0 & -1 & -1 & -1 \\ 0 & 0 & 0 & 0 & 0 & 0 & 0 & -1 & 0 \\ 0 & 0 & 0 & 0 & 0 & 0 & 0 & 0 & -1 \end{bmatrix}. \tag{8}$$

Some of the sets introduced are listed in Table 1 for the graph of the example in Figure 1.

	N_j	T_j
$j = 1$	$\{2, 4, 7\}$	$\{1, 2, 3, 4, 5, 6\}$
$j = 4$	$\{1, 2, 5, 6\}$	$\{4, 5, 6\}$
$j = 9$	$\{7, 8\}$	$\{9\}$

(a) Sets regarding edges.

	N_J	J_k
$J = \{2, 4, 5, 8\}$	$\{1, 3, 6, 7, 9\}$	$\{2, 4, 5\}, \{8\}$
$J = \{1, 7, 9\}$	$\{2, 4, 8\}$	$\{1, 7, 9\}$
$J = \{3, 5, 6\}$	$\{2, 4\}$	$\{3\}, \{5, 6\}$

(b) Sets regarding the set J.

Table 1: Definition of sets occurring in the graph in Figure 1

III   Equations of motion

Dynamical equations of the attitude motion of the satellite formation are derived in this section. The derivation follows the derivation in [5], but takes the general tree structure into account. To describe the attitude motion of the formation the orbit frame is introduced. The frame is centered at the center of mass (CM) of the formation and has the x-axis along the position vector from the Earth to the CM and the z-axis perpendicular to the orbit plane. The masses of the formation are described by a position vector $\boldsymbol{r}_i = [x_i \ y_i \ x_i]^T$ for $i = 0, \ldots, n$ and a vector along the positive direction of each rod is introduced as $\boldsymbol{\rho}_j = [\xi_j \ \eta_j \ \zeta_j]^T$ for $j = 1, \ldots, n$ (see Figure 2). Using the path matrix, the position of m_i for $i = 1 \ldots n$ can be found relative to m_0. To be able to describe the position of all masses, including m_0, by a single expression, the path matrix is expanded to $\widetilde{\boldsymbol{P}} \in \mathbb{R}^{n \times (n+1)}$ such that $\widetilde{\boldsymbol{P}} = [\boldsymbol{0}_n \ \boldsymbol{P}]$. The additional column of zeros $\boldsymbol{0}_n \in \mathbb{R}^n$ can be interpreted as representing the path from the root node to itself. This path does not contain any edges. Using $\widetilde{\boldsymbol{P}}$ the position vector of each mass can be written as a sum along the path to the mass,

$$\boldsymbol{r}_i = \boldsymbol{r}_0 - \sum_{j=1}^{n} \widetilde{P}_{j(i+1)} \boldsymbol{\rho}_j \qquad \text{for } i = 0, \ldots, n. \tag{9}$$

The sign of the sum originates from the fact that the vectors $\boldsymbol{\rho}_j$ are pointing away from the root, while the paths are directed towards the root. Since the frame is centered at the CM, the position vectors obey the relation $\sum_i m_i \boldsymbol{r}_i = 0$,
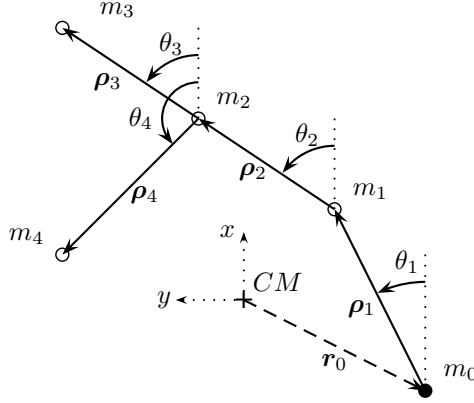
Figure 2: A tethered satellite formation in the orbit plane.

which combined with (9) leads to the position vector of m_0,

$$\boldsymbol{r}_0 = \sum_{j=1}^{n} \boldsymbol{\rho}_j \sum_{k=1}^{n} \widetilde{P}_{j(k+1)} \mu_k. \tag{10}$$

Substituting (9) back into (10) the position vectors of the masses in the formation are,

$$\boldsymbol{r}_i = -\sum_{j=1}^{n} \left(\widetilde{P}_{j(i+1)} - \sum_{k=1}^{n} \widetilde{P}_{j(k+1)} \mu_k \right) \boldsymbol{\rho}_j$$

$$= \sum_{j=1}^{n} \left(\sum_{k=1}^{n} \widetilde{P}_{j(k+1)} \left(\mu_k - \delta_{ik} \right) \right) \boldsymbol{\rho}_j, \tag{11}$$

where δ_{ik} is Kronecker's delta. Equation (11) gives the relation between the position of m_i and the directions of the rods l_j. By collecting x_i in a vector $\boldsymbol{x} \in \mathbb{R}^{n+1}$ and ξ_j in a vector $\boldsymbol{\xi} \in \mathbb{R}^n$ defined as

$$\boldsymbol{x} = \begin{bmatrix} x_0 & x_1 & \dots & x_n \end{bmatrix}^T, \tag{12}$$

$$\boldsymbol{\xi} = \begin{bmatrix} \xi_1 & \xi_2 & \dots & \xi_n \end{bmatrix}^T, \tag{13}$$

the relation of the x-component of (11) can be written in the compact form,

$$\boldsymbol{x} = \boldsymbol{\Gamma} \boldsymbol{P}^T \boldsymbol{\xi}. \tag{14}$$

The components of the matrix $\boldsymbol{\Gamma} \in \mathbb{R}^{(n+1) \times n}$ are given as,

$$\Gamma_{ik} = \mu_k - \delta_{i(k+1)}. \tag{15}$$

Introducing $\boldsymbol{y}, \boldsymbol{z} \in \mathbb{R}^{n+1}$ similar to $\boldsymbol{x}$ and $\boldsymbol{\eta}, \boldsymbol{\zeta} \in \mathbb{R}^n$ similar to $\boldsymbol{\xi}$, the relations can be expanded to the position along the y- and z-axes as,

$$\boldsymbol{y} = \boldsymbol{\Gamma} \boldsymbol{P}^T \boldsymbol{\eta}, \tag{16a}$$

$$\boldsymbol{z} = \boldsymbol{\Gamma} \boldsymbol{P}^T \boldsymbol{\zeta}. \tag{16b}$$

Note that the original path matrix $\boldsymbol{P}$ is used in this relation, not the expanded version $\widetilde{\boldsymbol{P}}$.

In the following, the equations of motion are derived under the assumption of constant length rods and a CM following a circular orbit with orbital rate ω. For simplicity, we first restrict the derivation of the dynamics of this formation to the motion in the orbit plane. The derivation for the general three dimensional motion is included in A. Due to the assumption of a circular orbit, ω is constant, and the true anomaly $\nu = \omega t$ is introduced as the time variable for the system. The in-plane angles θ_j are chosen as generalized coordinates and are collected in the vector $\boldsymbol{\theta} = [\theta_1, \ldots, \theta_n]^T$. The in-plane angle θ_j is defined with respect to axes parallel with the orbit frame centered at the initial node of l_j, as seen in Figure 2. The vectors along the rods are then,

$$\boldsymbol{\rho}_j = \begin{bmatrix} l_j \cos \theta_j \\ l_j \sin \theta_j \end{bmatrix}. \tag{17}$$

The velocity of each mass in the inertial frame can be written as $\boldsymbol{V}_i = \boldsymbol{V}_{CM} + \boldsymbol{v}_i$ for $i = 0, \ldots, n$, where $\boldsymbol{V}_{CM}$ is the velocity of the CM and $\boldsymbol{v}_i$ is the velocity of m_i relative to the CM. The relative velocity is,

$$\boldsymbol{v}_i = \begin{bmatrix} \omega \dot{x}_i - \omega y_i \\ \omega \dot{y}_i + \omega x_i \end{bmatrix}, \tag{18}$$

where $(\dot{\ })$ denotes the first derivative with respect to ν relative to the orbit frame. The total kinetic energy of the formation can be written as,

$$\mathcal{T} = \frac{m}{2} |\boldsymbol{V}_{CM}|^2 + \sum_{i=0}^{n} m_i \boldsymbol{V}_{CM} \cdot \boldsymbol{v}_i + \frac{1}{2} \sum_{i=0}^{n} m_i |\boldsymbol{v}_i|^2. \tag{19}$$

Only the last term of (19) contributes to the equations of motion, since the first term is constant and the second term vanishes in Lagrange's equation. With an assumption that the length of each rod l_j is much smaller than the orbit radius, the potential energy of the system can be approximated by,

$$\mathcal{V} = \mathcal{V}_{CM} + \frac{\omega^2}{2} \sum_{i=0}^{n} m_i \left(|\boldsymbol{r}_i|^2 - 3x_i^2 \right), \tag{20}$$

where $\mathcal{V}_{CM}$ is the constant orbital energy of the circular orbit, which will not contribute to the attitude motion. From the energy functions the equations of

motion can be found using Lagrange's equation,

$$\frac{d}{d\nu}\frac{\partial \mathcal{T}}{\partial \dot{\theta}_j} - \frac{\partial \mathcal{T}}{\partial \theta_j} + \frac{\partial \mathcal{V}}{\partial \theta_j} = 0, \qquad j = 1, \ldots, n. \tag{21}$$

Inserting (19) and (20) in (21) results in the equations of motion,

$$\mathcal{M}\ddot{\boldsymbol{\theta}} + \mathcal{G} = 0, \tag{22}$$

where

$$\mathcal{M} = \boldsymbol{E}_{\sin\theta}\boldsymbol{LGL}\boldsymbol{E}_{\sin\theta} + \boldsymbol{E}_{\cos\theta}\boldsymbol{LGL}\boldsymbol{E}_{\cos\theta}, \tag{23a}$$

$$\mathcal{G} = \left(\boldsymbol{E}_{\sin\theta}\boldsymbol{LGL}\boldsymbol{E}_{\cos\theta} - \boldsymbol{E}_{\cos\theta}\boldsymbol{LGL}\boldsymbol{E}_{\sin\theta}\right)\left(2\boldsymbol{I} + \boldsymbol{E}_{\dot{\theta}}\right)\dot{\boldsymbol{\theta}}$$
$$+ 3\boldsymbol{E}_{\sin\theta}\boldsymbol{LGL}\boldsymbol{E}_{\cos\theta}\boldsymbol{1}_n. \tag{23b}$$

The matrices $\boldsymbol{E}_{\cos\theta} \in \mathbb{R}^{n\times n}$ and $\boldsymbol{E}_{\sin\theta} \in \mathbb{R}^{n\times n}$ are diagonal matrices with $\cos\theta_j$ and $\sin\theta_j$, respectively, at the jth diagonal entry. Similarly $\boldsymbol{E}_{\dot{\theta}} \in \mathbb{R}^{n\times n}$ is diagonal with $\dot{\theta}_j$ at the jth diagonal entry. All elements of the vector $\boldsymbol{1}_n \in \mathbb{R}^n$ equal 1. All parameters of the model are then collected in a single matrix $\boldsymbol{LGL}$ where,

$$\boldsymbol{G} = \boldsymbol{P}\boldsymbol{\Gamma}^T\boldsymbol{\Lambda}\boldsymbol{\Gamma}\boldsymbol{P}^T. \tag{24}$$

Here $\boldsymbol{G} \in \mathbb{R}^{n\times n}$ is referred to as the mass matrix of the system. The mass matrix will be investigated further in the next section, in connection with determination of stationary configurations of the system.

IV   Stationary configuration in the orbit plane

In this section, the stationary configurations of the system are investigated. We restrict the investigation to the stationary configuration in the orbit plane. The in-plane stationary configuration can be treated separately, since the motion in the orbit plane is restricted to an invariant manifold in state space (see A). It should, however, be emphasized that there exist stationary configurations which are not situated in the orbit plane. In [14] these general stationary configurations have been investigated for a chain structure. The present investigation follows the same steps as [6] and is based on the same properties which are expanded to the present case with a tree structure.

a)   Properties of mass matrix

For the analysis of the stationary configuration the mass matrix $\boldsymbol{G}$ is of significant importance. We therefore start this section by stating some properties

regarding $\boldsymbol{G}$ which will be used when finding and analyzing the stationary configuration of the formation. Proofs of the properties of this section can be found in B. From (24) the matrix $\boldsymbol{W} \in \mathbb{R}^{n \times n}$ is defined as $\boldsymbol{W} = \boldsymbol{\Gamma}^T \boldsymbol{\Lambda} \boldsymbol{\Gamma}$ such that the mass matrix can be written as,

$$\boldsymbol{G} = \boldsymbol{P} \boldsymbol{W} \boldsymbol{P}^T. \tag{25}$$

From the definition of $\boldsymbol{\Gamma}$ in (15) the elements of $\boldsymbol{W}$ can be found as,

$$W_{ik} = \mu_i \delta_{ik} - \mu_i \mu_k. \tag{26}$$

The matrix $\boldsymbol{W}$ is clearly symmetric and obeys the following property.

Property 1. *The matrix $\boldsymbol{W}$ is positive definite and the elements of the inverse matrix are given as,*

$$W_{ki}^{-1} = \frac{1}{\mu_0} + \frac{\delta_{ki}}{\mu_i}. \tag{27}$$

Property 1 serves mainly to prove the statements regarding $\boldsymbol{G}$ in the next property.

Property 2. *The mass matrix $\boldsymbol{G}$ is symmetric and positive definite. The elements of its inverse satisfies the property that $G_{jk}^{-1} = 0$ for $k \notin N_j \wedge j \neq k$.*

The last point in Property 2 states that the transformation of $\boldsymbol{G}$ into a identity matrix can be made by linear combinations consisting only of columns corresponding to neighboring edges. This point is similar to Property 1 in [6]. The assumption $k \notin N_j$ is equivalent to $j \notin N_k$, which must be the case since $\boldsymbol{G}$ is symmetric.

The elements of $\boldsymbol{G}$ can be formulated by means of the sub-trees T_j of the graph introduced in Section II. This formulation is useful when proving Property 3 and it will be treated further in the proof of that property. First the sum M_{jk} is introduced as,

$$M_{jk} = \sum_{i \in T_j \cap T_k} \mu_i. \tag{28}$$

The definition is based on the nodes of two arbitrary sub-trees in the graph, T_j and T_k. The sum is taken over the intersection of the two trees, hence for M_{jk} to be different from zero T_j must be a sub-tree in T_k or vice versa. Using M_{jk} the elements for $\boldsymbol{G}$ can be written as,

$$G_{jk} = M_{jk} - M_{jj} M_{kk}. \tag{29}$$

Note that M_{jj} sums the nodes in the sub-tree T_j and is therefore always different from zero.

When solving the equation leading to the stationary configuration a reduced version of the mass matrix will occur. From an arbitrary set of rods J with complement $\bar{J}$ the reduced mass matrix $\widehat{G} \in \mathbb{R}^{|\bar{J}| \times |\bar{J}|}$ is defined by removing the rows and columns corresponding to rods in the set J. We connect a reduced graph with the set J. The graph occurs when the edges in the set J are removed

(a) Original Graph
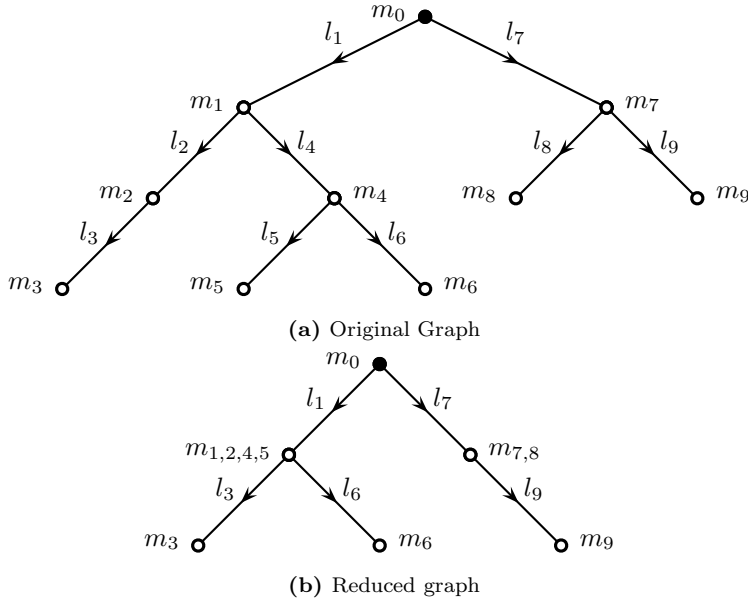
(b) Reduced graph

Figure 3: Graph and its by $J = \{2, 4, 5, 8\}$ reduced counterpart.

from the graph as shown in Figure 3. The reduction is done based on the decomposition of $J = \cup_k J_k$ introduced in Section II. Each component J_k forms a tree. The tree J_k can be assumed rooted at a node m_i if all edges $j \in J_k$ are included in sub-tree T_i. We denote m_i the root of J_k. The sub-tree T_i can be decomposed into J_k and a number of sub-trees. When the tree J_k is removed the from the graph, these sub-trees are connected to the root of J_k. The following property, which is illustrated in Figure 3, shows a relation between the graph reduced by the set J and the reduced matrix $\widehat{G}$.

Property 3. *Consider a graph reduced by the set $J = \cup_k J_k$ and the roots m_i of J_k. Assume that the nodes m_i are assigned the sum of the nodes in the sub-trees J_k, while the remaining nodes stay unchanged. Then the mass matrix of the reduced graph will equal the reduced mass matrix $\widehat{G}$ of the original graph.*

The important point regarding Property 3 is that $\widehat{G}$ is the mass matrix for a different graph, hence the statement in Property 2 also applies to $\widehat{G}$. When

working with the reduced graph we keep referring to the rods according to the original graph. This also applies when referring to rows, columns, and elements of the corresponding matrices and vectors.

The next property addresses the similarity between $\widehat{\boldsymbol{G}}^{-1}$ and $\boldsymbol{G}^{-1}$.

Property 4. *Assume that* $j, k \in \bar{J}$ *such that the element* $\widehat{G}_{jk}^{-1}$ *exists, then*

$$\widehat{G}_{jk}^{-1} = G_{jk}^{-1} \quad \text{for} \quad j, k \notin N_J. \tag{30}$$

This property states that the common elements of a row of $\widehat{\boldsymbol{G}}^{-1}$ representing an edge with no neighbors in J is unchanged compared to $\boldsymbol{G}^{-1}$, hence the reduction only introduces a local change in the inverse mass matrix. Furthermore, using Property 2 it can be seen that the elements excluded from the row compared to $\boldsymbol{G}^{-1}$ in this case equal zero. Note that $\widehat{\boldsymbol{G}}^{-1}$ is symmetric, hence the property could just as well be explained with respect to columns.

b)   Equation of stationary configuration

From the equations of motion (22) a stationary configuration $\boldsymbol{\theta}^*$ in the orbit plane is found as a solution to the equation,

$$\boldsymbol{E}_{\sin\theta}^* \boldsymbol{G} \boldsymbol{\xi}^* = \boldsymbol{0}_n, \tag{31}$$

where $\boldsymbol{\xi}^* = [l_1 \cos\theta_1^*, \ldots, l_n \cos\theta_n^*]^T$ and $\boldsymbol{E}_{\sin\theta}^*$ denotes $\boldsymbol{E}_{\sin\theta}$ evaluated at $\boldsymbol{\theta} = \boldsymbol{\theta}^*$. The first thing to note about (31) is that the stationary configurations are symmetric in the sense that if $\boldsymbol{\theta}^*$ is a stationary configuration so is $\bar{\boldsymbol{\theta}}^* = \pi\boldsymbol{1}_n - \boldsymbol{\theta}^*$. In a stationary configuration a rod is characterized as horizontal if $\cos\theta_k^* = 0$. If $\sin\theta_k^* = 0$ the rod is vertical. Eq. (31) is in general solved by choosing a set J containing vertical rods, hence $\sin\theta_j^* = 0$ for $j \in J$. Denoting the rows of $\boldsymbol{G}$ as $\boldsymbol{G}_j$ for $j = 1, \ldots, n$, the matrix equation (31) can be divided into n coupled scalar equations,

$$\sin\theta_j^* \boldsymbol{G}_j^T \boldsymbol{\xi}^* = 0 \qquad \text{for } j = 1, \ldots, n. \tag{32}$$

From (32) it is seen that for each vertical rod one of the n equations is solved, hence introducing J leaves $|\bar{J}|$ equations to be solved.

Two choices of J stand out from the general solution procedure. First $J = \emptyset$ where no rods are situated in a vertical position. In this case (31) reduces to,

$$\boldsymbol{G}\boldsymbol{\xi}^* = \boldsymbol{0}_n. \tag{33}$$

Due to Property 2 the equation has a unique solution $\boldsymbol{\xi}^* = \boldsymbol{0}_n$ corresponding to rods situated in a horizontal position. Each rod can have two different orientations in a horizontal position (corresponding to symmetric configurations), hence there are 2^n different configurations for $\boldsymbol{\xi}^* = \boldsymbol{0}_n$. The second special case is $\bar{J} = \emptyset$, i.e. all rods are in a vertical position. In this case, all n equations in (32) are solved immediately. A rod in a vertical position has two different orientations, which again leads to 2^n configurations. The existence of the 2^{n+1} configurations in the two special cases are independent of the parameters of the system. These stationary configurations are similar to the four stationary configurations induced by the gravity gradient for a single rod in orbit.

In the remaining cases where $J \neq \emptyset$ and $\bar{J} \neq \emptyset$ equation (31) can be written as,

$$\widehat{G}\hat{\boldsymbol{\xi}}^* = -\sum_{k \in J} \hat{g}_k \xi_k^*, \tag{34}$$

where $\hat{\boldsymbol{\xi}}^*$ equals $\boldsymbol{\xi}^*$ reduced by the set J. The vector $\hat{g}_k$ is the kth column of $\boldsymbol{G}$ reduced by the elements in J. Note that $\hat{g}_k$ does not equal the kth column of the reduced mass matrix $\widehat{G}$ since $k \in J$. Eq. (34) gives the relation between the rods fixed in a vertical position ξ_k^* for $k \in J$ and the orientation of the remaining rods are collected in $\hat{\boldsymbol{\xi}}^*$. The vertical orientation implies that $\xi_k^* = \pm l_k$ for $k \in J$, hence (34) actually includes $2^{|J|}$ equations taking all sign combinations into account. According to Property 3 the matrix $\widehat{G}$ has full rank, and the solution of (34) is unique for each right-hand side. The existence of each configuration can be investigated from the vector $\hat{\boldsymbol{\sigma}} \in \mathbb{R}^{|\bar{J}|}$,

$$\hat{\boldsymbol{\sigma}} = -\widehat{\boldsymbol{L}}^{-1}\widehat{\boldsymbol{G}}^{-1}\sum_{k \in J} \hat{g}_k \xi_k^*, \tag{35}$$

where $\widehat{\boldsymbol{L}}$ is a reduced version of $\boldsymbol{L}$. The elements of $\hat{\boldsymbol{\sigma}}$ equal $\hat{\sigma}_j = \cos\theta_j^*$ for $j \in \bar{J}$. Hence the stationary configuration exists if the absolute value of all elements of $\hat{\boldsymbol{\sigma}}$ are less than one, $|\hat{\sigma}_j| < 1$ for $j \in \bar{J}$. Note that the case $|\hat{\sigma}_j| = 1$ is not included, since this would contradict the assumption that $j \in \bar{J}$.

The similarity between $\boldsymbol{G}^{-1}$ and $\widehat{\boldsymbol{G}}^{-1}$ stated in Property 4 can be used together with the knowledge of the zero elements of $\boldsymbol{G}^{-1}$ from Property 2 to conclude that,

$$(\widehat{\boldsymbol{G}}_j^{-1})^T \hat{g}_k = 0 \qquad \text{for } k \in J, j \notin N_J \tag{36}$$

where $\widehat{\boldsymbol{G}}_j^{-1}$ denotes the jth column of $\widehat{\boldsymbol{G}}^{-1}$. From (35) it is seen that this implies that $\hat{\sigma}_j = 0$ if $j \notin N_J$. The geometrical interpretation of this property is that, in a stationary configuration, only the neighbors of a vertical rod will be affected, while all others will remain horizontal. Hence it can be concluded that the stationary configuration consists of groups of either horizontal or vertical rods,

which are separated by no more than one inclined rod. This was also concluded in [6] for a chain structure. The vertical groups are orthogonal to the horizontal groups and therefore no forces can be transferred along the inclined rods, in stationary configurations. This furthermore shows that all horizontal groups are placed along the y-axis where the centrifugal force cancels the gravitational force. A detailed stability analysis of the configurations is not in the scope of this article, but the above description indicates that all formation with one or more horizontal groups will be unstable, since the masses of these groups will balance at the unstable equilibrium between the centrifugal and the gravitational force.

Since both G and $\widehat{G}$ have full rank, the described method will result in all possible stationary configurations of the system. The total number of possible stationary configurations can be found by realizing that the set J can be chosen in 2^n different ways. Each rod have two possible orientations, hence there are $2^{|J|}2^{|\bar{J}|} = 2^n$ possible orientations for each choice of J. This leads to a total number of possible configurations of 2^{2n}. This limit is the same as was obtained for a chain structure in [6].

V   Example

This example will consider five satellites in a Y-formation illustrated in Figure 4. The nodes m_0 and m_2 are marked to better illustrate the formation. This
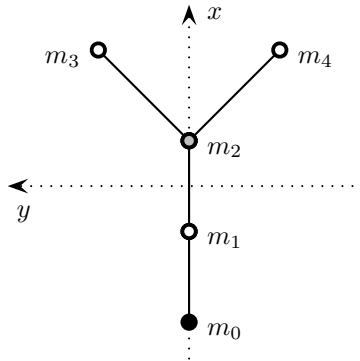
Figure 4: Y-formation.

is also done in the Figures 5 to 7. The incidence matrix of the Y-formation is given as,

$$B = \begin{bmatrix} 1 & 0 & 0 & 0 \\ -1 & 1 & 0 & 0 \\ 0 & -1 & 1 & 1 \\ 0 & 0 & -1 & 0 \\ 0 & 0 & 0 & -1 \end{bmatrix}. \tag{37}$$

Using this incidence matrix and (25) the mass matrix is,

$$\boldsymbol{G} = \begin{bmatrix} \mu_0(1-\mu_0) & \mu_0\mu_{2,3,4} & \mu_0\mu_3 & \mu_0\mu_4 \\ \mu_0\mu_{2,3,4} & (1-\mu_0-\mu_1)\mu_{2,3,4} & (1-\mu_0-\mu_1)\mu_3 & (1-\mu_0-\mu_1)\mu_4 \\ \mu_0\mu_3 & (1-\mu_0-\mu_1)\mu_3 & (1-\mu_3)\mu_3 & -\mu_3\mu_4 \\ \mu_0\mu_4 & (1-\mu_0-\mu_1)\mu_4 & -\mu_3\mu_4 & (1-\mu_4)\mu_4 \end{bmatrix}, \tag{38}$$

where $\mu_{2,3,4} = \mu_2 + \mu_3 + \mu_4$. The inverse is given as,

$$\boldsymbol{G}^{-1} = \begin{bmatrix} \frac{\mu_0+\mu_1}{\mu_0\mu_1} & -\frac{1}{\mu_1} & 0 & 0 \\ -\frac{1}{\mu_1} & \frac{\mu_1+\mu_2}{\mu_1\mu_2} & -\frac{1}{\mu_2} & -\frac{1}{\mu_2} \\ 0 & -\frac{1}{\mu_2} & \frac{\mu_2+\mu_3}{\mu_2\mu_3} & \frac{1}{\mu_2} \\ 0 & -\frac{1}{\mu_2} & \frac{1}{\mu_2} & \frac{\mu_2+\mu_4}{\mu_2\mu_4} \end{bmatrix}. \tag{39}$$

According to the previous section, the total number of possible stationary configurations is 256 for this example. The qualitatively different configurations are illustrated in Figures 5 to 7. The configurations are found by fixing the masses

(a) $J = \emptyset$ **(b)** $J = \{1\}$

(c) $J = \{2\}$ **(d)** $J = \{3\}, \{4\}$
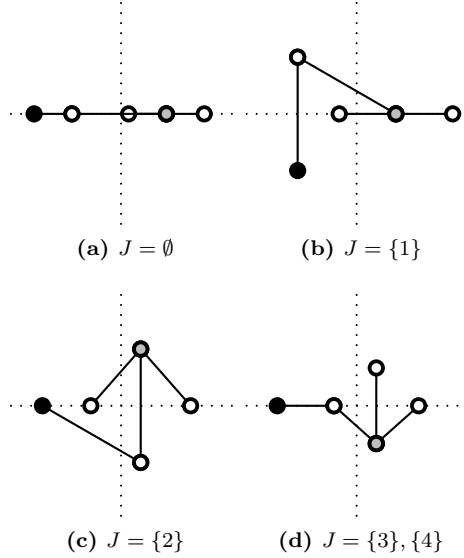
Figure 5: Y-formations with $|J| = 0$ or $|J| = 1$.

uniformly and adjusting the length of the rods to illustrate the formation best possible and ensure that a stationary configuration actually exists. It is emphasized that the figures only exemplify configurations, since for each choice of J, there exist 16 configurations divided into 8 symmetric pairs. The formations illustrate that a horizontal rod only affects its neighboring rods, while the remaining rods will maintain their vertical orientation. It is also seen that masses not connected to a rod in the set J are placed along the y-axis. Examining the

(a) $J = \{1, 2\}$ **(b)** $J = \{1, 3\}, \{1, 4\}$

(c) $J = \{2, 3\}, \{2, 4\}$ **(d)** $J = \{3, 4\}$
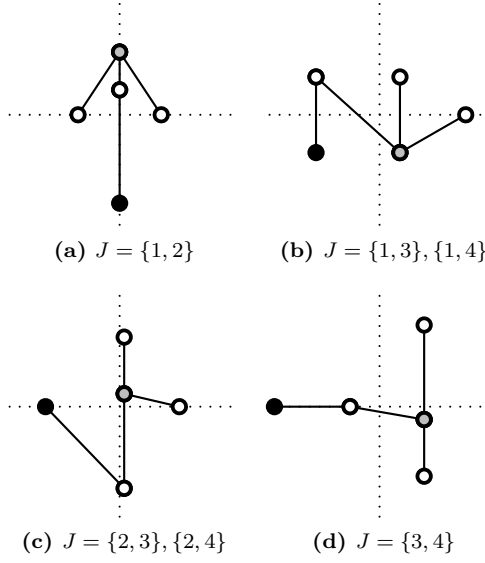
Figure 6: Y-formations with $|J| = 2$.

(a) $J = \{1, 2, 3\}, \{1, 2, 4\}$ **(b)** $J = \{1, 3, 4\}$

(c) $J = \{2, 3, 4\}$ **(d)** $J = \{1, 2, 3, 4\}$
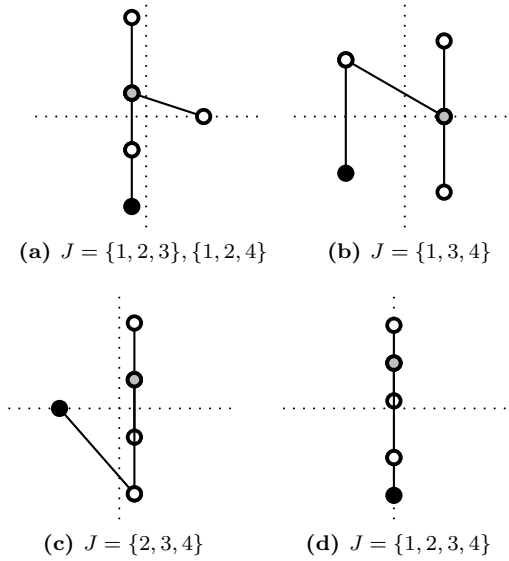
Figure 7: Y-formations with $|J| = 3$ or $|J| = 4$.

configurations it is seen that rods that are neither vertical nor horizontal, and are connected to a group at both ends, separate two groups of either horizontal

or vertical rods. Such rods cannot affect either of the groups with forces, since the configuration is stationary.

VI   Conclusions

With the aim of easing the task of modeling dynamics of tethered satellite formations, and determine stationary configurations, this paper combined graph theory with Lagrange formalism to obtain a generic framework for modeling. Imposing an assumption of a tree structure on the formation, enabled the path between the satellites, along the tethers, to be unique. Furthermore it allowed the paths from sub-satellites to a main satellite to be described by a single matrix quantity. A generic method for modeling was obtained by using this path matrix together with Lagrange formalism and the equations of motion were derived for both the in-plane motion and for the general three dimensional case. Constant-length rigid tethers and a circular orbit were assumed for the formation. The assumption of a tree structure simplified the equations, since the absence of algebraic constraints around cycles in the formation resulted in a formulation where each tether represents a single degree of freedom. A particular feature of the methodology was that the equations of motion were given in a matrix formulation, with the desirable property that all physical parameters, as well as the formation description, were captured by a single matrix. Furthermore, a method of finding the stationary configurations in the orbit plane was suggested, using the generic equations of motion. These configurations were classified based on the numbers of rods situated in a vertical equilibrium position and the upper limit of stationary configurations was determined to be the same as that of a chain structure. The method could be expanded to take stationary configurations into account that were not situated in the orbit plane. This would complicate the method and an upper limit would need be established for this case. The main advantage of the modeling based on graph theory presented in this article is that a broad class of formation can be treated collectively, and that both dynamic and stationary properties can be dealt with through this formalism.

Appendix

A   Equations of motion in three dimensions

A two degree of freedom model taking both in-plane and out-of-plane motion into account is deduced in this appendix. The procedure is identical to the one used for the in-plane motion in Section III, but the derivation becomes more cumbersome due to the additional states and the interaction between in-plane and out-of-plane motions. Denoting the out-of-plane angle φ, the vectors along the rods can be written as,

$$\boldsymbol{\rho}_j = \begin{bmatrix} l_j \cos \theta_j \cos \varphi_j \\ l_j \sin \theta_j \cos \varphi_j \\ l_j \sin \varphi_j \end{bmatrix}. \tag{40}$$

The relative velocity of the mass m_i is expanded with an out-of-plane component, compared to (18),

$$\boldsymbol{v}_i = \begin{bmatrix} \omega \dot{x}_i - \omega y_i \\ \omega \dot{y}_i + \omega x_i \\ \omega \dot{z}_i \end{bmatrix}. \tag{41}$$

The kinetic and the potential energies are unchanged compared to (19) and (20). Inserting the energies including the out-of-plane motion into Lagrange's equation, the system can be written as,

$$\begin{bmatrix} \mathcal{M}_{11} & \mathcal{M}_{12} \\ \mathcal{M}_{12}^T & \mathcal{M}_{22} \end{bmatrix} \begin{bmatrix} \ddot{\boldsymbol{\theta}} \\ \ddot{\boldsymbol{\varphi}} \end{bmatrix} + \begin{bmatrix} \mathcal{G}_1 \\ \mathcal{G}_2 \end{bmatrix} = 0, \tag{42}$$

where the matrices can be found to be,

$$\mathcal{M}_{11} = \boldsymbol{E}_{\sin\theta} \boldsymbol{E}_{\cos\varphi} \widetilde{\boldsymbol{G}} \boldsymbol{E}_{\sin\theta} \boldsymbol{E}_{\cos\varphi} + \boldsymbol{E}_{\cos\theta} \boldsymbol{E}_{\cos\varphi} \widetilde{\boldsymbol{G}} \boldsymbol{E}_{\cos\theta} \boldsymbol{E}_{\cos\varphi}, \tag{43a}$$

$$\mathcal{M}_{22} = \boldsymbol{E}_{\cos\theta} \boldsymbol{E}_{\sin\varphi} \widetilde{\boldsymbol{G}} \boldsymbol{E}_{\cos\theta} \boldsymbol{E}_{\sin\varphi} + \boldsymbol{E}_{\cos\varphi} \widetilde{\boldsymbol{G}} \boldsymbol{E}_{\cos\varphi},$$
$$+ \boldsymbol{E}_{\sin\theta} \boldsymbol{E}_{\sin\varphi} \widetilde{\boldsymbol{G}} \boldsymbol{E}_{\sin\theta} \boldsymbol{E}_{\sin\varphi} \tag{43b}$$

$$\mathcal{M}_{12} = \boldsymbol{E}_{\sin\theta} \boldsymbol{E}_{\cos\varphi} \widetilde{\boldsymbol{G}} \boldsymbol{E}_{\cos\theta} \boldsymbol{E}_{\sin\varphi} - \boldsymbol{E}_{\cos\theta} \boldsymbol{E}_{\cos\varphi} \widetilde{\boldsymbol{G}} \boldsymbol{E}_{\sin\theta} \boldsymbol{E}_{\sin\varphi}, \tag{43c}$$

$$\mathcal{G}_1 = \big(\boldsymbol{E}_{\sin\theta} \boldsymbol{E}_{\cos\varphi} \widetilde{\boldsymbol{G}} \boldsymbol{E}_{\cos\theta} \boldsymbol{E}_{\cos\varphi}$$
$$- \boldsymbol{E}_{\cos\theta} \boldsymbol{E}_{\cos\varphi} \widetilde{\boldsymbol{G}} \boldsymbol{E}_{\sin\theta} \boldsymbol{E}_{\cos\varphi} \big) \big((2\boldsymbol{I} + \boldsymbol{E}_{\dot\theta}) \dot{\boldsymbol{\theta}} + \boldsymbol{E}_{\dot\varphi} \dot{\boldsymbol{\varphi}} \big)$$
$$- 2 \big(\boldsymbol{E}_{\sin\theta} \boldsymbol{E}_{\cos\varphi} \widetilde{\boldsymbol{G}} \boldsymbol{E}_{\sin\theta} \boldsymbol{E}_{\sin\varphi}$$
$$+ \boldsymbol{E}_{\cos\theta} \boldsymbol{E}_{\cos\varphi} \widetilde{\boldsymbol{G}} \boldsymbol{E}_{\cos\theta} \boldsymbol{E}_{\sin\varphi} \big) \big(\boldsymbol{I} + \boldsymbol{E}_{\dot\theta} \big) \dot{\boldsymbol{\varphi}}$$
$$+ 3 \boldsymbol{E}_{\sin\theta} \boldsymbol{E}_{\cos\varphi} \widetilde{\boldsymbol{G}} \boldsymbol{E}_{\cos\theta} \boldsymbol{E}_{\cos\varphi} \boldsymbol{1}_n, \tag{43d}$$

$$
\begin{aligned}
\mathcal{G}_2 = \big(& \boldsymbol{E}_{\cos\theta} \boldsymbol{E}_{\sin\varphi} \widetilde{\boldsymbol{G}} \boldsymbol{E}_{\cos\theta} \boldsymbol{E}_{\cos\varphi} \\
& + \boldsymbol{E}_{\sin\theta} \boldsymbol{E}_{\sin\varphi} \widetilde{\boldsymbol{G}} \boldsymbol{E}_{\sin\theta} \boldsymbol{E}_{\cos\varphi} \big) \big((2\boldsymbol{I} + \boldsymbol{E}_{\dot\theta}) \dot{\boldsymbol{\theta}} + \boldsymbol{E}_{\dot\varphi} \dot{\boldsymbol{\varphi}} \big) \\
& - \boldsymbol{E}_{\cos\varphi} \widetilde{\boldsymbol{G}} \boldsymbol{E}_{\sin\varphi} \boldsymbol{E}_{\dot\varphi} \dot{\boldsymbol{\varphi}} \\
& + 2\big(\boldsymbol{E}_{\sin\theta} \boldsymbol{E}_{\sin\varphi} \widetilde{\boldsymbol{G}} \boldsymbol{E}_{\cos\theta} \boldsymbol{E}_{\sin\varphi} \\
& - \boldsymbol{E}_{\cos\theta} \boldsymbol{E}_{\sin\varphi} \widetilde{\boldsymbol{G}} \boldsymbol{E}_{\sin\theta} \boldsymbol{E}_{\sin\varphi} \big) \big(\boldsymbol{I} + \boldsymbol{E}_{\dot\theta} \big) \dot{\boldsymbol{\varphi}} \\
& + 3 \boldsymbol{E}_{\cos\theta} \boldsymbol{E}_{\sin\varphi} \widetilde{\boldsymbol{G}} \boldsymbol{E}_{\cos\theta} \boldsymbol{E}_{\cos\varphi} \mathbf{1}_n + \boldsymbol{E}_{\cos\varphi} \widetilde{\boldsymbol{G}} \boldsymbol{E}_{\sin\varphi} \mathbf{1}_n.
\end{aligned}
\tag{43e}
$$

The matrices $\boldsymbol{E}_{\cos\varphi}$ and $\boldsymbol{E}_{\sin\varphi}$ are defined similarly to $\boldsymbol{E}_{\cos\theta}$ and $\boldsymbol{E}_{\sin\theta}$, while $\boldsymbol{E}_{\dot\varphi}$ is defined in the same way as $\boldsymbol{E}_{\dot\theta}$. All parameters are collected in the matrix $\widetilde{\boldsymbol{G}} = \boldsymbol{L}\boldsymbol{G}\boldsymbol{L}$, in the same way as for the in-plane motion. The equations shows that motion in the orbit plane does not give rise to a motion out of the plane, hence the in-plane motion compose an invariant manifold. By contrast, the opposite is not the case. An out-of-plane motion will excite the in-plane dynamics.

B Proof of properties

Proof of Property 1. To prove that $\boldsymbol{W}$, $W_{ik} = \mu_i \delta_{ik} - \mu_i \mu_k$, is positive definite, it is used that $\boldsymbol{W}$ is symmetric. The Sylvester Criterion [16, 7.2.5, p. 404] states that a Hermitian is positive definite if the determinant of all upper left sub-matrices as well as the matrix itself are positive definite. First $\boldsymbol{W}$ is rewritten in the matrix form,

$$
\boldsymbol{W} = \widetilde{\boldsymbol{\Lambda}} - \boldsymbol{\mu}\boldsymbol{\mu}^T
\tag{44}
$$

where $\widetilde{\boldsymbol{\Lambda}} \in \mathbb{R}^{n \times n}$ is a diagonal matrix $\widetilde{\Lambda}_{ik} = \mu_i \delta_{ik}$ and $\boldsymbol{\mu} = [\mu_1 \ \ldots \ \mu_n]^T$. The matrix determinant lemma can be used to find the determinant of the sub-matrices. The upper left square matrices can be found by truncating $\widetilde{\boldsymbol{\Lambda}}$ and $\boldsymbol{\mu}$. The truncated versions containing ℓ elements are denoted $\boldsymbol{W}_\ell, \widetilde{\boldsymbol{\Lambda}}_\ell \in \mathbb{R}^{\ell \times \ell}$ and $\boldsymbol{\mu}_\ell \in \mathbb{R}^\ell$. The matrix determinant lemma states that $\det\left(\boldsymbol{A} + \boldsymbol{u}\boldsymbol{v}^T\right) = \left(1 + \boldsymbol{v}^T \boldsymbol{A}^{-1} \boldsymbol{u}\right) \det \boldsymbol{A}$, which, applied to the sub-matrices, leads to,

$$
\det \boldsymbol{W}_\ell = \left(1 - \boldsymbol{\mu}_\ell \widetilde{\boldsymbol{\Lambda}}_\ell^{-1} \boldsymbol{\mu}_\ell^T\right) \det \widetilde{\boldsymbol{\Lambda}}_\ell = \left(\mu_0 + \sum_{j=\ell+1}^n \mu_j\right) \prod_{j=1}^\ell \mu_j > 0.
\tag{45}
$$

For $\ell = n$ the determinant of $\boldsymbol{W}$ is,

$$
\det \boldsymbol{W} = \prod_{i=0}^n \mu_i > 0,
\tag{46}
$$

which means that W is positive definite. The inverse of W can be found from (44) using the Sherman-Morrison formula [16, 0.7.4, pp. 18-19],

$$W^{-1} = \widetilde{\Lambda}^{-1} + \frac{\mathbf{1}_n \mathbf{1}_n^T}{\mu_0}. \tag{47}$$

$\square$

Proof of Property 2. Since P has full rank and W is positive definite, it can be concluded, using [16, 7.1.6 p. 399], that $G = PWP^T$ is symmetric and positive definite. The last part of the property states that $G_{jk}^{-1} = 0$ for $k \notin N_j \wedge j \neq k$. This is proved using the fact that $P^{-1} = A$, hence $G^{-1} = A^T W^{-1} A$. The product is easily found since each column of A has no more than two non-zero elements. Denoting the initial nodes of l_j and l_k by m_p and m_q, respectively, the inverse matrix can be written as,

$$G_{jk}^{-1} = \frac{1}{\mu_j}\delta_{jk} - \frac{1}{\mu_p}\delta_{pk} - \frac{1}{\mu_j}\delta_{jq} + \frac{1}{\mu_p}\delta_{pq}, \tag{48}$$

assuming that $m_p \neq m_0$ and $m_q \neq m_0$. The first term represents the diagonal of G^{-1}. The next terms include the entries of upper and lower neighbors of l_j in the path to the root. The last term represents the situation where l_j and l_k have a common upper neighbor. Hence only entries representing neighbors of l_j are different from zero in the jth column of G^{-1}. Similar calculations show that the property is also valid in case $m_p = m_0$ and/or $m_q = m_0$. $\square$

Proof of Property 3. First it is proved that $G_{jk} = M_{jk} - M_{jj}M_{kk}$, using the fact that the jth row of P can be expressed by means of the sub-tree T_j as in (6). By insertion it is seen that the first part of the product $G = PWP^T$ can be written,

$$(PW)_{ji} = \sum_{k=1}^{n} P_{jk}W_{ki} = -\sum_{k \in T_j} \mu_k \delta_{ik} + \sum_{k \in T_j} \mu_k \mu_i = -\mu_i d_{ij} + \mu_i M_{jj}, \tag{49}$$

where $d_{ij} = 1$ if $i \in T_j$, and zero otherwise. The elements of G are then found,

$$G_{jk} = \sum_{i=1}^{n} (PW)_{ji} P_{ki} = -M_{jj} \sum_{i \in T_k} \mu_i + \sum_{i \in T_k} \mu_i d_{ij} = M_{ij} - M_{ii}M_{jj}, \tag{50}$$

hence (29) is proved. The sum of the nodes in a sub-tree T_j is not affected by the reduction, which together with (29) proves the property. $\square$

Proof of Property 4. Denote again the nodes incident to l_j by m_j and m_p, and assume that $m_p \neq m_0$. The elements of $\boldsymbol{G}^{-1}$ are given in (48), which is also valid for $\widehat{\boldsymbol{G}}^{-1}$ using the node values of the reduced graph. If $G_{jk}^{-1} = 0$ then $k \in N_j$ or equivalently, $j \in N_k$. This can only be changed by the reduction if there exists an edge $q \in J$ such that $q \in N_j$ and $q \in N_J$. This implies that $j \in N_J$ and $k \in N_k$, which is in contradiction to the assumption, hence the property holds for $G_{jk}^{-1} = 0$. The entry $G_{jk}^{-1} \neq 0$ if $j = k$ or $k \in N_j$ (equivalent $j \in N_k$). This neighboring relation cannot be changed by the reduction since $j, k \notin J$. The quantity G_{jk}^{-1} only depends on μ_j and μ_p, which will only change by the reduction if there exists an edge $q \in J$ incident to m_j or m_p. This means that $q \in N_j$ and consequently $j \in N_J$, which is again in contradiction to the assumption. Hence the property is proved for $m_p \neq m_0$. A similar argument can be made for $m_p = m_0$. $\qquad\square$

References

[1] M. L. Cosmo and E. C. Lorenzini, editors. *Tethers in space handbook.* NASA Marshall Space Flight Center, 3rd edition, 1997.

[2] E C Lorenzini, M Cosmo, S Vetrella, and A Moccia. Dynamics and control of the tether elevator/crawler system. *Journal of Guidance, Control, and Dynamics*, 12(3):404–411, may-jun 1989. ISSN 0731-5090.

[3] N Takeichi, MC Natori, and N Okuizumi. Dynamic behavior of a tethered system with multiple subsatellites in elliptic orbits. *Journal of Spacecraft and Rockets*, 38(6):914–921, NOV-DEC 2001. ISSN 0022-4650.

[4] C. Bombardelli, E. C. Lorenzini, and M. B. Quadrelli. Retargeting dynamics of a linear tethered interferometer. *Journal of Guidance, Control, and Dynamics*, 27(6):1061–1067, nov-dec 2004. ISSN 0731-5090.

[5] A. K. Misra and V. J. Modi. Three-dimensional dynamics and control of tether-connected n-body systems. *Acta Astronautica*, 26(2):77–84, 1992. ISSN 0094-5765.

[6] A D Guerman. Equilibria of multibody chain in orbit plane. *Journal of Guidance, Control, and Dynamics*, 26(6):942–948, nov-dec 2003. ISSN 0731-5090.

[7] V. V. Beletsky and E. M. Levin. Stability of a ring of connected satellites. *Acta Astronautica*, 12(10):765–769, 1985. ISSN 0094-5765.

[8] Ary Pizarro-Chong and Arun K. Misra. Dynamics of multi-tethered satellite formations containing a parent body. *Acta Astronautica*, 63(11-12):

1188–1202, dec 2008. ISSN 0094-5765. doi: 10.1016/j.actaastro.2008.06.
021.

 [9] Jun Zhao and Zhiqin Cai. Nonlinear dynamics and simulation of multi-
tethered satellite formations in Halo orbits. *Acta Astronautica*, 63(5-6):
673–681, sep 2008. ISSN 0094-5765. doi: 10.1016/j.actaastro.2008.04.007.

[10] S. G. Tragesser and A. Tuncay. Orbital design of earth-oriented tethered
satellite formations. *Journal of the Astronautical Sciences*, 53(1):51–64,
jan-mar 2005. ISSN 0021-9142.

[11] A. K. Misra, Z. Amier, and V. J. Modi. Attitude dynamics of three-boby
tethred systems. *Acta Astronautica*, 17(10):1059–1068, 1988. ISSN 0094-
5765.

[12] Anna D. Guerman, Georgi Smirnov, P. Paglione, and A. M. Vale Seabra.
Stationary configurations of a tetrahedral tethered satellite, formation.
Journal of Guidance, Control, and Dynamics, 31(2):424–428, mar-apr 2008.
ISSN 0731-5090. doi: 10.2514/1.31979.

[13] M. Keshmiri, A. K. Misra, and V. J. Modi. General formulation for n-
body tethered satellite system dynamics. *Journal of Guidance, Control,
and Dynamics*, 19(1):75–83, jan-feb 1996. ISSN 0731-5090.

[14] AD Guerman. Spatial equilibria of multibody chain in a circular orbit.
Acta Astronautica, 58(1):1–14, jan 2006. ISSN 0094-5765. doi: 10.1016/j.
actaastro.2005.05.002.

[15] W. K. Chen. *Graph theory and its engineering applications*, volume 5 of
Advanced Series in Electrical and Computer Engineering. World Scientific,
1996. ISBN 980-02-1859-1.

[16] Roger A. Horn and Charles R. Johnson. *Matrix analysis*. Cambridge Uni-
versity Press, Cambridge, 1990. ISBN 0-521-38632-2. Corrected reprint of
the 1985 original.

Decentralized control of tethered satellite formations using electrodynamic tethers[1]

Abstract

Tethered satellite formations have gained increasing attention over the last years, since tethered formations can be advantageous for example for interferometry missions. This paper investigates the use of electrodynamic tethers for formation control of a broad class of formations. Actuation of the attitude dynamics is accomplished by control of electric currents through the tethers, giving rise to Lorentz forces along the tethers, through interaction with the magnetic field of the Earth. Control of the currents is possible through adjustable voltage sources situated at the satellites of the formation, providing potential differences to the ionosphere. The paper considers formations forming a tree structure and uses graph theory to describe these formations. Modeling of the electrical network formed by the tethers is likewise graph-based, and the result is a very generic model. A decentralized control algorithm is proposed such that each satellite can generate its control signal based on its own observations and without communicating with other satellites in the formation. The control strategy is divided into two parts: One controller stabilizes the currents through the tethers and another deals with attitude dynamics.

---

[1]Submitted to *Journal of Guidance, Control, and Dynamics.*

I Introduction

Tethered satellite formations are interesting in connection with several tasks in space. Recently, tethered interferometers have received massive attention due to the Submillimeter Probe of the Evolution of Cosmic Structure (SPECS) concept proposed by NASA [1]. Tethered satellite formations are also proposed in several other connections, for example for elevator systems used at space stations and atmospheric probes [2]. A large variety of different formations have been investigated. The most examined formation is a chain structure. For an N-body chain structure the equations of motion were investigated in [3, 4] and a simple relation between the in-plane and the out-of-plane natural frequencies was stated. In [5] the stationary configurations situated in the orbit plane for an N-body chain were found and an upper limit on the number of possible configurations was stated. The investigation was expanded in [6] to include general stationary configurations taking both the in-plane and the out-of-plane dimensions into account. Recently, we have studied the dynamics and the stationary configurations of a general tree structure [7], which can be seen as several connected chains. More complicated formations have also been considered, mainly in connection with spinning satellite formations. The so-called hub-and-spoke formation is a formation consisting of a parent satellite to which several sub-satellites are tethered. In the case where the sub-satellites furthermore are tethered in a ring, the formation is denoted a closed-hub-and-spoke formation. The stability properties of these formations, spinning around different axes, were investigated in [8]. Another spinning formation is a double pyramid formation. This formation consists of a number of satellites tethered in a plane, and two anchor satellites tethered at each side of the formation. The formation spins around an axis through the anchor satellites. Such a formation was investigated for its stability properties in [8] and [9].

In [10, 11] a decentralized control strategy was developed for the in-plane dynamics chain structure include three satellites. The control design considered the attitude of each satellite and used reaction wheels situated at each satellite to actuate the system. The strategy was decentralized in the sense that each satellite generated a control signal based on its own orientation and the spinning rate of the formation. Ref. [12] investigated the control of a three satellite tethered interferometer forming a chain structure. An open-loop control strategy was developed for this spinning formation to change the plane of rotation. The strategy applied electrical thrusters at two of the three satellites and solved the attitude equations analytically by means of a perturbation method.

The use of electrodynamic tethers is a well established concept when considering single tether systems. The main interest in this connection is the systems ability to actuate the orbit motion. Missions have been flown to investigate the concept

[13] and several control strategies have been proposed both for the orbital motion [14] and the attitude motion [15, 16, 17]. The investigations have shown that, in the case where only the current through the tether is controlled, the system is under-actuated. It has also been shown, that it is not possible to stabilize both in-plane and out-of-plane motion at an equilibrium point, and several articles have therefore studied the possibility of stabilizing periodic solutions. Utilizing magnetic fields for formation control is also the idea behind a so-called electromagnetic formation flight (EMFF). In an EMFF system each satellite of the formation is generating a magnetic field and the formation is controlled through the interconnection of these fields. In [18] an EMFF was investigated as an alternative to a tethered formation.

This article proposes the use of electrodynamic tethers in connection with the control of tethered satellite formations. A main contribution of this article is a generic formulation of the electrical network formed by the formation when using electrodynamic tethers. Combined with a corresponding generic model of the in-plane attitude motion, an overall nonlinear model is stated for the system. The electrical circuit is closed via the ionosphere through a phantom loop. These connections to the ionosphere are modeled by resistors with non-linear current-voltage characteristics. The current in the electrical network is controlled by adjustable voltage source placed at each satellite determine the current flow to the ionosphere. The tether currents give rise to forces acting along the tether through interactions with the Earth's magnetic field. These forces are used to actuate the attitude motion. The modeling covers formations forming tree structures. Another contribution is a decentralized control strategy applicable for the system. The strategy is decentralized in the sense that each satellite can apply a control signal based on own observations and without communication between satellites. The control design is obtained in two steps. First, a control law stabilizes the current along the tethers using the voltage sources at the satellites. Second, a control law for the attitude dynamics stabilizes the formation in a desired shape. Both the model and the control laws are based on graph theoretical quantities describing the formation structure and the electrical circuit, which occur as parameters in the system descriptions. This enables both the dynamics and the control laws to cover a variety of different models.

The remaining part of this article is organized as follows. Section II treats the modeling of the system. The graph description is introduced and the unforced dynamics are briefly considered. The electrodynamic actuation of the system is examined and the modeling of the electrical network formed by the tethers is treated in detail. Section III treats the control design for the system. A control law providing asymptotic stability of the tether currents is introduced and the motion control is treated. In both cases the constraints to guarantee a decentralized control configuration are stated. The control design is exemplified

using a Y-formation in Section IV. Finally, the main conclusions of the work
are stated in Section V.

II   Model

The model presented in this section considers the attitude motion in the or-
bit plane of a tethered satellite formation. The in-plane motion is actuated
by means of electrodynamic tethers, while the out-of-plane motion is assumed
stabilized by another set of actuators. This assumption is mainly introduced
to avoid an under-actuated system occurring when a single current through a
tether, controls both the in-plane and the out-of-plane motion. The modeling
is based on two graphs: One describing the interconnection of satellites in the
formation and another describing the electrical circuit formed by the electro-
dynamic tethers. The formations under consideration form a tree structure.
This assumption simplifies the equations of motion, since each tether repre-
sents a single degree of freedom and algebraic constraints around the cycles are
avoided.

a)   Graph theoretical description

The formation under consideration consists of n tethers. Since the formation is
assumed to form a tree structure the number of satellites in the formation equals
$n + 1$. The satellites are modeled as point masses denoted m_i for $i = 0, \ldots, n$
and the tethers are assumed massless and of constant length l_j for $j = 1, \ldots, n$.
The total mass of the formation is denoted $m = \sum_i m_i$ and the relative mass
of each satellite is $\mu_i = \frac{m_i}{m}$. The formation is described by a directed graph
where the nodes represent the satellites and the edges represent the tethers.
The notations m_i and l_j are reused to refer to the nodes and edges, respectively.
The formation is described relative to the node m_0 called the root of the tree,
which can be chosen arbitrarily. Each edge is assigned a direction and it is
assumed, without loss of generality, that all edges are directed away from the
root m_0. Furthermore, the edges are ordered such that the edge l_j is connected
to m_j and directed towards m_j. A directed graph with n edges and $n + 1$
nodes can be described by an incidence matrix $\boldsymbol{B} \in \mathbb{R}^{(n+1) \times n}$. Each column of
$\boldsymbol{B}$ represents an edge of the graph. The elements of the incidence matrix are

defined as,

$$
B_{ij} = \begin{cases} 1 & \text{if } l_j \text{ is connected to and pointing away from } m_i \\ -1 & \text{if } l_j \text{ is connected to and pointing towards } m_i \\ 0 & \text{if } l_j \text{ is not connected to } m_i \end{cases} \tag{1}
$$

This definition is general and can also be applied to directed graphs not forming a tree structure. Assuming a tree structure, the incidence matrix $\boldsymbol{B}$ has full rank and all paths along the tethers are unique. The paths from the nodes m_i for $i = 1, \ldots, n$ to the root m_0 are described by the path matrix $\boldsymbol{P} \in \mathbb{R}^{n \times n}$ with elements,

$$
P_{ji} = \begin{cases} 1 & \text{if } l_j \text{ is in the path from } m_i \text{ to } m_0 \text{ directed towards } m_0 \\ -1 & \text{if } l_j \text{ is in the path from } m_i \text{ to } m_0 \text{ directed towards } m_i \\ 0 & \text{if } l_j \text{ is not in the path from } m_i \text{ to } m_0 \end{cases} \tag{2}
$$

Figure 1 shows a simple Y-formation consisting of five satellites connected by
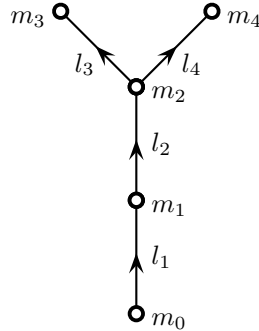
Figure 1: Y-formation with five satellites.

four tethers. The corresponding matrices are given as,

$$
\boldsymbol{B} = \begin{bmatrix} 1 & 0 & 0 & 0 \\ -1 & 1 & 0 & 0 \\ 0 & -1 & 1 & 1 \\ 0 & 0 & -1 & 0 \\ 0 & 0 & 0 & -1 \end{bmatrix}, \qquad \boldsymbol{P} = \begin{bmatrix} -1 & -1 & -1 & -1 \\ 0 & -1 & -1 & -1 \\ 0 & 0 & -1 & 0 \\ 0 & 0 & 0 & -1 \end{bmatrix}. \tag{3}
$$

b)   Equations of motion

The derivation of the unforced equations of motion is treated in detail in [7] and will therefore only be briefly described here. The center of mass (CM) of

the formation is assumed to follow a circular orbit with orbital rate ω. The formation is described in an orbit frame centered at the CM, with its x-axis directed along the position vector of the CM relative the Earth, and the y-axis is in the direction of the orbit velocity. The orientation of each tether is
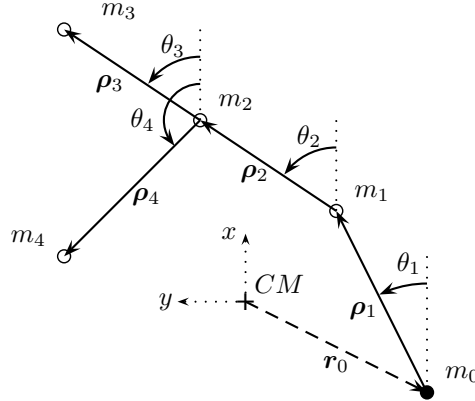
Figure 2: A tethered satellite formation situated in the orbit plane.

described by an angle θ_j for $j = 1, \ldots, n$ defined relative to translations of the orbit frame as shown in Fig. 2. These angles are chosen as the generalized coordinates of the system. A vector $\boldsymbol{\rho}_j$ is introduced along each tether,

$$\boldsymbol{\rho}_j = \begin{bmatrix} l_j \cos \theta_j \\ l_j \sin \theta_j \end{bmatrix}. \tag{4}$$

The basic idea of the derivation is to describe the position of each satellite by a sum of the vectors $\boldsymbol{\rho}_k$ following the path from satellite m_0. These sums can be found from the path matrix $\boldsymbol{P}$. For the formation in Fig. 2 the position of m_4 is found as the sum of $\boldsymbol{\rho}_1$, $\boldsymbol{\rho}_2$ and $\boldsymbol{\rho}_4$, which corresponds to the non-zero elements of the fourth column of the path matrix in (3). The position vector $\boldsymbol{r}_0$ describing m_0 relative to the CM can be determined from the weighted sum defining the CM, and consequently the position of all satellites relative to the CM can be calculated. The Lagrangian of the system is found and using Lagrange's equation the equations of motion occurs as,

$$\mathcal{M}\ddot{\boldsymbol{\theta}} + \mathcal{G} = \frac{\boldsymbol{\tau}}{m\omega^2}, \tag{5}$$

where $\boldsymbol{\theta} \in \mathbb{R}^n$ is a vector of the angles θ_j and $\boldsymbol{\tau} \in \mathbb{R}^n$ comprise the generalized forces. The derivatives of the generalized coordinates are denoted $\dot{\boldsymbol{\theta}}$. When considering circular orbits it is common to scale time by the orbital rate, creating a non-dimensional time variable. The derivatives are taken with respect to this

non-dimensional time. To describe the attitude motion of the formation the derivatives are taken relative to the orbit frame. The quantities $\boldsymbol{\mathcal{M}} \in \mathbb{R}^{n \times n}$ and $\boldsymbol{\mathcal{G}} \in \mathbb{R}^n$ are nonlinear functions of the generalized coordinates and velocities given as,

$$\boldsymbol{\mathcal{M}} = \boldsymbol{E}_{\sin} \boldsymbol{G} \boldsymbol{E}_{\sin} + \boldsymbol{E}_{\cos} \boldsymbol{G} \boldsymbol{E}_{\cos}, \tag{6}$$

$$\boldsymbol{\mathcal{G}} = \left(\boldsymbol{E}_{\sin} \boldsymbol{G} \boldsymbol{E}_{\cos} - \boldsymbol{E}_{\cos} \boldsymbol{G} \boldsymbol{E}_{\sin} \right) \left(2 \boldsymbol{I}_n + \boldsymbol{E}_{\dot{\theta}} \right) \dot{\boldsymbol{\theta}} + 3 \boldsymbol{E}_{\sin} \boldsymbol{G} \boldsymbol{E}_{\cos} \boldsymbol{1}_n, \tag{7}$$

where $\boldsymbol{I}_n$ is an identity matrix of size $n \times n$ and $\boldsymbol{1}_n$ denotes a vector of size n with one at all entries. The diagonal matrices $\boldsymbol{E}_{\cos} \in \mathbb{R}^{n \times n}$ and $\boldsymbol{E}_{\sin} \in \mathbb{R}^{n \times n}$ have $\cos \theta_j$ and $\sin \theta_j$, respectively, in diagonal entry j. The diagonal matrix $\boldsymbol{E}_{\dot{\theta}} \in \mathbb{R}^{n \times n}$ is defined similarly with $\dot{\theta}_j$ in diagonal entry j. The symmetric matrix $\boldsymbol{G} \in \mathbb{R}^{n \times n}$ collects all the parameters of the unforced dynamics as well as the formation topology. It can be written from the path matrix $\boldsymbol{P}$ as,

$$\boldsymbol{G} = \boldsymbol{L} \boldsymbol{P} \boldsymbol{W} \boldsymbol{P}^T \boldsymbol{L}, \tag{8}$$

where $\boldsymbol{L} \in \mathbb{R}^{n \times n}$ is a diagonal matrix with l_j in diagonal entry L_{jj}. The elements W_{ik} of the matrix $\boldsymbol{W} \in \mathbb{R}^{n \times n}$ is based on the relative masses,

$$W_{ik} = \mu_i \delta_{ik} - \mu_i \mu_k, \tag{9}$$

where δ_{ik} denotes Kronecker's delta.

c)   Electrodynamic actuation

The electrical circuit formed by the tethers is closed via phantom loops through the ionosphere. This means that each satellite has the ability to exchange electrons with the plasma either through collectors or active electron emitters. The currents through the tethers interact with the magnetic field of the Earth and give rise to Lorentz forces acting along the tethers. These forces are utilized to actuate the attitude dynamics. The distributed Lorentz force acting along a unit section of tether k is,

$$\boldsymbol{F}_k = \frac{\alpha_k}{l_k} \boldsymbol{\rho}_k \times \boldsymbol{B}_e \qquad \text{for } k = 1, \dots, n, \tag{10}$$

where α_k is the current through the tether and $\boldsymbol{B}_e$ is the magnetic field vector. Since only the in-plane motion is under consideration it is assumed that $\boldsymbol{B}_e$ is perpendicular to the orbit plane with magnitude B_z. The generalized force τ_j can be found by projecting the total Lorentz force onto the generalized coordinate θ_j. The Lorentz forces acting along the tethers are found by integrating the distributed force along the tethers, and the total force affecting the system

is the sum over all tethers. Consequently, the generalized forces are,

$$\tau_j = \sum_{k=1}^{n} \int_0^{l_k} \boldsymbol{F}_k^T \frac{\partial \boldsymbol{\rho}_k}{\partial \theta_j} \frac{s}{l_k} ds = \int_0^{l_j} \boldsymbol{F}_j^T \frac{\partial \boldsymbol{\rho}_j}{\partial \theta_j} \frac{s}{l_j} ds. \tag{11}$$

The right-hand side reflects that the sum only contains one term since $\boldsymbol{\rho}_j$ only depends on θ_j. Inserting (10) into (11) the generalized force is shown to be proportional to the tether current,

$$\tau_j = -\frac{1}{2} l_j^2 B_z \alpha_j. \tag{12}$$

Collecting the currents in a vector $\boldsymbol{\alpha} \in \mathbb{R}^n$, $\boldsymbol{\alpha} = [\alpha_1 \ \ldots \ \alpha_n]^T$, the generalized forces can be written as,

$$\frac{\boldsymbol{\tau}}{m\omega^2} = \boldsymbol{\Lambda}\boldsymbol{\alpha}, \tag{13}$$

where $\boldsymbol{\Lambda} \in \mathbb{R}^{n \times n}$ is a constant diagonal matrix introduced as $\boldsymbol{\Lambda} = -\frac{1}{2} \frac{B_z}{m\omega^2} \boldsymbol{L}^2$. The total system description can be written as,

$$\dot{\boldsymbol{x}} = \boldsymbol{f}(\boldsymbol{x}) + \boldsymbol{\Gamma}\boldsymbol{\alpha}, \tag{14}$$

where $\boldsymbol{x} = [\boldsymbol{\theta} \ \dot{\boldsymbol{\theta}}]^T$ is the state vector and $\boldsymbol{\Gamma} = [\boldsymbol{0}_{n \times n} \ \boldsymbol{\Lambda}]^T$ is the input matrix. The function $\boldsymbol{f}(\boldsymbol{x})$ can be written as,

$$\boldsymbol{f}(\boldsymbol{x}) = \begin{bmatrix} \dot{\boldsymbol{\theta}} \\ \boldsymbol{\mathcal{M}}^{-1}\boldsymbol{\mathcal{G}} \end{bmatrix} \tag{15}$$

d)   Electrical circuit description

The network of electrodynamic tethers resembles an electrical circuit, and it is natural to model this circuit using graph theory to maintain the generic system description. The formulation presented here is based on [19, chap. 2], with the expansion of including resistors with nonlinear current-voltage characteristics.

The first step in the modeling is to consider the electrical circuit of a single electrodynamic tether. An equivalent circuit is shown in Figure 3a. The circuit is described in detail in [20]. The voltage W induced along the tether occurs when the system is passing through the magnetic field. By exchanging electrons with the ionosphere the current I can flow through the tether. The resistances R_{SH+} and R_{SH-} are associated with collecting and emitting electrons, respectively, and obey a quite complicated current-voltage relation due to Debye shield and other phenomena. The phantom loop through the ionosphere is characterized by the resistance R_P, while the tether resistance is R_T. According to [20] the

(a) Equivalent circuit   (b) Controlled circuit
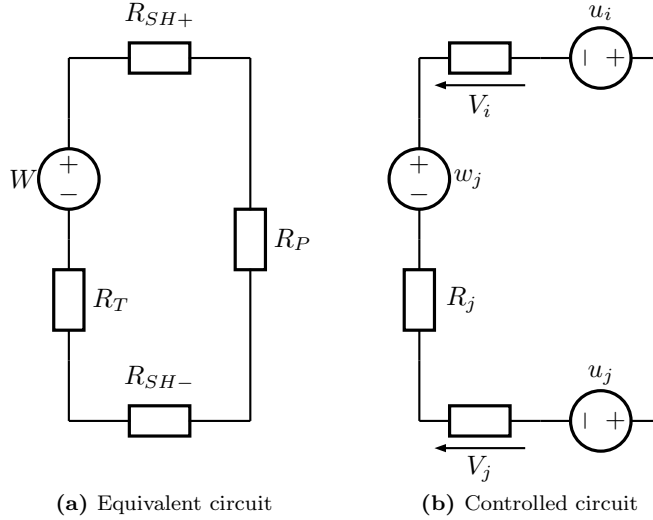
Figure 3: Equivalent electric circuits of a single tether system.

resistance R_P is negligible compared to the other resistances and is therefore omitted in this work. Consequently, the ionosphere can be regarded as having a single potential, and therefore be represented by a single node in the electrical circuit.

To control the currents in the tethers, each satellite can generate an adjustable potential difference u_i relative to the ionosphere. This leads to the controlled circuit shown in Fig. 3b. A resistor with a nonlinear current-voltage characteristic is placed in series with u_i. The voltage over this resistor is given as $V_i(\beta_i)$, where β_i is the current through the resistor. It is assumed that $V_i(\beta_i)$ is strictly increasing. The nonlinear current-voltage relations are collected in the vector function $\boldsymbol{V}$, which have a special structure since V_i only depends on β_i. This resistor can be seen as a combination of R_{SH+} and R_{SH-}, since the system is designed for currents to be able to flow both to and from the ionosphere at all satellites. The controlled voltages are collected in $\boldsymbol{u} \in \mathbb{R}^{n+1}$ and the currents β_i in $\boldsymbol{\beta} \in \mathbb{R}^{n+1}$. The induced voltages w_j and the resistances R_j of the tethers are collected in a vector $\boldsymbol{w} \in \mathbb{R}^n$ and a diagonal matrix $\boldsymbol{R} \in \mathbb{R}^{n \times n}$.

When using graph theory to model electrical circuits, junctions are represented by nodes and the connections between them by edges. The satellites of the formation can be seen as junctions in the circuit and the graph describing the circuit can therefore be written as an expansion of the graph describing the tethered formation. The set of edges is expanded by $n + 1$ edges, representing the connections to the ionosphere at each satellite. The edges are arranged such

that the first n edges coincide with the edges representing tethers, while edge $n+1$ represents the connection at m_0, the edge $n+2$ the connection at m_1, and so on until edge $2n+1$, which represents the connection at m_n. The graph is expanded by a single node representing the ionosphere and the total number of nodes becomes $n+2$. The first $n+1$ nodes represent the satellites and the last node represents the ionosphere. Without loss of generality, the edges connected to the ionosphere are directed away from the ionosphere. This choice leads to an incidence matrix $\boldsymbol{B}_c \in \mathbb{R}^{(n+2) \times (2n+1)}$ for the circuit graph given as,

$$\boldsymbol{B}_c = \begin{bmatrix} \boldsymbol{B} & -\boldsymbol{I}_{n+1} \\ \boldsymbol{0}_n^T & \boldsymbol{1}_{n+1}^T \end{bmatrix}, \tag{16}$$

where the elements are defined as in (1). The vector $\boldsymbol{0}_n \in \mathbb{R}^n$ has zero at all entries. The graph described by $\boldsymbol{B}_c$ is connected and its nullity is therefore n according to [19, Def. 1.12 p.11]. The cycles of $\boldsymbol{B}_c$ correspond to the loops of the electrical circuit. The directed cycles can be described by the matrix $\boldsymbol{Q}_c \in \mathbb{R}^{n \times (2n+1)}$. Each row of $\boldsymbol{Q}_c$ describes a cycle of the graph and its elements are given as,

$$(Q_c)_{kj} = \begin{cases} 1 & \text{if edge } j \text{ is included in cycle } k \text{ in the same} \\ & \text{direction as the cycle} \\ -1 & \text{if edge } j \text{ is included in cycle } k \text{ in the opposite} \\ & \text{direction as the cycle} \\ 0 & \text{if edge } j \text{ is not included in cycle } k \end{cases} \tag{17}$$

The cycles of the graph are not uniquely determined, but $\boldsymbol{Q}_c$ contains a complete set of linear independent cycles. The matrix $\boldsymbol{Q}_c$ can be found from the right nullspace of $\boldsymbol{B}_c$,

$$\boldsymbol{B}_c \boldsymbol{Q}_c^T = \boldsymbol{0}_{(n+2) \times n}. \tag{18}$$

A set of linear independent cycles can be chosen such that each tether is only included in one cycle. This is done by assuming that left $n \times n$ sub-matrix of $\boldsymbol{Q}_c$ is an identity matrix. Using this structure, $\boldsymbol{Q}_c$ can be found by inserting (16) into (18),

$$\boldsymbol{Q}_c = \begin{bmatrix} \boldsymbol{I}_n & \boldsymbol{B}^T \end{bmatrix}. \tag{19}$$

The currents and potential differences along the branches of the network are collected in $\boldsymbol{i}$ and $\boldsymbol{v}$, respectively. In accordance with the ordering of the edges $\boldsymbol{i}$ can be written as,

$$\boldsymbol{i} = \begin{bmatrix} \boldsymbol{\alpha} \\ \boldsymbol{\beta} \end{bmatrix}, \tag{20}$$

The current along a branch can be seen as a sum with a term for each loop including the branch. Consequently, all currents in the network can be written

as functions of these currents called the loop currents $\boldsymbol{i} \in \mathbb{R}^n$. The loop currents fulfills,

$$\boldsymbol{i} = \boldsymbol{Q}_c^T \boldsymbol{i}_m. \tag{21}$$

Combining (19), (20), and (21) it is seen that the loop currents equal the tether currents, $\boldsymbol{i}_m = \boldsymbol{\alpha}$, which is a consequence of the fact that each tether is only included in one loop. Furthermore, it is seen that,

$$\boldsymbol{\beta} = \boldsymbol{B}\boldsymbol{\alpha}, \tag{22}$$

which shows that the net tether current at a satellite is transferred along the branch to the ionosphere.

The circuit equations is found from Kirchhoff's voltage law, which can be formulated from the cycle matrix,

$$\boldsymbol{Q}_c \boldsymbol{v} = \boldsymbol{0}_n. \tag{23}$$

The potential differences along the branches are a combination of the voltage sources and voltages drops over the resistors, hence $\boldsymbol{v}$ is,

$$\boldsymbol{v} = \begin{bmatrix} \boldsymbol{w} + \boldsymbol{R}\boldsymbol{\alpha} \\ \boldsymbol{u} + \boldsymbol{V}(\boldsymbol{\beta}) \end{bmatrix}. \tag{24}$$

Inserting this into Kirchhoff's law (23) utilizing the structure of $\boldsymbol{Q}_c$ stated in (19) leads to the circuit equations,

$$\boldsymbol{R}\boldsymbol{\alpha} + \boldsymbol{B}^T \boldsymbol{V}(\boldsymbol{\beta}) = -\boldsymbol{w} - \boldsymbol{B}^T \boldsymbol{u}. \tag{25}$$

To illustrate the setup consider the simple two-tether chain in Fig. 4. The
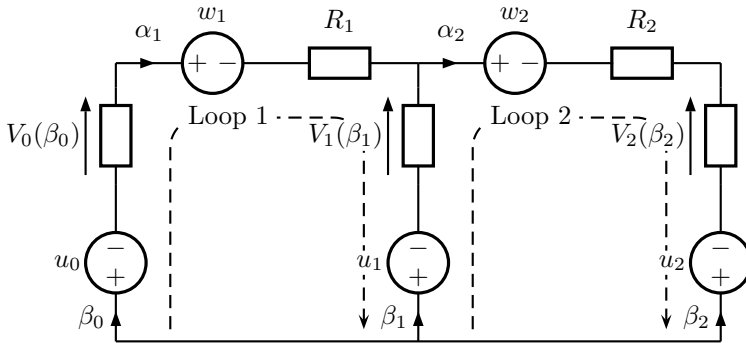

Figure 4: Equivalent electrical circuit of a two-tether formation.

incidence and the cycle matrices are,

$$\boldsymbol{B} = \begin{bmatrix} 1 & 0 \\ -1 & 1 \\ 0 & -1 \end{bmatrix}, \qquad \boldsymbol{Q}_c = \begin{bmatrix} 1 & 0 & 1 & -1 & 0 \\ 0 & 1 & 0 & 1 & -1 \end{bmatrix}. \qquad (26)$$

The direction of the two cycles are shown in Fig. 4. In this example (22) gives,

$$\boldsymbol{\beta} = \begin{bmatrix} 1 & 0 \\ -1 & 1 \\ 0 & -1 \end{bmatrix} \boldsymbol{\alpha} = \begin{bmatrix} \alpha_1 \\ \alpha_2 - \alpha_1 \\ -\alpha_2 \end{bmatrix}, \qquad (27)$$

which is seen to describe Kirchhoff's current law for the tree nodes representing the satellites of the formation.

III   Control design

The control design is divided into two parts. The solutions to both parts is decentralized in the sense that the control signal applied at a satellite depends only on quantities, that can be measured from the same satellite. A control law is first designed to stabilize the tether currents at a desired level. The resulting closed-loop system will be the actuator for attitude control. The challenge in this problem is to control the n currents with the $n + 1$ voltage sources, where each current depends on all voltage sources. The second part of the control design will be a control law for the attitude motion.

a)   Control of tether currents

The tether currents are determined by the circuit equation found in the previous section,

$$\boldsymbol{R}\boldsymbol{\alpha} + \boldsymbol{B}^T \boldsymbol{V}(\boldsymbol{\beta}) = -\boldsymbol{w} - \boldsymbol{B}^T \boldsymbol{u}. \qquad (28)$$

The induced voltage $\boldsymbol{w}$ will depend on the magnetic field vector and the velocity of the formation. It will not be difficult to obtain an estimate $\widehat{\boldsymbol{w}}$ of $\boldsymbol{w}$ and have this available at each satellite in the formation. Using this estimate, $\boldsymbol{w}$ can be compensated for using the input,

$$\boldsymbol{u} = \left(\boldsymbol{B}^+\right)^T \widehat{\boldsymbol{w}} - \bar{\boldsymbol{u}} \qquad (29)$$

where $\bar{\boldsymbol{u}}$ is a new input. The matrix $\boldsymbol{B}^+$ is the left pseudoinverse of $\boldsymbol{B}$, which is guaranteed to exist since $\boldsymbol{B}$ has full rank. In general the inverse $\boldsymbol{B}^+$ does

not have a sparse structure, hence the compensation (29) requires that the
formation topology is known. Assuming a perfect estimate $\widehat{\boldsymbol{w}} = \boldsymbol{w}$, the system
can be written as,

$$\boldsymbol{R}\boldsymbol{\alpha} + \boldsymbol{B}^T \boldsymbol{V}(\boldsymbol{\beta}) = -\boldsymbol{B}^T \bar{\boldsymbol{u}}. \tag{30}$$

To stabilize the tether currents the following control law based in integral action
is proposed,

$$\dot{\bar{\boldsymbol{u}}} = \boldsymbol{K}_i \boldsymbol{B} \left(\boldsymbol{\alpha} - \boldsymbol{\alpha}_d \right), \tag{31}$$

where $\boldsymbol{K}_i \in \mathbb{R}^{(n+1)\times(n+1)}$ is a positive definite diagonal matrix, $\boldsymbol{K}_i > 0$, and the
vector $\boldsymbol{\alpha}_d \in \mathbb{R}^n$ is the desired loop currents. To find the closed-loop description
the derivative of (30) is needed,

$$\boldsymbol{R}\dot{\boldsymbol{\alpha}} + \boldsymbol{B}^T \frac{\partial \boldsymbol{V}}{\partial \boldsymbol{\beta}} \boldsymbol{B}\dot{\boldsymbol{\alpha}} = -\boldsymbol{B}^T \dot{\bar{\boldsymbol{u}}}, \tag{32}$$

where it is utilized that the vector function $\boldsymbol{V}(\boldsymbol{\beta})$ can be written as $\boldsymbol{V}(\boldsymbol{B}\boldsymbol{\alpha})$ using
(22), hence the derivative $\frac{\partial \boldsymbol{V}}{\partial \boldsymbol{\beta}} \boldsymbol{B}\dot{\boldsymbol{\alpha}}$. The Jacobian has a diagonal structure since
V_i only depends on β_i, and using the assumption that V_i is strictly increasing
the Jacobian becomes positive definite. Since $\boldsymbol{B}$ has full rank, $\boldsymbol{B}^T \frac{\partial \boldsymbol{V}}{\partial \boldsymbol{\beta}} \boldsymbol{B}$ and
$\boldsymbol{B}^T \boldsymbol{K}_i \boldsymbol{B}$ are positive definite. Inserting the control law (31) in (32) the closed-
loop actuator dynamics are,

$$\dot{\boldsymbol{\alpha}} = - \left(\boldsymbol{R} + \boldsymbol{B}^T \frac{\partial \boldsymbol{V}}{\partial \boldsymbol{\beta}} \boldsymbol{B} \right)^{-1} \boldsymbol{B}^T \boldsymbol{K}_i \boldsymbol{B} \left(\boldsymbol{\alpha} - \boldsymbol{\alpha}_d \right). \tag{33}$$

The stability of this nonlinear closed-loop system can be investigated using the
Lyapunov function $V = \frac{1}{2} \left(\boldsymbol{\alpha} - \boldsymbol{\alpha}_d \right)^T \left(\boldsymbol{\alpha} - \boldsymbol{\alpha}_d \right)$, which has the negative definite
time derivative,

$$\dot{V} = - \left(\boldsymbol{\alpha} - \boldsymbol{\alpha}_d \right)^T \left(\boldsymbol{R} + \boldsymbol{B}^T \frac{\partial \boldsymbol{V}}{\partial \boldsymbol{\beta}} \boldsymbol{B} \right)^{-1} \boldsymbol{B}^T \boldsymbol{K}_i \boldsymbol{B} \left(\boldsymbol{\alpha} - \boldsymbol{\alpha}_d \right). \tag{34}$$

Hence the closed-loop system will converge asymptotically towards $\boldsymbol{\alpha}_d$

To realize that the control law (31) can be implemented in a decentralized way,
the factor $\boldsymbol{B}\boldsymbol{\alpha}$ is considered. According to (22) this quantity equals the currents
in the branches connected to the ionosphere $\boldsymbol{\beta}$, and the element β_i represents
a current, that can be measured at satellite i. The input u_i represents in the
same way a voltage, which can be applied at satellite i. The diagonal structure
of the controller gain $\boldsymbol{K}_i$ ensures that the measurements are kept separate, and
that the control signal u_i only depends on the measurement of β_i. To use the
introduced actuator dynamics in a decentralized manner, it is advantageous to
be able to connect the reference signal to measurements at the satellites. This
can be done by introducing the new reference signal $\boldsymbol{\beta}_d = \boldsymbol{B}\boldsymbol{\alpha}_d$, again using
(22). Using $\boldsymbol{\beta}_d$, the desired tether currents are expressed using the current

exchanged with the ionosphere at each satellite. The reference signal $\boldsymbol{\beta}_d$ is, however, an over-representation of the tether currents and must be subjected to the constraint,

$$\mathbf{1}_{n+1}^T \boldsymbol{\beta}_d = 0. \tag{35}$$

This constraint states that the net current to the node representing the ionosphere must be zero. In a practical context one could argue that this is actually not necessary, but that the constraint is reflecting the way the circuit is modeled. The decentralized current stabilization is shown in Figure 5. The control
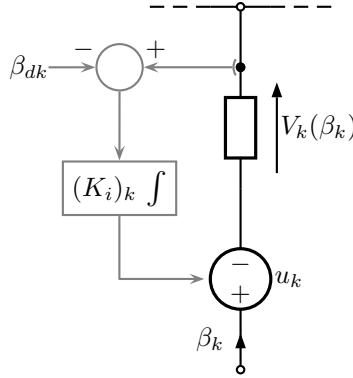
Figure 5: Current stabilizing control scheme.

scheme is stabilizing the current through the nonlinear resistor based on a measurement of the same current. Hence the control scheme can be seen as a way of implementing controllable current sources based on adjustable voltage sources, and in that way controlling the current flow to the ionosphere.

In summary the total actuator dynamics can be written as,

$$\dot{\boldsymbol{\alpha}} = \boldsymbol{f}_a(\boldsymbol{\alpha}) + \boldsymbol{g}_a(\boldsymbol{\alpha})\boldsymbol{\beta}_d \tag{36}$$

where the nonlinear functions $\boldsymbol{f}_a$ and $\boldsymbol{g}_a$ are given as,

$$\boldsymbol{f}_a = -\left(\boldsymbol{R} + \boldsymbol{B}^T \frac{\partial \boldsymbol{V}}{\partial \boldsymbol{\beta}} \boldsymbol{B}\right)^{-1} \boldsymbol{B}^T \boldsymbol{K}_i \boldsymbol{B} \boldsymbol{\alpha}, \tag{37}$$

$$\boldsymbol{g}_a = \left(\boldsymbol{R} + \boldsymbol{B}^T \frac{\partial \boldsymbol{V}}{\partial \boldsymbol{\beta}} \boldsymbol{B}\right)^{-1} \boldsymbol{B}^T \boldsymbol{K}_i \boldsymbol{\beta}_d. \tag{38}$$

b)   Decentralized formation control

Turning to attitude control, it is assumed that each satellite can measure its orientation in the orbit frame and the orientations θ_j of the tethers incident

to the satellite. Furthermore, it is assumed that the time derivatives of the measurements are available. The control design is based on a system dynamics of the form,

$$\dot{\boldsymbol{x}} = \boldsymbol{f}(\boldsymbol{x}) + \boldsymbol{\Gamma}\boldsymbol{\alpha}. \tag{39}$$

The measurements $\boldsymbol{y} \in \mathbb{R}^{2n+2}$ of the system are,

$$\boldsymbol{y} = \boldsymbol{C}\boldsymbol{x} = \begin{bmatrix} \boldsymbol{B} & \boldsymbol{0} \\ \boldsymbol{0} & \boldsymbol{B} \end{bmatrix} \boldsymbol{x}. \tag{40}$$

The elements y_i and y_{n+1+i} for $i = 1, \ldots, n+1$ represent measurements at each satellite. The first y_i is a linear combination of the orientation of the tethers connected to the satellite. The linear combination is determined by the direction of the edges representing the tethers. Outgoing edges contribute with positive signs in the linear combination, and ingoing edges with negative signs. This structure of the measurement originates from the definition of $\boldsymbol{B}$ in (1) and guarantees that the signal y_i is measurable from satellite i. The measurement y_{n+1+i} equals $\dot{y}_i$. The definition of the measurements are quite restrictive, even in a decentralized setup. The definition has, however, the advantage of introducing the incidence matrix $\boldsymbol{B}$ in output matrix $\boldsymbol{C}$ and thereby connecting the measurements with the satellites instead of the tethers. The proposed feedback law is,

$$\boldsymbol{\beta}_d = \boldsymbol{K}\boldsymbol{y} = \begin{bmatrix} \boldsymbol{K}_p & \boldsymbol{K}_d \end{bmatrix} \boldsymbol{y}, \tag{41}$$

where the matrices $\boldsymbol{K}_p, \boldsymbol{K}_d \in \mathbb{R}^{(n+1)\times(n+1)}$ are diagonal to ensure the decentralized structure. The total control setup is illustrated in Fig. 6.

Figure 6: Block diagram of the total control scheme.

The constraint on the reference signal $\boldsymbol{\beta}_d$ imposes some restrictions in the choice of controller gains. To investigate these, the feedback law (41) is combined with

the constraint in (35),

$$\begin{bmatrix} \mathbf{1}_{n+1}^T \boldsymbol{K}_p \boldsymbol{B} & \mathbf{1}_{n+1}^T \boldsymbol{K}_d \boldsymbol{B} \end{bmatrix} \boldsymbol{x} = 0. \tag{42}$$

Using that $\mathbf{1}_{n+1}^T \boldsymbol{B} = \mathbf{0}_n^T$, it is seen that the constraint can be fulfilled by using the same controller gains at all local controllers. This imposes the structures $\boldsymbol{K}_p = k_p \boldsymbol{I}_{n+1}$ and $\boldsymbol{K}_d = k_d \boldsymbol{I}_{n+1}$ on the controller gains. In a practical context this constraint can lead to some difficulties, since it can be hard to guarantee identical gains in all sub-controllers.

The control design is mainly presented to show that a decentralized control strategy is possible. It could be improved in several ways, for example by using the measurements in a less restrictive way. Furthermore, a full or partial observer design could by applied at each satellite, enabling a less restrictive control scheme, while maintaining the decentralized structure.

IV   Example

Consider as an example an Y-formation shown in Figures 1 and 2. The orbit is assumed to be equatorial, and the magnetic field constant and perpendicular to the orbit plane, when using a non-tilted dipole to model the magnetic field of the Earth. The constant $\boldsymbol{\Lambda}$ can then be written as,

$$\boldsymbol{\Lambda} = -\frac{1}{2} \frac{1}{m} \frac{\mu_m}{\mu} \boldsymbol{L}^2 \tag{43}$$

where $\mu_m = 7.79 \times 10^{15}$ Nm^{2}A^{-1} is the strength of the magnetic field and $\mu = 3.986 \times 10^{14}$ m^{3}s^{-1} is the standard gravitational parameter of the Earth. Let all tethers have a length of 5 km and a resistance of 55.7×10^{-3} Ω/m. The resistances modeling the ionosphere connections are assumed to follow the current-voltage relation $V_i(\beta_i) = 150 \text{ sign}(\beta_i)\beta_i^2$, where sign denotes the sign function. This choice is inspired by the characteristics of a spherical electron collector presented in [20]. The relation shows that the characteristics for collecting and emitting electrons are equal. This is a conservative assumption since the emitting of electrons is connected with a much lower resistance in reality. The relation $V_i(\beta_i)$ is not strictly increasing as required for stability, but since $\frac{\partial V_i}{\partial \beta_i} = 0$ only for $\beta_i = 0$ the stability conclusions are not affected. The masses are chosen as $m_0 = m_1 = 89.1$ kg, $m_2 = 200$ kg, and $m_3 = m_4 = 50$ kg. The masses of the satellites are chosen such that the configuration $\boldsymbol{\theta}^* = [0° \; 0° \; 135° \; 135°]^T$ is stationary, and the system will operate around this configuration. The controller gain $\boldsymbol{K}_i$ must be chosen to obtain actuator dynamics which allows the desired performance of the overall controller. The gain is chosen as,

$$\boldsymbol{K}_i = 5000 \; \boldsymbol{I}_5 \; \frac{\text{V}}{\text{As}}. \tag{44}$$

Figure 7 shows the tether currents and the control voltages of a simulation of actuator dynamics. The desired currents are $\boldsymbol{\alpha}_d = [1 \ -0.2 \ -0.8 \ \ 0.3]^T$. It is
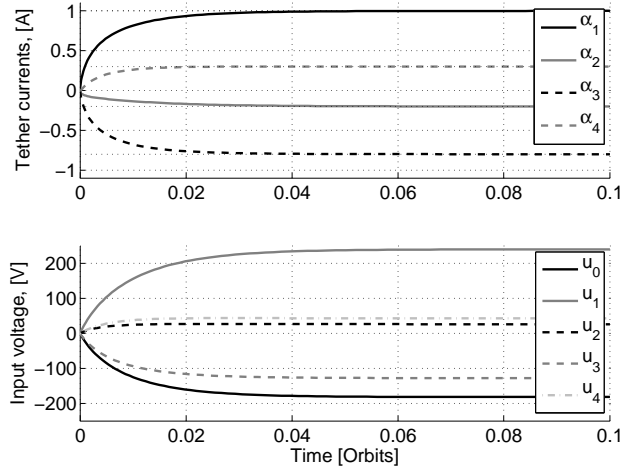

Figure 7: Simulation of the actuator dynamics.

seen that the system can stabilize the tether current within a tenth of an orbit.

Figure 8 shows two simulations, one of an large attitude maneuver and another of an attitude correction. The control gains used in the simulations are shown in Table 1. During the maneuver shown in Fig. 8a the tether currents exceed the

	Maneuver	Correction
k_p	$-20 \ \frac{\text{A}}{\text{rad}}$	$-10 \ \frac{\text{A}}{\text{rad}}$
k_d	$-10 \ \frac{\text{A}}{\text{rad/s}}$	$-5 \ \frac{\text{A}}{\text{rad/s}}$
$\boldsymbol{K}_i$	$10^4 \ \boldsymbol{I}_5 \ \frac{\text{V}}{\text{As}}$	$5000 \ \boldsymbol{I}_5 \ \frac{\text{V}}{\text{As}}$

Table 1: Controller gains for simulation in Fig. 8

level, which are feasible to drive through tethers of this length. Consequently the control voltages are very large. Figure 8b shows that minor attitude correction are feasible and can be done within about one orbit. This simulation is carried out around the same stationary configuration $\boldsymbol{\theta}^*$, and to emphasize the convergence properties, deviation in states are shown. Combined, the simulations show that additional actuators must be utilized when making large orbit maneuvers, however, the electrodynamics tethers are capable of operating the system around an open-loop stationary configuration.
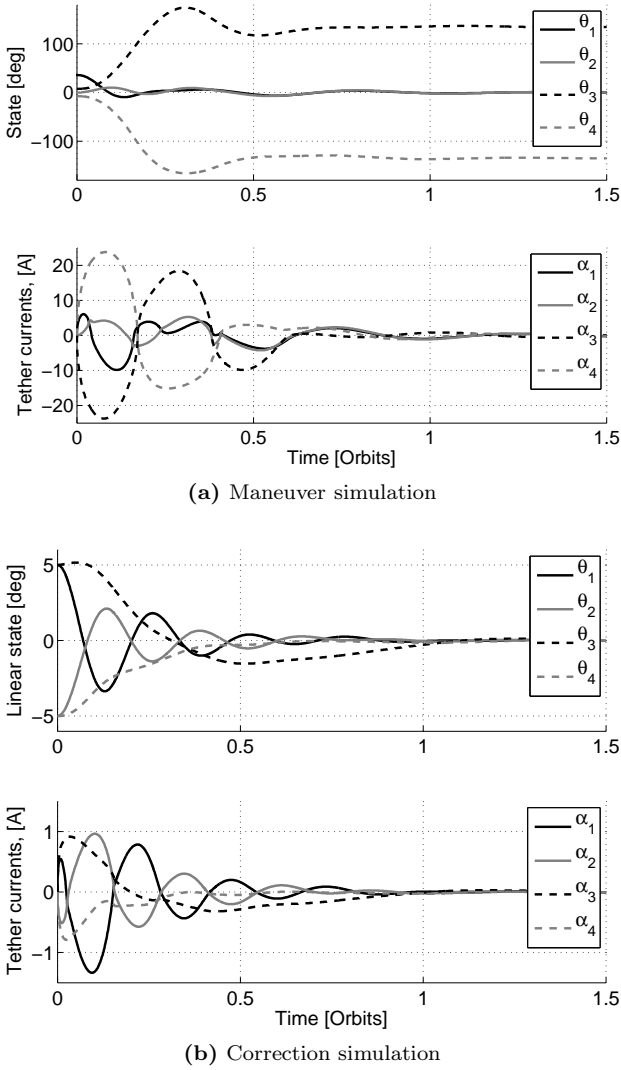
(a) Maneuver simulation

(b) Correction simulation

Figure 8: Simulation of Y-formation.

V   Conclusions

This article has investigated the use of electrodynamic tethers for formation control of tethered satellite formations. The main contribution was a generic way of modeling the electrical circuit formed by the tethers. The circuit included the

resistance of the tethers, the nonlinear current-voltage characteristics connected with the exchange of electrons with the ionosphere, and controllable voltage sources situated at the satellites. Combining this with a previously investigated generic formulation of the attitude dynamics gave an actuated system, which is valid for all formations forming a tree structure. The model was restricted to the motion in the orbit plane and tethers were modelled as rigid rods. Based on the model a generic control law was designed, using the formation structure as a parameter. The control law was decentralized in the sense that each satellite can apply a control signal without communication with other satellites in the formation. This feature makes the strategy suited for large formations. The control law was divided into one part stabilizing the tether currents and another controlling the attitude dynamics. The generic formulation was made possible by the use of graph theory, which was employed to describe both the formation structure and the electrical circuit.

An interesting extension of the control design would be to investigate the tension along the tethers. In the case where the tension along the tethers can be guaranteed by the controller, it would be interesting to investigate control strategies where the flexibility of the tethers was taken into account. Extending the model to include spinning satellite formations could also be of interest in this context, since they provide a centrifugal force to induce tension along the tethers.

References

[1] D. Leisawitz, J. C. Mather, S. H. Moseley, and X. L. Zhang. The submillimeter probe of the evolution of cosmic structure (SPECS). *Astrophysics and Space Science*, 269:563–567, 1999. ISSN 0004-640X.

[2] M. L. Cosmo and E. C. Lorenzini, editors. *Tethers in space handbook*. NASA Marshall Space Flight Center, 3rd edition, 1997.

[3] A. K. Misra and V. J. Modi. Three-dimensional dynamics and control of tether-connected n-body systems. *Acta Astronautica*, 26(2):77–84, 1992. ISSN 0094-5765.

[4] M. Keshmiri, A. K. Misra, and V. J. Modi. General formulation for n-body tethered satellite system dynamics. *Journal of Guidance, Control, and Dynamics*, 19(1):75–83, jan-feb 1996. ISSN 0731-5090.

[5] A D Guerman. Equilibria of multibody chain in orbit plane. *Journal of Guidance, Control, and Dynamics*, 26(6):942–948, nov-dec 2003. ISSN 0731-5090.

[6] AD Guerman. Spatial equilibria of multibody chain in a circular orbit. *Acta Astronautica*, 58(1):1–14, jan 2006. ISSN 0094-5765. doi: 10.1016/j. actaastro.2005.05.002.

[7] M. B. Larsen, R. S. Smith, and M. Blanke. Modeling of tethered satellite formations using graph theory (submitted). *Acta Astronautica*, 2010.

[8] Ary Pizarro-Chong and Arun K. Misra. Dynamics of multi-tethered satellite formations containing a parent body. *Acta Astronautica*, 63(11-12): 1188–1202, dec 2008. ISSN 0094-5765. doi: 10.1016/j.actaastro.2008.06. 021.

[9] S. G. Tragesser and A. Tuncay. Orbital design of earth-oriented tethered satellite formations. *Journal of the Astronautical Sciences*, 53(1):51–64, jan-mar 2005. ISSN 0021-9142.

[10] Soon-Jo Chung, Jean-Jacques E. Slotine, and David W. Miller. Nonlinear model reduction and decentralized control of tethered formation flight. *Journal of Guidance, Control, and Dynamics*, 30(2):390–400, MAR-APR 2007. ISSN 0731-5090. doi: 10.2514/1.21492. AIAA Guidance, Navigation, and Control Conference, Keystone, CO, AUG 21-24, 2006.

[11] Soon-Jo Chung and David W. Miller. Propellant-free control of tethered formation flight, part 1: Linear control and experimentation. *Journal of Guidance, Control, and Dynamics*, 31(3):571–584, may-jun 2008. ISSN 0731-5090.

[12] C. Bombardelli, E. C. Lorenzini, and M. B. Quadrelli. Retargeting dynamics of a linear tethered interferometer. *Journal of Guidance, Control, and Dynamics*, 27(6):1061–1067, nov-dec 2004. ISSN 0731-5090.

[13] E Lorenzini and J Sanmartin. Electrodynamic tethers in space. *Scientific American*, 291(2):50–57, AUG 2004. ISSN 0036-8733.

[14] Paul Williams. Optimal orbital transfer with electrodynamic tether. *Journal of Guidance, Control, and Dynamics*, 28(2):369–372, 2005. ISSN 0731-5090.

[15] J. Peláez and E. C. Lorenzini. Libration control of electrodynamic tethers in inclined orbit. *Journal of Guidance, Control, and Dynamics*, 28(2):269–279, 2005. ISSN 0731-5090.

[16] Paul Williams. Libration control of electrodynamic tethers using predictive control with time-delayed feedback. *Journal of Guidance, Control, and Dynamics*, 32(4):1254–1268, 2009. ISSN 0731-5090. doi: 10.2514/1.41039.

[17] M. B. Larsen and M Blanke. Passivity-based control of a rigid electrodynamic tether (submitted). *Journal of Guidance, Control, and Dynamics*, 2010.

[18] R J Sedwick and S A Schweighart. Propellantless spin-up of tethered or electromagnetically coupled sparse apertures. In H. A. MacEwen, editor, *Highly Innovative Space Telescope Concepts*, volume 4849 of *Proceedings of the Society of Photo-Optical Instrumentation Engineers (SPIE)*, pages 193–204. SPIE-International Society for Optical Engineering, 2002. ISBN 0-8194-4628-9.

[19] W. K. Chen. *Graph theory and its engineering applications*, volume 5 of *Advanced Series in Electrical and Computer Engineering*. World Scientific, 1996. ISBN 980-02-1859-1.

[20] L. Iess, C. Bruno, C. Ulivieri, U. Ponzi, M. Parisse, G. Laneve, M. Dobrowolny, F. De Venuto, B. Bertotti, L. Anselmo, and Giuliano Vannaroni. Satellite de-orbiting by means of electrodynamic tethers part I: General concepts and requirements. *Acta Astronautica*, 50(7):399–406, 2002. ISSN 0094-5765.